TECHNISCHE UNIVERSITÄT MÜNCHEN

Lehrstuhl für Proteomik und Bioanalytik

Application of mass spectrometry-based proteomics to study cancer drug resistance mechanisms

Heiner Matthias Koch

Vollständiger Abdruck der von der Fakultät Wissenschaftszentrum Weihenstephan für Ernährung, Landnutzung und Umwelt der Technischen Universität München zur Erlangung des akademischen Grades eines

Doktors der Naturwissenschaften

genehmigten Dissertation.

Vorsitzender: Prof. Dr. D. Langosch

Prüfer der Dissertation:
1. Prof. Dr. B. Küster
2. Prof. Dr. F. Bassermann

Die Dissertation wurde am 12.07.2016 bei der Technischen Universität München eingereicht und durch die Fakultät Wissenschaftszentrum Weihenstephan für Ernährung, Landnutzung und Umwelt am 20.09.2016 angenommen.

Table of Content

Abstract V

Zusammenfassung VI

Chapter I General Introduction 1

Chapter II Chemical proteomics uncovers EPHA2 as a mechanism of acquired resistance to small molecule EGFR kinase inhibition 49

Chapter III Phosphoproteome profiling reveals molecular mechanisms of growth factor mediated kinase inhibitor resistance in EGFR overexpressing cancer cells 73

Chapter IV Time resolved proteomic and phosphoproteomic analysis of adaptation to kinase inhibition 109

Chapter V General discussion 135

List of publications 144

Danksagung | Acknowledgment 145

Curriculum vitae 146

Abstract

In recent years an increasing number of small molecule kinase inhibitors were approved for targeted cancer therapies. Targeted therapies have less toxic side effects than conventional chemotherapeutics and promise efficacious personalized treatments. Although some molecules improved the outcome of selected patient groups, resistance almost invariably develops and represents a major clinical challenge. There is an intensive effort to circumvent emerging resistance by the development of new targeted agents or the combination of approved molecules. However, the molecular alterations that render cancer cells resistant are still poorly understood. Due to the pivotal role of mass spectrometry-based proteomics for the system-wide quantification of proteins and protein modifications, proteomic techniques should be applied to study the molecular mechanisms involved in drug resistance in more detail.

In the first part of this thesis, the differences in kinome expression between EGFR inhibitor sensitive and resistant cells were investigated. For this purpose a chemical proteomics approach comprising kinase affinity purification (Kinobeads) and mass spectrometry-based quantification was applied. This allowed the identification of known resistance mechanisms including the clinically observed amplification of MET, but also the discovery of new actionable targets including the kinase EPHA2 that was 10-fold overexpressed in resistant cells. Cell based assays could confirm that EPHA2 is an actionable drug target for combination with EGFR inhibition in resistant cells and proved that chemical proteomics is a broadly applicable approach for the discovery of drug resistance mechanisms.

It has been shown that growth factors secreted by the tumor microenvironment can render kinase inhibitors ineffective. To improve the molecular understanding of growth factor induced resistance in a simplified model, the global molecular consequences of FGF2 mediated gefitinib resistance were assessed on the proteome and phosphoproteome level. A tandem mass tag (TMT) labeling strategy was developed and allowed the identification and quantification of ~22,000 phosphopeptides and ~8,800 proteins in biological triplicates without missing values. A large number of kinases and kinase phosphorylation sites was downregulated by the drug but restored by the growth factor, indicating that these sites may represent reactivated signaling. Molecularly rationalized combination treatments with EGFR/MEK or PI3K/mTOR prevented growth factor mediated rescue and thus provide a potential strategy to target the tumor microenvironment.

Adaptation to kinase inhibitor treatment arises within days after treatment and results in proteome reprogramming and network rewiring. To investigate early drug adaptation mechanisms a TMT based time resolved analysis to EGFR and FGFR inhibition was conducted over 10 time points in 4 cell lines on the proteome and phosphoproteome level. Mostly, adaptation mechanisms of cell lines to kinase inhibition were very different on the proteome and on the phosphoproteome level. However, the inhibition of ERK1/2 activity in response to EGFR inhibition was apparent in almost all cells and the adaptation to EGFR inhibition revealed elevated expression of E-cadherin over time and correlated with a more aggregative phenotype. These results confirm that TMT labeling is also well suited for the investigation of time resolved adaptation mechanisms that occur in response to kinase inhibition.

Zusammenfassung

In den vergangenen Jahren wurde eine steigende Anzahl niedermolekularer Kinaseinhibitoren für die Behandlung von Krebserkrankungen zugelassen. Obwohl manche Substanzen den Gesundheitszustand von Patienten deutlich verbessert haben, kommt es jedoch fast immer zu einer Resistenzentwicklung und einem erneuten Tumorwachstum. Es gibt daher starke Bemühungen entstehende Resistenzen durch neue Inhibitoren, Inhibitorkombinationen oder individualisierte Behandlungen aufzuhalten. Die molekularen Ursachen die zu der Resistenzentwicklung beitragen sind allerdings noch immer wenig verstanden. Da die Massenspektrometrie basierte Proteomik eine leistungsfähige Technologie zur Charakterisierung des Proteoms und der Signaltransduktion darstellt, sollten in dieser Arbeit verschiedene Methoden der Proteomik angewendet werden um die molekularen Ursachen der Resistenzentwicklung systematisch zu untersuchen.

Im ersten Teil der Arbeit wurden die Unterschiede in der Zusammensetzung des Kinoms bei EGFR Inhibitor sensitiven und resistenten Zellen untersucht. Hierfür wurden Kinasen durch eine Affinitätsmatrix (Kinobeads, chemische Proteomik) angereichert um anschließend die Unterschiede durch Massenspektrometrie zu charakterisieren. Hierdurch konnte die aus klinischen Studien bekannte Amplifikation der Rezeptortyrosinkinase MET neben der bis dahin unbekannte Überexpression der Rezeptortyrosinkinase EPHA2 in resistenten Zellen nachgewiesen werden. Die Anwendung von weiteren zellbasierten Assays bestätigte die Rolle von EPHA2 bei der Resistenzentstehung und zeigte, dass die Kombination von EGFR und EPHA2 einen zusätzlichen Nutzen bringt. Es konnte somit auch gezeigt werden, dass chemische Proteomik für die Identifikation neuer Resistenzmechanismen geeignet ist.

Wachstumsfaktoren im Tumor können die Wirkung von Kinaseinhibitoren herabsetzen oder beseitigen. In einem komplexitätsreduzierten Modell mit Gefitinib und FGF2 wurden die Mechanismen der Wachstumsfaktor induzierten Resistenz deshalb genauer untersucht. Hierzu wurde eine Strategie zur chemischen Markierung durch Tandem Mass Tags (TMT) entwickelt, die die parallelisierte Quantifizierung von ~22.000 Phosphopeptiden und ~8.800 Proteinen in biologischen Replikaten ermöglichte. Die Auswertung des Datensatzes zeigte, dass viele Phosphorylierungsstellen durch Gefitinib inhibiert und durch FGF2 reaktiviert werden. Molekular rationalisierte Kombinationsbehandlungen mit EGFRi/MEKi oder PI3Ki/mTORi verhinderten die Wachstumsfaktor induzierte Resistenz und stellen somit eine potentielle Strategie zu einer besseren Behandlung dar.

Eine Anpassung an die Behandlung mit Kinaseinhibitoren findet innerhalb von wenigen Tagen statt und führt zum Umprogrammieren von Proteom und Signaltransduktion. Um die parallelisierte Untersuchung von Proteom und Phosphoproteom nach EGFR und FGFR Inhibition über 10 Zeitpunkte in 4 Zelllinien zu untersuchen, wurde eine Strategie mit TMT Markierung angewendet. Es zeigte sich, dass die Anpassungsmechanismen auf Proteom- und Phosphoproteomebene in den Zelllinien sehr unterschiedlich sind. Allerdings wurde in fast allen Zelllinien eine zeitabhängige Reduktion der ERK1/2 Aktivität nach EGFR Inhibition gefunden und es konnte gezeigt werden, dass die Überexpression von E-cadherin mit sichtbarer zellulärer Aggregation korreliert. Dies bestätigte, dass die TMT Markierung auch für die zeitlich aufgelöste Erforschung von Adaptionsmechanismen durch Proteomik geeignet ist.

Chapter I

General Introduction

Targeted cancer therapies

Protein kinases and signal transduction

Cells are densely packed with biomolecules including lipids, proteins and DNA. While lipids define cellular structures and DNA contains the genetic information, proteins take care and control all actions in the cell. About ~20,000 protein coding genes are annotated and recent large scale proteomics studies found evidence for 18,097 [1] and 17,294 [2] proteins, respectively. However, the complexity of the proteome is not reflected by these two numbers. Allelic variations, alternative splicing of the mRNA, endogenous proteolysis and post-translational modifications increase the number of so called proteoforms. A proteoform can be described as the number of all sources of combinations that can exist of each single protein coding gene [3]. This number of combinations consequently results in an exponential increase of protein and functional complexity in the cell. The complexity that is not reflected in the relatively fixed genome but in the proteome can lead to very different cellular functions and cellular specialization in multicellular organisms.

To achieve a certain flexibility, the communication within the cell is essential and allows the cell to adapt to different conditions and allows to perform different tasks in a multicellular organism. Intracellular communication is achieved by protein kinases, a protein family that has catalytic activity and transfers the high energy γ-phosphate group of ATP to serine, threonine or tyrosine residues of the target protein substrate. The human protein kinase family consists of 518 genes, covers approximately 1.7% of the human genome and thereby represents one of the largest but also functionally diverse gene families [4]. Based on the amino acids that are phosphorylated in the substrates, kinases can be classified into protein-serine/threonine kinases, protein-tyrosine kinases or tyrosine like proteins [4]. Protein kinases can be furthermore clustered into 7 families (TK, CMGC, CAMK, AGC, CK1, STE, TKL) and seven subfamilies, based on the sequence similarity of their catalytic kinase domains, general sequence similarity and biological functions (Fig.1A). Due to their shared functional characteristics, the structure of the protein kinase catalytic domain is largely conserved. The catalytic domain consists of ~250 amino acids and two lobes, the amino-terminal lobe (N-lobe) that contains β-strands and the larger carboxy-terminal lobe (C-lobe) that contains mostly α-helices. The catalytic loop in the C-lobe contains highly conserved residues that are required for the transfer of a phosphate group from ATP to the kinase substrate and the conserved amino acid sequence of Asp-Phe-Gly (DFG) that controls access to the active site [5-7] (Fig.1B). The N-lobe contains the glycine-rich loop which is important for the positioning of ATP and proper binding in the ATP binding pocket between the two lobes.

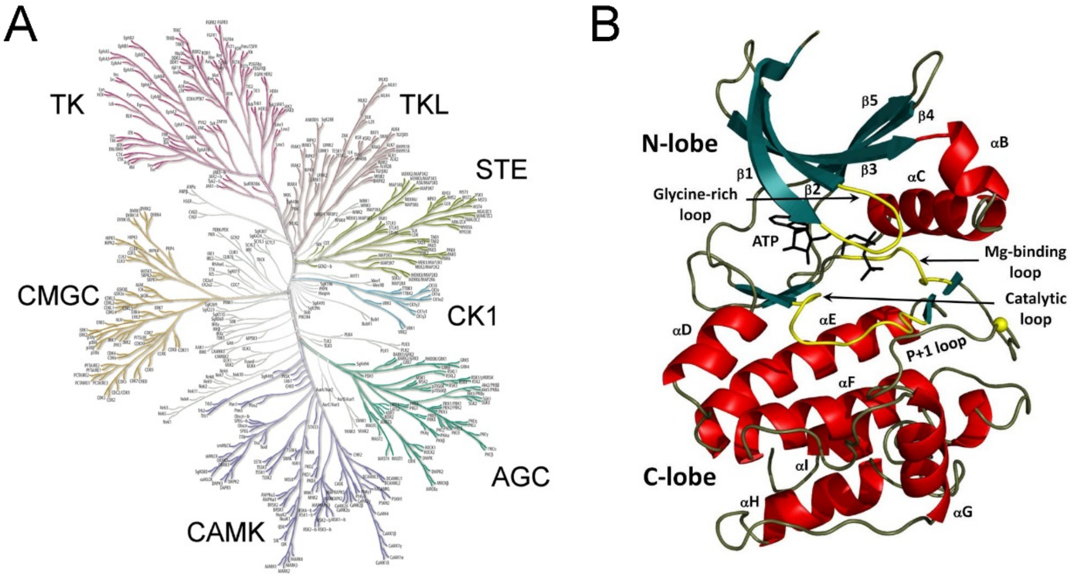

Figure 1: Phylogenetic tree of kinase families and kinase core structure. A) Similarity based relationship of 518 protein kinases in the human genome. Kinases are grouped in seven kinase families (TK, CMGC, CAMK, AGC, CK1, STE, TKL) based on their sequence similarity and biological functions (© Cell Signaling Technology). B) Protein kinase domain of PKC. Conserved kinase structure consisting of the β-strand containing N-lobe and the larger α-helical C-lobe. The C-lobe contains the catalytic and activation loop with the highly conserved DFG motif. The N-lobe contains the glycine-rich loop that positions ATP in the ATP binding pocket between N- and C-lobe (Adapted from [5]).

Protein phosphorylation can change the molecular function of a protein by regulation of domain activity or protein-protein interactions [8]. Kinases can activate other kinases by phosphorylation and thereby lead to signal transduction cascades where one kinase is activating one or several other kinases. Due to its importance in cellular signaling, phosphorylation is one of the best studied post-translational modification and has been estimated to occur on 90% of all proteins in eukaryotes [9]. Phosphorylation can be found on serine (pS), threonine (pT) and tyrosine (pY) residues in different densities. The ratio for phosphorylations on these residues was estimated in the early 80s as 92 : 8 : 0.04 (pS, pT, pY) [10] by autoradiography and was later confirmed to be in a similar range by large scale phosphoproteomics [9, 11]. According to aggregated data from different experiments that are compiled on the PhosphoSitePlus database (www.phosphosite.org) there are currently approximately 250,000 phosphosites known, underscoring the importance of this post-translational modification (PTM) in biological systems and the need for a better understanding of kinase substrate relationships and signal transduction on a systems biology level. If there are hundreds of thousands of possible kinase substrates, kinase substrate specificities are highly desirable to enable transduction of specific signals in the cell that control cell fate and certain cellular functions. The number of substrates that is known for a single kinase can vary [12], indicating that kinases have narrow and broad substrate specificities. Despite, kinases have conserved catalytic domains, they need to specifically recognize different substrates. The active site of the kinase and the structural characteristics serves as the first level to accomplish substrate specificity. Specific features of the active site, as the depth of the catalytic cleft or the charge and hydrophobicity of surrounding amino acids can determine certain substrate specificities. Tyrosine kinases for example have a deeper catalytic cleft than Ser/Thr kinases [7]. The amino acids that are in close proximity to the p-site of the substrate also contribute significantly to the substrate recognition [7, 13]. Kinases recognize phosphorylation motifs in their substrates that contain certain amino acids at distinct positions around the phosphorylation site. Apart from those amino acids, motifs in close proximity to the phosphorylation site serve as distal docking motifs. The distal docking site can be around 50-100 residues away from the desired phosphorylation site and increases the affinity of the kinase to the substrate [14, 15]. Further mechanisms that increase the substrate specificity include targeting subunits, proteins that recruit the substrates to specific kinases, or scaffold proteins that recruit the kinase and the substrate to the same complex [7].

The described specificity of kinases together with the ability of protein phosphatases to remove phosphorylation events results in a reversible biological regulation mechanism that is the basis for dynamic regulation in the cell. Especially the phosphorylation on tyrosine residues was found to be very stringently regulated by phosphatases and is just low abundant under physiologic conditions. Phosphorylation on tyrosine residues only increases in abundance in response to very specific signaling activation [9]. The regulation of cellular signaling by phosphorylation of tyrosine residues is tightly controlled and can be considered as a three component system of writer, reader and eraser. The writer is the phosphotyrosine kinase (pTK), the reader a SRC homology domain 2 (SH2) domain containing protein that binds the phosphorylated substrate and directs other proteins to the complex, and the eraser, a protein tyrosine phosphatase (PTP) that removes the phosphate residue from the substrate [16]. The generation of positive and negative feedback-loops in cellular signaling can be explained by such writer, reader eraser systems. In positive feedback loops the reader recognizes a phosphorylated kinase substrate and directs a pTK to the substrate to phosphorylate the substrate on another residue that amplifies the signal. In negative feedback loops the reader directs the eraser PTP to the substrate to remove a phosphorylated residue and thereby stops signal transduction [16]. Positive and negative feedback loops can carefully regulate signal transduction networks and are joining points to interconnect signaling events in all directions in the cell not only from the cytoplasmic membrane to the nucleus.

Small molecule kinase inhibitors for cancer therapies

Kinases are the executors of cell signaling and influence the cell fate by the control of almost every cellular function [4]. Apart from their physiological roles in a healthy individual they also control aberrant signaling in many diseases including cancer. It is therefore not surprising that kinases have emerged as one of the most intensively pursued targets for the treatment of cancer. There are essentially two major principles for the inhibition of kinases. Monoclonal antibodies bind the extracellular domain of RTKs, antagonistically block the binding of ligands and thus prevent receptor dimerization and autophosphorylation of intracellular domains [17, 18]. In contrast, small molecule kinase inhibitors bind competitively or irreversibly to the ATP binding pocket or prevent binding of ATP by allosteric mechanisms.

As described above, kinases transfer the γ-phosphate group of ATP to a substrate. The catalytic domain of all kinases is largely similar because all of them need structural characteristics that allow the binding of ATP and the transfer of the phosphate group. ATP binds into a cleft between the N-lobe and the C-lobe and most kinase inhibitors mimic ATP and bind into this cleft. Inhibitors can be divided into irreversible and reversible inhibitors. Irreversible inhibitors covalently bind to a cysteine residue in the ATP binding pocket via Michael addition and thereby make the pocket inaccessible for ATP [19]. Reversible inhibitors can be classified into four main types based on the conformation of the ATP binding pocket and the DFG motif [20, 21]. Type I inhibitors bind to the active form of kinases. The aspartate residue of the DFG motif in the activation loop is faced into the active site of the kinase (DFG-in) to enable binding to Mg^{2+} ions that coordinate ATP (Fig. 2). Type II inhibitors in contrast bind to the inactive form of the kinase with the aspartate residue of the DFG motif facing outward of the ATP kinase binding site (DFG-out). The movement of the activation loop to the DFG-out conformation exposes additional hydrophobic binding sites adjacent to the ATP binding site that enable the interaction with the inhibitor [22]. Type III inhibitors bind only to an allosteric pocket that is adjacent to the ATP pocket but do not interact with any amino acid residue in the ATP binding pocket [21]. A trend towards the discovery of more selective inhibitors resulted in molecules that target the kinases at allosteric pockets that are remote from the ATP binding site. Allosteric binding sites in kinases can be more specifically targeted than the similar ATP binding pocket. Type IV inhibitors should therefore have at least in theory a higher selectivity [23] (Fig. 2).

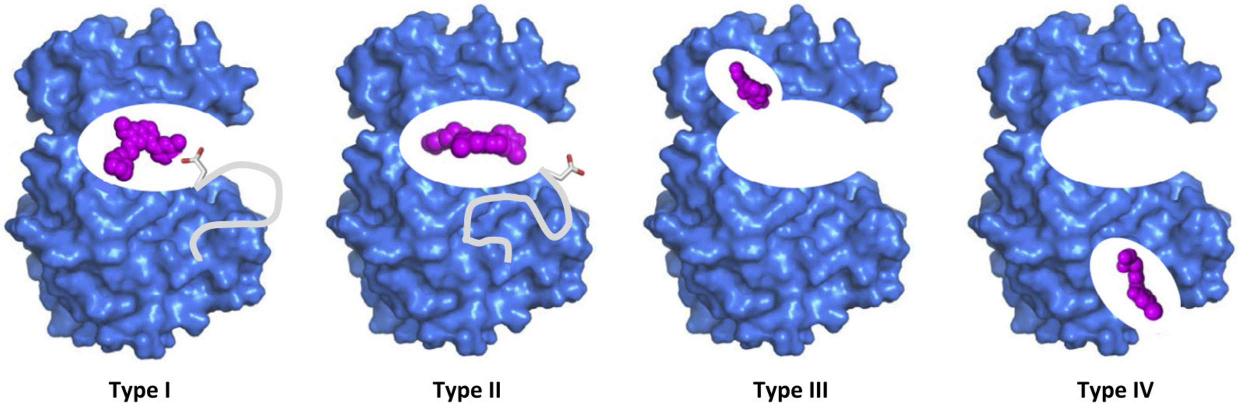

Figure 2: Classes of reversible small molecule kinase inhibitors. Class I inhibitors bind the active form of the kinase with the aspartate residue of the DFG motif pointing inside of the ATP binding pocket. Type II inhibitors bind and stabilize the inactive conformation of the kinase and the aspartate residue is facing outwards of the ATP binding pocket. Type III inhibitors bind an allosteric pocket that is adjacent to the ATP binding site and type IV inhibitors bind an allosteric pocket that is separated from the ATP binding site (Adapted from [21]).

Until 2015 there were 28 small molecule kinase inhibitors approved by the FDA and in recent years up to 6 new inhibitors were approved per year [21]. This illustrates that kinase inhibition is a clinically successful strategy and that there is a strong interest of pharmaceutical companies to develop new inhibitors to expand current applications. The epidermal growth factor receptor family (ERBB) is one of the most intensively investigated targets for small molecule kinase inhibition, which is reflected by the development of the inhibitors gefitinib (AstraZeneca), erlotinib (OSI Pharmaceuticsls), lapatinib (GlaxoSmithKline) and afatinib (Boehringer Ingelheim). Gefitinib was the first inhibitor for EGFR and is the second small molecule kinase inhibitor that was approved by the Food and Drug Administration (FDA, approval in 2003) but only one year later the EGFR inhibitor erlotinib reached the market. Both inhibitors are structurally largely similar and are used for the treatment of patients with non-small cell lung cancer [24-26]. Gefitinib and erlotinib were developed as type I inhibitors that bind the active conformation of EGFR [27, 28]. Lapatinib reached the market in 2007 and was developed for the treatment of ERBB2 overexpressing breast cancer [29]. Compared to gefitinib and erlotinib, lapatinib contains an additional fluorophenyl group that binds into an allosteric pocket. This allosteric pocket is formed after the conformational change of the DFG motif (DFG out) [30] and may explain the extremely high selectivity of lapatinib.

The most recent inhibitor approved for the epidermal growth factor receptor is afatinib, which is an irreversible kinase inhibitor. By incorporation of a Michael acceptor functionality, this inhibitor binds to a cysteine residue in the active site of EGFR which is expected to increase the selectivity and potency. Afatinib was also developed to inhibit mutated EGFR T790M which is an often observed resistance mutation to EGFR inhibitors (discussed later) [21]. The constant development of EGFR inhibitors in recent years illustrates that EGFR is a target of very high interest which may be due to two reasons. First, EGFR has oncogenic roles in various types of cancers and new inhibitors are approved for different cancer entities. Second, the constant appearance of new mutations in the EGFR receptor renders previous inhibitors ineffective and improved inhibitors are developed (e.g. afatinib). The development of new inhibitors is a continuous process to keep mutated EGFR as a druggable target.

Resistance to targeted cancer therapies

Targeted cancer therapy has become a major clinical option, reflected by the increasing number of small molecule kinase inhibitors that are clinically approved or in development stages. If molecular markers are available that can predict the clinical response of a drug, patients can undoubtedly have an improved prognosis and outcome. However, there is a major drawback of targeted cancer therapies. Patients develop resistance to anticancer agents which is accompanied with a clinical relapse. The underlying molecular processes that drive resistance are diverse but include the modification of the target that is inhibited (Fig. 3A), pathway reactivation in downstream signaling (Fig. 3B), pathway bypass activation (Fig. 3C) or the tumor microenvironment that can rescue the cells by pro-survival factors, cell to cell interactions and cell matrix interactions (Fig. 3D) [31].

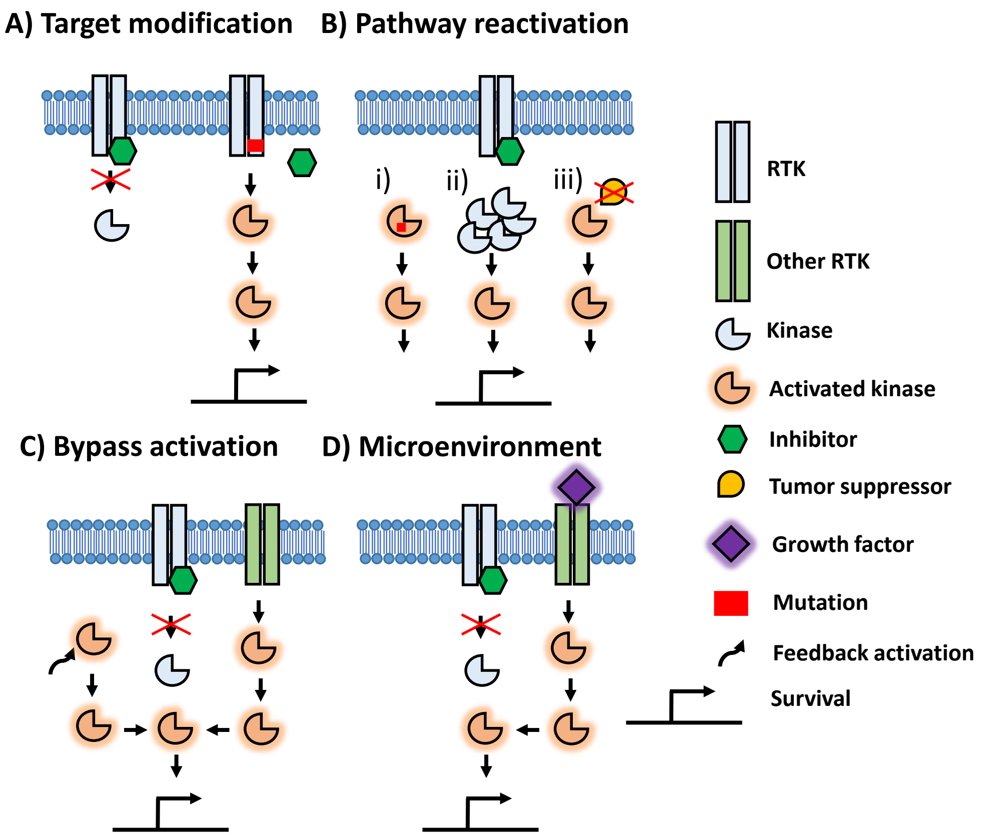
A) Target modification
B) Pathway reactivation
i)
ii)
iii)
C) Bypass activation
D) Microenvironment
RTK
Other RTK
Kinase
Activated kinase
Inhibitor
Tumor suppressor
Growth factor
Mutation
Feedback activation
Survival

Figure 3: Resistance mechanisms to targeted cancer therapies. A) Target modification of the inhibited target. Mutation based mechanisms in the ATP binding pocket decrease the affinity of the inhibitors and increase the affinity to ATP. B) Inhibition of the target facilitates downstream pathway reactivation b i) kinase activating mutations, ii) kinase overexpression in the pathway, iii) tumor suppressors are not expressed or lose their function. C) Bypass activation by overexpression of members in alternative pathways or pro-survival feedback loops that activate bypass signaling. D) Growth factors secreted by other cells or autocrine mechanisms stimulate alternative RTKs and activate bypass signaling tracks.

Target modification

Modification of the drug target is an often observed mechanism that is associated with a minimal change in the cells. Target modifications are often located in the ATP binding pocket and decrease the affinity of the inhibitor while increasing the ATP affinity. Target modification was found in BCR-ABL positive chronic myeloid leukemia patients after treatment with imatinib [32]. In this type of resistance, mutations in the phosphate binding p-loop were the most frequent [33]. MEK mutations were furthermore shown to confer resistance to MEK inhibitors [34] and FLT3 mutations can confer resistance to FLT3 inhibitors [35]. Another well described example for target modification is the gatekeeper mutation T790M in EGFR that emerges after treatment with gefitinib or erlotinib in lung cancer [36]. Mechanistic analysis revealed that the amino acid exchange does not influence the affinity to gefitinib. Instead the binding affinity of ATP is enhanced by more than an order of magnitude [37]. Gefitinib and erlotinib are competitive binders of the ATP binding pocket, a shift towards better ATP binding therefore increases the kinase activity and activates downstream signaling again. The T790M mutation accounts for 50% of acquired resistance in non-small cell lung cancer [38, 39] and therefore represents the most prominent cause of acquired resistance. The clinically observed response to EGFR kinase inhibitors lasts usually of around 10 months (median overall survival and progression free survival is 9.7 months) [24]. Considering these numbers it is apparent that genetic alterations in the target need some months to establish in the tumor and are compared to the other resistance mechanisms (discussed later) relatively slow. However, due to the large proportion of target mutation based resistance mechanisms, second generation inhibitors that covalently bind in the ATP binding pocket were developed. An example that represents this development is afatinib. As described above, afatinib is an irreversible inhibitor of EGFR, EGFR T790M, ERBB2, and ERBB4 that binds to Cys797 of EGFR, Cys805 of ERBB2, or Cys803 of ERBB4 in the ATP binding pocket [40]. Irreversible binding to ERBB family members prevents dissociation of afatinib from the ATP binding pocket and increased ATP affinity as apparent in the T790M mutation does not affect the inhibition of EGFR. As a consequence, irreversible inhibition of kinases may be more successful than competitive binding but there are still a lot of further possibilities for the cell to develop resistance.

Pathway reactivation

Reactivation of the targeted pathway represents a further mechanism for cells to become resistant. This reactivation can be mediated by upstream or downstream perturbations in the targeted pathway that recover the signaling in this axis. Essentially, there are three mechanisms known that confer this kind of pathway reactivation. Activating mutations in kinases (oncogenes), overexpression of one or more kinases in the pathway or loss of function/expression of a tumor suppressor in the pathway [31]. Activating mutations of MEK1 were found to confer resistance to inhibition of the upstream target BRAF [34], a mechanism where the signaling axis becomes independent on upstream activation. But also amplification of BRAF conferred resistance to MEK1 inhibition [41]. Breast cancers with ERBB2 amplifications are clinically treated with lapatinib or trastuzumab and the PI3K/AKT/mTOR signaling pathway is a highly important downstream signaling axis of ERBB2 [42]. In recent years, many alterations in this signaling axis were found to mediate resistance to the upstream inhibition of ERBB2. The tumor suppressor phosphatase and tensin homolog (PTEN) is a negative regulator of PI3K. Accordingly, loss of PTEN and the knockdown of PTEN in large siRNA screens results in resistance to ERBB2 inhibition [43, 44]. Oncogenic mutations of the catalytic subunit PIC3CA of PI3K represent another downstream resistance mechanism to ERBB2 inhibition [45, 46].

Bypass activation

The rationale for target based therapies is based on the observation that tumor cells are addicted on a certain oncogenic pathway. This pathway is then targeted by specific inhibitors that prevent oncogenic signaling and induce cell death. However, cells do not have one single pathway, instead they have a complex network that includes redundant signaling nodes. Inhibition of oncogenic pathways that drive the tumor cells therefore often leads to evasion of the original signaling by activation of bypass routes in the kinase network. Activation of such signaling routes is often a result of kinase amplification or feedback loops that activate bypass signaling tracks. One of the first described mechanisms of kinase amplification was the observation of hepatocyte growth factor (MET) overexpression in response to EGFR inhibition in lung cancer [47]. Later it became clear that MET overexpression is a very common mechanism of drug resistance that occurs in response to a broad range of inhibitors and in different cancer entities [48-51]. Other kinases that are amplified or activated after inhibition of members in the ERBB family by gefitinib, erlotinib or lapatinib include AXL [52, 53], IGFR1 [54], FGFR [55] or the kinase inactive ERBB3 that can serve as interaction partner of ERBB family members for transphosphorylation [56]. The mentioned examples illustrate that the inhibition of a receptor tyrosine kinase often results in very short bypass activation of other receptor tyrosine kinases at the cellular membrane. It is feasible that these RTK’s directly interact with each other and heterodimers or oligomers compensate for blocked interaction partners. Feedback activation mechanisms represent another possibility of bypass activation. Stat3 feedback activation is evident after MEK inhibition and affects cancer cells driven by diverse activated kinases, including EGFR, HER2, ALK, MET and mutant KRAS [57]. There is also a growing amount of literature that reports activation of the MAPK pathway after targeted inhibition. Inhibition of mTORC1 seems to be able to induce MAPK potentially via a feedback loop involving the S6K-PI3K-Ras pathway [58]. In another investigation, the PI3K-mTOR inhibition in ERBB2 amplified cells conferred activation of ERK, which was concomitant with ERBB2 activation [59]. Conversely, inhibition of MEK induced the activation of the PI3K pathway which was demonstrated in-vitro and in-vivo [60, 61]. A couple of further findings that indicate feedback loop activation of either the MAPK pathway by PI3K inhibition or vice versa fostered the idea that both pathways need to be inhibited at the same time [62]. Numerous further examples reported in the literature indicate that bypass signaling via kinase amplification and feedback loops is a very common principle. Hence, a deeper understanding of important signaling nodes and redundancy in signal transduction networks will be important to develop more effective combination therapies and to avoid trial and error approaches.

Tumor microenvironment

In an in-vivo situation, the tumor consists of various different cell types and a surrounding extracellular matrix. The cancer cells that proliferate constantly and uncontrolled, are surrounded by cancer associated fibroblasts (CAF) and immune inflammatory cells (IC) that can support the growth of the tumor cells by secreted growth factors. Stimulation by cell to cell contacts moreover provides a growth niche for the cancer cells. Interactions with the extracellular matrix (ECM) support the tumor cells and provide a protected microenvironment, the tumor niche. Digestion of the ECM by proteases in aggressive and metastasizing cancer cells, releases sequestered growth factors and cells from the primary tumor (Fig. 4). The importance of the tumor microenvironment is widely accepted and concepts were extensively reviewed by Hanahan and Weinberg in 2011 [63].

One of the early findings that has been described to rescue cancer cells from targeted cancer drugs is the stimulation of survival pathways by β-integrin ECM interactions. This mechanism of adhesion mediated drug resistance was found in chronic myelogenous leukemia cells after treatment with BCR-\ABL inhibitors [64], in breast cancer cells after treatment with ERBB2 inhibitor lapatinib [65] and in ovarian cancer after treatment with PI3K/mTOR inhibitors [66]. Consequently, the findings that integrin interactions with the ECM can rescue cells from a lot of specific kinase inhibitors resulted in combination treatments with antibodies against β-integrin [65]. Another principle of tumor microenvironment mediated resistance, based on the secretion of soluble growth factors and cytokines, has been investigated in many studies [67-69]. A prominent growth factor that mediates resistance to targeted inhibition is HGF. This growth factor is not secreted by the cancer cells, but tumor associated fibroblasts release this factor into the stroma [70]. Soluble HGF binds to the MET receptor in the cancer cells and can stimulate survival signaling after inhibition of EGFR, ERBB2 and RAF [48, 69, 71].

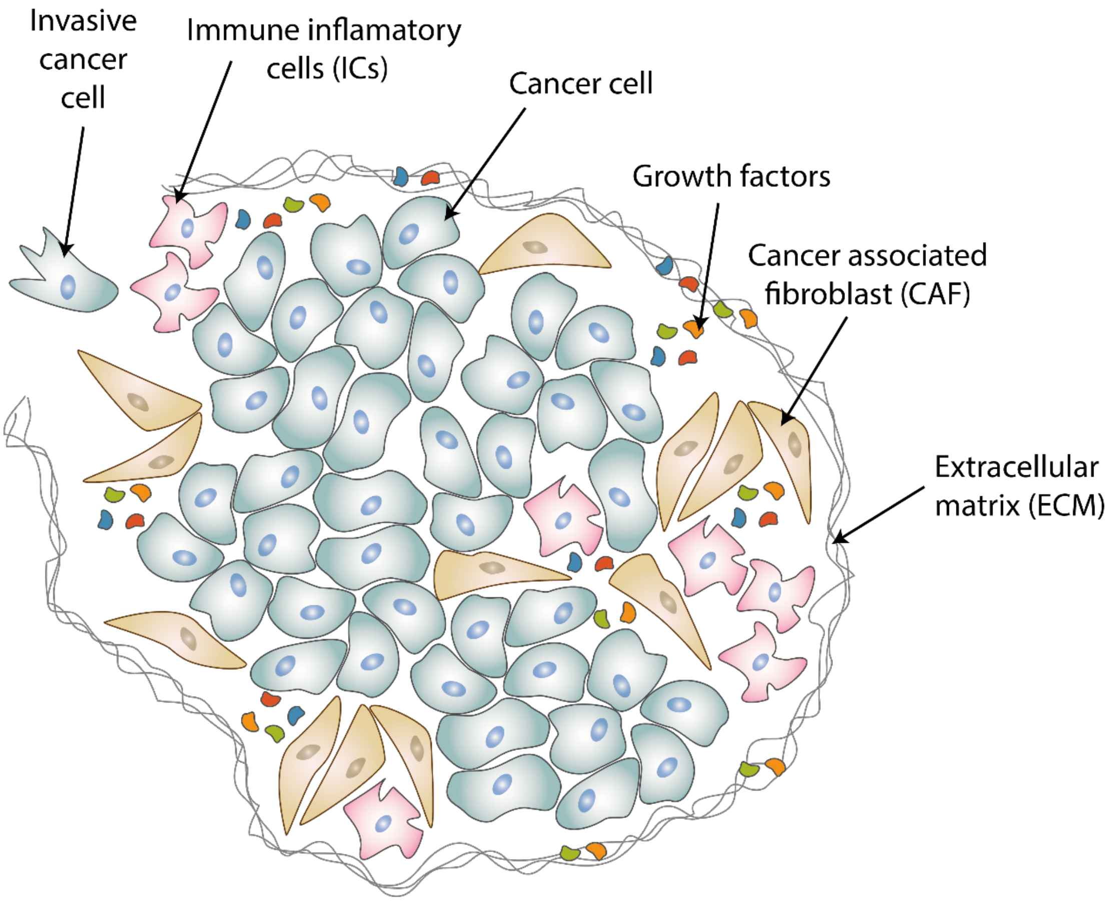
Invasive cancer cell
Immune inflamatory cells (ICs)
Cancer cell
Growth factors
Cancer associated fibroblast (CAF)
Extracellular matrix (ECM)

Figure 4: Tumor microenvironment. Cancer cells are surrounded by various other cells and components of the extracellular matrix (ECM) that provide a microenvironment were tumor cells can grow. Cancer associated fibroblasts (CAF) and immune inflammatory cells (ICs) secrete mitogens and cytokines that promote tumor growth, metastasis and resistance to specific kinase inhibitors by activation of bypass signaling. Sequestered growth factors in the extracellular matrix are released by proteases in cancer cells and invasive cancer cells can leave the primary tumor (Adapted from [63]).

Also growth factors of the FGF or IGF family can mediate drug resistance [72, 73]. To shed more light to the potential of growth factor mediated drug resistance, Wilson et al. [68] treated 41 oncogene dependent cancer cell lines from different entities with growth factors secreted by autocrine (cancer cells) and paracrine (CAFs, other cells) mechanisms. After some first experiments they selected HGF (MET receptor), FGF2 (FGFR), IGF1 (IGFR), NRG1 (HER3), PDGF (PDGFR) and EGF (EGFR) to test for their potential to rescue from selective inhibition by kinase inhibitors. Importantly, they found a very widespread potential for growth factor driven resistance. HGF, FGF2, NRG1 and EGF rescued from lapatinib, erlotinib, sunitinib and vemurafenib, ALKi and FGFRi, whereas IGF1 was just partially effective and PDGF did not affect the effectiveness of the tested inhibitors. The study illustrates the effectiveness of growth factors to activate bypass signaling and confirms that the activation of alternative RTKs is broadly relevant. Hence, a better understanding of common downstream signaling will provide the basis to understand redundant signal transduction which will improve targeted therapies.

Mass spectrometry-based proteomics

The so called "omics" technologies became a key technology in the twenty first century and enabled the investigation of biological systems on a global scale. Whereas the genomics area profited from developments in gene sequencing and sequencing analyzers, characterization of whole proteomes is so far dependent on mass spectrometry technology developments [74].

The human genome was sequenced in the very beginning of this century and resulted in the coverage of 99% of the eukaryotic genome. However, unexpectedly for the scientific community, the human genome encoded only approximately 20,000 genes [75]. The relative low number of genes was puzzling, especially when apparently less complex and less developed organisms had the same or even more coding genes [76, 77]. Consequently, one outcome of these studies was that the complexity of an organism cannot be explained by the number of coding genes. Instead, the number of proteins and protein isoforms that are expressed from a single gene as well as protein modifications determine the complexity and development status of an organism.

The qualitative and quantitative characterization of proteins, protein interactions and protein modifications that are present in a cell at a certain time point lead to the emergence of the field of proteomics [78]. In contrast to the genome, the proteome is not static and dynamically regulated and therefore better represents the status of a cell. However, genes are transcribed into mRNA which is translated into proteins that can again result in altered gene transcription resulting in dependencies of all layers of biological information. Proteomics therefore complements genomics and transcriptomics approaches and can measure the functional and executive repertoire of the cell directly. The mentioned higher complexity that is not visible on the genome and transcriptome level can only be captured by investigations on the proteome level. In this line, protein isoforms that are generated from alternative gene splicing [79], protein interactions and interaction based functions [80] as well as different post-translational modifications and their occupancies can be derived from proteomics experiments [11, 81].

Bottom-up proteomics

Three technological setups are used within the proteomics field to characterize proteomes. The top-down approach that is focused on protein purification and analysis of intact protein by mass spectrometry, middle-down approaches for the analysis of large polypeptides and bottom-up proteomics where the whole proteome is digested into smaller peptides before analysis [79, 82-

84]. Of all mentioned approaches, bottom-up (or shotgun) proteomics represents the most widely used technique as it is comparably less time consuming and more comprehensive when applied to large scale investigations of proteomes.

The bottom-up proteomic workflow includes multiple steps that need to take place before analysis by mass spectrometry. These steps are depicted in figure 5. First proteins are extracted from cells or tissues by cell lysis. If needed, a sub protein fraction of proteins can be enriched by affinity enrichment techniques (e.g. chemical proteomics (Kinobeads), immunoprecipitations) for subsequent digestion. Alternatively all proteins are digested directly by sequence specific proteases like trypsin. Trypsin cleaves very specifically at the C-terminus of lysine and arginine [85] and thereby generates peptides that are well ionized and analyzed by current mass spectrometers. However, due to naturally high abundance of lysine and arginine sites, peptides are often too short (56% of all generated peptides are ≤6 residues) and contain no protein specific information [86]. Further proteases or protease combinations (e.g. Lys-C, Asp-N, Lys-N, Glu-C, Chymotrypsin) were used to improve protein identifications and the sequence coverage of proteins [87-90]. The analytic capabilities of a mass spectrometer are still too low to handle the complexity of peptide digests, but peptides can be fractionated by chromatography to enhance the number of identifications. Specific peptides can be enriched from crude peptide digests based on physicochemical characteristics (e.g. phosphopeptide enrichment). All following methodologies depicted in the bottom-up workflow are now described in more detail with a special emphasis on the methodologies used for the work in this thesis.

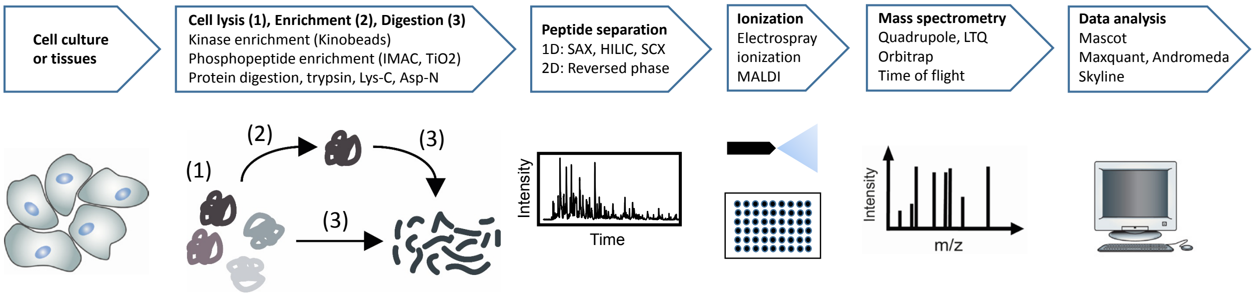
Cell culture or tissues
Cell lysis (1), Enrichment (2), Digestion (3)
Kinase enrichment (Kinobeads)
Phosphopeptide enrichment (IMAC, TiO2)
Protein digestion, trypsin, Lys-C, Asp-N
Peptide separation
1D: SAX, HILIC, SCX
2D: Reversed phase
Ionization
Electrospray ionization
MALDI
Mass spectrometry
Quadrupole, LTQ
Orbitrap
Time of flight
Data analysis
Mascot
Maxquant, Andromeda
Skyline
(1)
(2)
(3)
(3)
Intensity
Time
Intensity
m/z

Figure 5: Bottom-up proteomics workflow for deep proteome analysis (Adapted from [91]).

Chromatographic peptide separation

The bottom-up workflow generates a tremendous analytical challenge. From all of the proteins that are present in cells or body fluids the protein digestion creates an even higher complexity. Mass spectrometers have a limited acquisition speed and dynamic range which results in the requirement of peptide separation by chromatography. Efficient separation reduces the number of ions that enter the mass spectrometer in a certain timespan (lower complexity) and thereby allows a more comprehensive identification of peptides from a proteomic digest. The chromatographic principle is based on three types of interactions. The interaction of the stationary phase and the peptide, the peptide and mobile phase interactions as well as the interactions of the stationary phase with the mobile phase. All the three interactions influence the retention time of a peptide in the column and discriminates the elution time of peptides with different physicochemical characteristics. The mobile phase serves as the variable component in a chromatography system. Gradient flows start with a mobile phase that has weak interactions with the stationary phase and turn to increasing concentrations of a strong interacting solvent. The peptide is eluted from the stationary phase as soon as the mobile to stationary phase interaction equals the peptide to stationary phase interaction. Accordingly, a complex peptide mixture elutes sequentially from the column dependent on interactions to the stationary phase.

The columns used in proteomics for LC-MS/MS measurements are usually packed columns with reversed phase C18 (RP) silica beads (1-5 µm) that separate peptides based on hydrophobicity [92]. The C18 material consists of a hydrophobic side chain of 18 carbon atoms that can interact with hydrophobic sidechains of amino acids. An added amphiphilic acid (usually FA or TFA) additionally increases charged residue interactions between the peptide and the stationary phase. A LC-solvent gradient from low to high hydrophobicity (addition of acetonitrile) is applied to elute peptides from the stationary phase. In proteomics, a high resolution and peak capacity is desired to increase peptide identifications. Practically, this is achieved by long columns and small particle diameters, which results in high pressure (HPLC) and ultra-high pressure (UHPLC) chromatography systems [93, 94].

If a more comprehensive analysis to a depth of 10,000 proteins or more is desired, one chromatographic dimension is not sufficient. A second chromatographic dimension can be added by using an orthogonal chromatographic material. In the last years online and offline approaches were developed to increase peak capacity and analytical depth in proteomic experiments [95-98]. Even if online workflows can be very reproducible, they are often restricted to specific applications and require more technical expertise. Offline workflows are technically independent from each other and are therefore easier to perform and more generally used in a lot of laboratories. Widely applied chromatography materials that are used in a first dimension before reversed phase (RP) separation include anion- and cation exchangers (SAX, SCX) [95, 99, 100] or hydrophilic interaction liquid chromatography (HILIC) [101]. Alternatively, due to the high resolution, it became recently popular to use high- and low pH reversed-phase chromatography as a two dimensional system. High- and low pH reversed-phase chromatography is only partially orthogonal. This makes the pooling of fractions after separation in the first dimension (usually high pH) necessary. Samples are most often pooled in a concatenated way before separation in the second dimension is performed [96, 102]. By such pooling techniques full orthogonality is finally achieved. The second dimension of liquid chromatography is usually directly coupled to a mass spectrometer and peptides get ionized by electrospray ionization (ESI). Alternatively fractionated peptides are spotted on a target plate for ionization by matrix assisted laser desorption ionization (MALDI).

Protein and peptide affinity enrichment

Even though it is nowadays possible to analyze whole proteomes by applying intensive fractionation, it is sometimes desired or more informative to enrich a target class and interactors in advance to LC-MS/MS analysis. For this purpose proteins can be enriched with specific antibodies (immuno-affinity enrichments), where the antibodies are immobilized to sepharose, agarose or magnetic beads. Immuno-affinity enrichments are usually performed to identify binding partners of a bait protein of interest and to determine quantities and stoichiometries of protein complexes [103, 104]. This principle was applied in large scale studies very recently to investigate the whole interactome of cells [80, 105].

Kinases control cellular processes by active regulation of signal transduction. A change in kinase activity and abundance can cause different cellular behaviors and is often responsible for human diseases. Although it is important to understand functional relationships between kinases and disease phenotypes, mass spectrometry-based quantification of low abundant kinases from crude proteome digests requires intensive measurement time. Alternatively, kinases can be specifically enriched in advance to mass spectrometry analysis. It has been demonstrated that kinase enrichment with immobilized small-molecule kinase inhibitors can be very powerful [106, 107]. In these approaches, specific kinase inhibitors or broad spectrum kinase inhibitors are covalently attached to sepharose beads for immobilization. Immobilized kinase inhibitors are in the following incubated with cell lysates and bind kinases in their ATP binding pocket. Afterwards kinases are purified and eluted from the beads for quantification. This affinity based enrichment of kinases from crude cell lysates and the subsequent analysis by LC-MS/MS is termed chemical proteomics and allows identification of up to 260 kinases in a single experiment when unselective broad spectrum kinase inhibitors are used [107]. Chemical proteomics is not restricted to enrichment of kinases and can be used to enrich other specific binders of small-molecules including histone deacetylases (HDAC) [108], ATP/ADP binding proteins [109], cAMP, cGMP binders [110] or binders of tankyrases [111]. The simple enrichment of specific binding proteins by chemical probes is just one possibility, but this technology also enables the selectivity profiling of drugs. For this purpose, desired drugs can be added to cells or cell lysates before incubation with the immobilized inhibitor matrix is performed. The drugs thereby compete with the interactions of immobilized inhibitors on the drug matrix. If the drugs are added in an increasing concentration and occupy the target, they prevent the binding of the target to the immobilized small molecule matrix. Enrichment of drug targets thereby decreases with increasing drug concentrations. Decreased enrichment results in decreased intensity in the mass spectrometry readout and a sigmoidal dose response characteristic. This principle has been applied to kinase inhibitor selectivity screenings and offers determination of drug affinities to their targets under physiological conditions [106, 112].

In proteomics, affinity enrichments are also regularly applied to enrich peptides that contain low abundant and often substoichiometric post-translational modifications. The antibody can thereby specifically bind phosphorylated (most often phosphotyrosine), methyl-arginine, acetyl-lysine or ubiquitinated (diglycyl-lysine affinity) peptides to enrich them from a highly complex peptide sample [113, 114]. By applying this enrichment, high abundant peptides are removed from the modified low abundant peptides and dynamic range of the sample is decreased. Increasing speed and effective affinity enrichments of post-translational modifications (PTMs) facilitated large scale investigations and, enabled a holistic view into signal transduction pathways and improved our understanding of the function of protein modifications [115, 116]. Investigations on protein phosphorylation are often exceptionally interesting as they reflect protein activity. Kinases can activate themselves by autophosphorylation and activate other kinases by phosphorylation, leading to signal transduction cascades and signaling networks in the cell. It is therefore not surprising that phosphorylation is the most extensively studied PTM. Apart from the biologically interesting function it became very easy to identify this kind of modification because of developments in affinity enrichment techniques. Especially metal ion and metal oxide chromatography are the method of choice to enrich phosphorylated peptides in a large scale [9, 90, 117]. Immobilized metal affinity chromatography (IMAC) is based on chelating agents, usually nitrilotriacetic acid (NTA) or iminodiacetic acid (IDA), that are immobilized on a polymer matrix. Chelating agents can than coordinatively bind to the free orbitals of metal ions, usually Fe^{3+}, that then binds the negatively charged phosphate group. Specificity of phosphorylated peptide binding is usually achieved at a low pH where carboxyl side chains are protonated and cannot bind to metal ions. However, unspecific binding of glutamic acid and aspartic acid residues cannot be completely prevented and is usually responsible for co-enrichment of unphosphorylated peptides [118]. Metal oxide affinity chromatography (MOAC) is a widely applied alternative to IMAC and is reported to be very selective and orthogonal to IMAC enrichment [119, 120]. This orthogonality was recently called into question and could be largely explained by insufficient capacity, inefficient elution, and the stochastic nature of data-dependent acquisition in mass spectrometry [121]. All three described methods enrich phosphopeptides according to their natural abundances in the cells. Serine and threonine sites account together for more than 98% of all phosphorylation sites [9]. Hence, the enrichment of phosphorylated peptides with IMAC or MOAC is very well suited for analysis of serine and threonine phosphorylation, the phosphotyrosine phosphorylation is underrepresented. However, phosphotyrosine containing peptides can be specifically enriched with phosphotyrosine specific antibodies as mentioned above.

Mass spectrometry

Mass spectrometers use the characteristics of charged particles that are accelerated in electric fields. The result of this analysis is a mass spectrum that represents the abundance and mass to charge ratios (m/z). The abundance of atoms and molecules within a sample can be derived from the area under the curve of each m/z. Mass spectrometry enables the determination of the m/z ratio of peptides and peptide fragments that can be used to identify and quantify proteins in a large scale. A mass spectrometer consists of an ionization source to transfer analytes into the gas phase, a mass analyzer that separates ions based on m/z and a detector that detects the current of moving charges in an electric field.

Electrospray ionization

A mass spectrometer can only identify charged particles and their mass to charge ratio (m/z). Hence, the first step for peptide analysis by mass spectrometry is the ionization process and the transfer into the gas phase. Electrospray ionization (ESI) is today the most widely used technique for the ionization of biomolecules and in proteomics [122]. The technique was introduced in the late 80s, was shown to be very effective and did not destroy the analytes during ionization. It is therefore known as a soft ionization technique [123, 124]. Beside the soft and protective ionization, ESI can be coupled online to any case of liquid chromatography. This combination renders this technology to be an extremely effective and a high performing ionization technique for large scale proteomics experiments.

The solved analytes are transferred in nanoliter flow rates through a small stainless steel capillary needle where a high voltage of several kilovolts is applied. The voltage applied to the needle tip, charges emerging liquid at the spray needle (Fig. 6A). The liquid leaves the needle and anions and cations get separated by the applied electric field, leading to a tailor cone. When a certain threshold is reached and the electrostatic field becomes stronger than the surface tension, the tailor cone is transformed into a thin jet stream. With increasing distance to the spray needle, small droplets appear from the jet stream and generate a fine spray (Fig. 6A). Evaporation of the liquid from those droplets enhances the charge density until the coulomb repulsion becomes stronger than the surface tension and the Rayleigh limit is reached. Coulomb explosion than leads to the formation of several smaller droplets from a big one. This process is repeated until only the analyte remains in a small droplet which is released as a charged ion after evaporation (charge residue model, CRM, Fig. 6B) [122, 125]. Another model describes the generation of ions as the result of evaporation and shrinking droplets. When droplets shrink, the field strength increases as a consequence of charge density and single ions are ejected from the droplets (ion evaporation model, IEM, Fig. 6B) [126, 127].

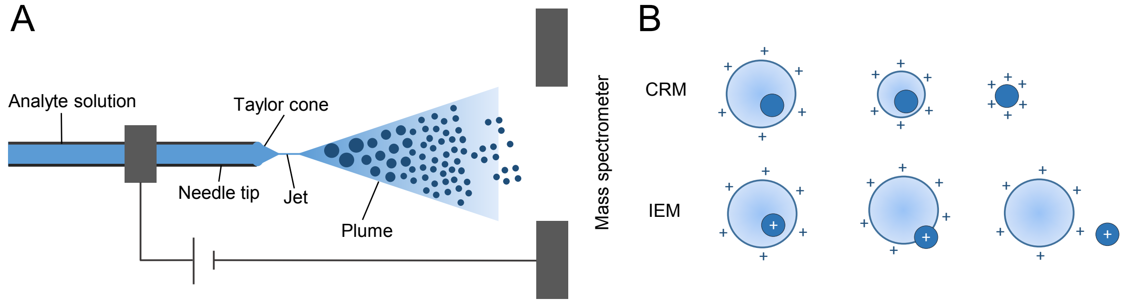

Figure 6: Electrospray ionization principle. (A) Analyte solution is transferred through a spray needle. Formation of a tailor cone by electrophoretic charge separation, jet stream induction when the electrostatic field is stronger than the surface tension and generation of droplets. (B) Models for the generation of ions from droplets. Charged residue model (CRM) and ion evaporation model (IEM).

Electrospray ionization preferentially produces multiply charged ions. This is an advantage as mass analyzers have often a restricted m/z range and a high charge reduces the m/z, which enables the identification of large peptides and even intact proteins in a narrow m/z range [123].

Moreover, effectiveness of the electrospray ionization increases with decreasing flow volumes which matches very well to nano-LC separations. Miniaturization of the electrospray ion source and low flow rates increase the generation of small droplets and more analyte molecules are successfully ionized [128]. It was recently shown that the addition of low percentages of DMSO to liquid chromatography solvents can reduce the surface tension of droplets, leading to smaller droplets and increased ionization and sensitivity [129].

Mass analyzers

After ionization, analytes enter the mass spectrometer and are separated in the mass analyzers according to their m/z. Different mass analyzers have been developed and are used in commercially available mass spectrometers. Mass analyzers have various characteristics regarding to their mass accuracy (ability to measure the true mass of an analyte), mass resolution (ability to separate very similar masses as two distinct different masses), m/z range (the m/z range they can record in a mass spectrum), sensitivity (lowest amount of molecules that can be detected) and dynamic range (difference between lowest and highest abundant ions that can be detected). Characteristics of often used mass analyzers are summarized in table 1.

Table 1: Characteristics of mass analyzers. Adapted from [130, 131].

	TOF	Quadrupole	LTQ / ion trap	FTICR	Orbitrap
Mass accuracy	<2ppm	>500 ppm	100–500 ppm	<2 ppm	<5ppm
Mass resolution	>20,000	1000	2000	>750,000	>100,000
m/z range	>50,000	200–4000	200–4000	200–4000	200–4000
Sensitivity	femtomole	picomole	femtomole	femtomole	femtomole
Dynamic range	10^4	10^3	10^4	10^3	4*10^3

Time of flight (TOF) mass analyzers record the time that ions with a certain m/z value need to travel from a source to the detector in a flight tube. Ions leaving the ion source do not have the same starting times and kinetic energies. As a consequence they reach the flight tube not all at the same time, resulting in decreased resolution. To compensate for this differences TOFs are often equipped with a reflectron that compensate for different kinetic energies at the same m/z and improve resolution [132].

Quadrupole analyzers consists out of four rod electrodes and an inner axial space for ion transmission. Application of an RF voltage to the two opposing rods generates the electric field of the quadrupole and enables oscillation based trajectories of ions with a certain m/z along the inner axis. Ions can either get lost during this transmission, collide with the electrodes or are successfully transmitted if the RF fits to their m/z. Quadrupoles are therefore also termed mass filters and can select single m/z.

Ion traps (linear ion traps) store ions in an electric field that is similar to a quadrupole. Ions are then kept on stable trajectories in this electric field for a certain duration of time. The changing of applied voltages induces m/z dependent ejections of ions to the surrounding detector [133, 134].

Orbitraps are a special case of ion traps. They have a spindle shaped central electrode and two symmetrical outer electrodes that complement the shape of the central electrode. Ion packages are injected from an external storing device (C-trap) and enter the orbitrap tangential to the axis of the central electrode. Application of a voltage to the electrodes pushes injected ions on a radial orbit between the outer and inner electrode, tangential injection leads to circular movement and axial movement is induced by the shape of the electrodes (Fig. 7).

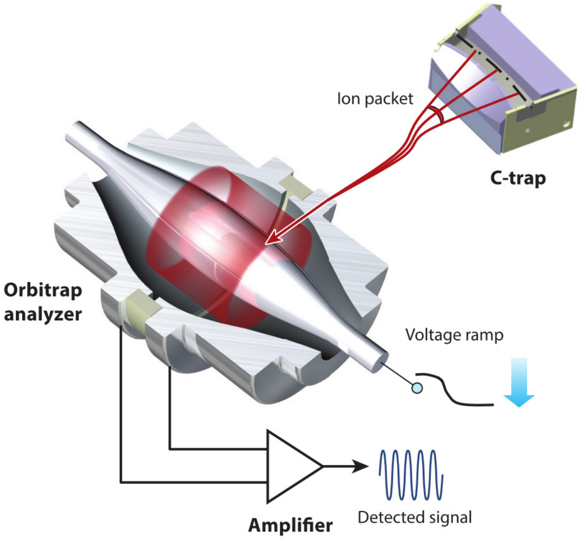

Figure 7: Orbitrap mass analyzer and C-trap ion accumulation device. Ions are injected from an external trapping device (C-trap) and oscillate around the inner spindle electrode. Frequencies of oscillating ions are detected as image current and transferred to m/z values by Fourier transform (Adapted from [74]).

Only the axial oscillations of ions are independent on initial injection velocity or injection angle and can be used for m/z analysis. Consequently, the frequencies of axial ion movement along the central electrode induce an image current that can be recorded. Fourier transform of the detected and amplified signal then translates to the m/z value of trapped ions [74, 135, 136].

Hybrid mass spectrometers

The large-scale analysis of proteomes is performed on hybrid mass spectrometers. Hybrid mass spectrometers consist of two or more mass analyzers and thereby combine the strengths of these analyzers to improve resolution, sequencing speed and sensitivity. Furthermore, selected ions need to be accumulated in storing devices (linear ion traps, LTQ) or selected (quadrupoles) to allow fragmentation of single peptides into peptide fragments (tandem-mass spectrometry). There are some advances in hybrid quadrupole time-of-flight (QTOF) instruments [131], but hybrid technologies using an orbitrap as the high accuracy and resolution mass analyzer became the backbone of many proteomics laboratories. The developments of orbitrap hybrid instruments for proteomics are therefore described in the following in more detail.

The combination of a high resolution orbitrap combined with the sensitivity of a linear ion trap mass analyzer was introduced in 2005 in the commercially available instrument Orbitrap XL [137] (Fig. 8A). This instrument allowed the high accuracy readout of MS1 spectra in the orbitrap which enabled the search of intact peptide m/z in a narrow parts-per-million (ppm) range in databases and therefore reduced false positive peptide identifications [138]. The hybrid design furthermore enabled the parallel acquisition of precursor m/z in the orbitrap while precursors were selected and fragmented. This principle termed as tandem mass spectrometry is described in the next section. By parallel acquisition of m/z information from peptide precursors and peptide fragments, peptide identifications could be acquired in a reasonable timescale. In the following years improvements in the design of the LTQ (dual-pressure ion trap) [139] and the Orbitrap (high field orbitrap) [140] improved the acquisition speed and resolution at a fixed acquisition time. The implementation of beam type fragmentation (HCD) enabled high resolution acquisition of MS1 and MS2 in the orbitrap and provided an alternative for a better localization of PTM's in post-translationally modified peptides [141]. HCD fragmentation was developed to perform acquisition of MS2 spectra in the orbitrap. However, the speed of hybrid mass spectrometers was only high if acquisition was performed for MS1 in the orbitrap and for MS2 in the ion-trap. To fill the need of the community to perform both readouts at high resolution without too much loss in sequencing speed, the hybrid mass spectrometer was modified. The hybrid design of a mass storage (LTQ) plus orbitrap was changed to a mass filter (quadrupole) plus orbitrap, commercially available as the Q Exactive [142](Fig. 8B).

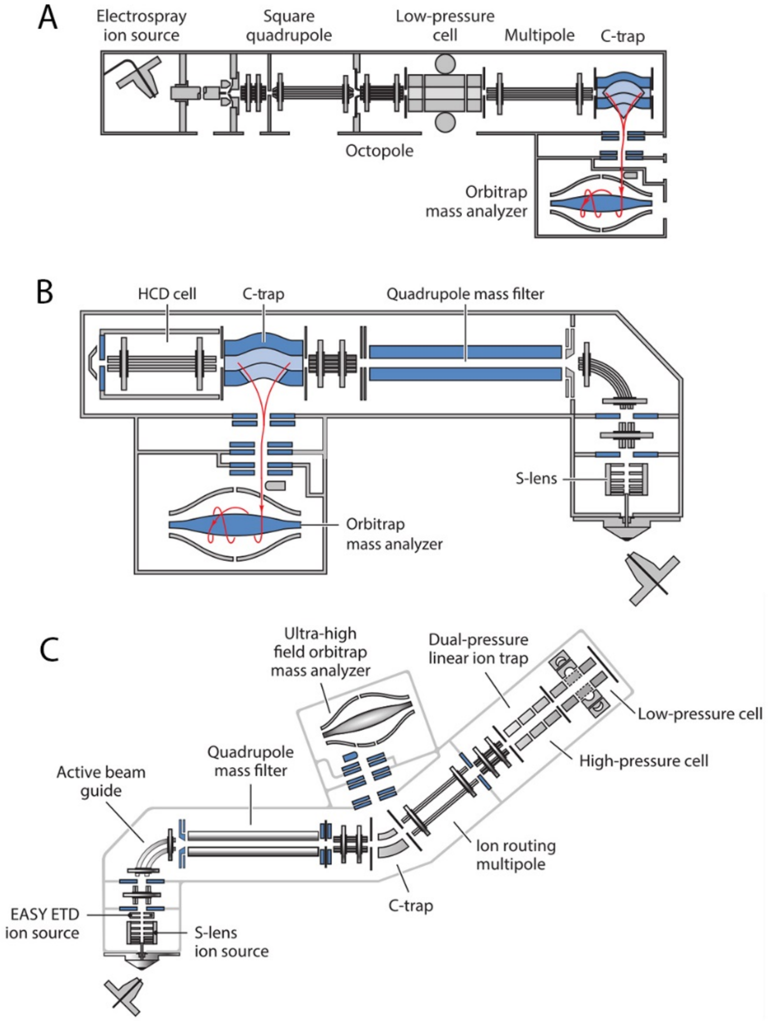
A
Electrospray ion source
Square quadrupole
Low-pressure cell
Multipole
C-trap
Octopole
Orbitrap mass analyzer
B
HCD cell
C-trap
Quadrupole mass filter
S-lens
Orbitrap mass analyzer
C
Ultra-high field orbitrap mass analyzer
Dual-pressure linear ion trap
Low-pressure cell
High-pressure cell
Quadrupole mass filter
Active beam guide
Ion routing multipole
C-trap
EASY ETD ion source
S-lens ion source

Figure 8: Schematic representation of the evolution of hybrid orbitrap devices. A) First commercially available hybrid orbitrap mass spectrometer, the Orbitrap XL. Combination of a linear ion trap and the orbitrap combines high sensitivity and mass accuracy. B) The Q Exactive, a mass filter (quadrupole) orbitrap hybrid instrument to combine speed and accuracy. C) The orbitrap Fusion, a hybrid mass spectrometer consisting of a quadrupole, orbitrap and ion trap mass analyzer (Adapted from [74]).

The filtering of ions in a quadrupole instead of accumulation in an LTQ thereby allowed faster acquisition speeds. Hybrid mass spectrometers of the Q-Exactive type achieve high acquisition speeds but they cannot collect ions and are therefore less sensitive than ion trap orbitrap hybrid mass spectrometers. To have an instrument that fuels the need for high flexibility at the side of fragmentation and that can provide detection in the orbitrap and the ion trap while achieving a high acquisition speed, the orbitrap Fusion was developed (Fig. 8C) [143]. The Fusion combines the LTQ, a quadrupole and the orbitrap from previous mass spectrometer generations. The experimental possibilities are therefore expanded when compared to previous hybrid mass spectrometers.

Tandem mass spectrometry

Before peptides can be identified from complex protein digests, the intact mass and peptide fragment masses need to be determined. Mass spectrometers therefore need to analyze the intact peptide m/z (precursor), select this peptide for fragmentation and measure the peptide mass of generated peptide fragments. This principle of time domain separated m/z measurement of precursor masses in a first spectrum (MS1) and fragment masses in the following spectra (MS2) is termed tandem mass spectrometry. Tandem mass spectrometry can be performed as “tandem in time”, when mass analysis and fragmentation are recorded in the same mass analyzer in a consecutive manner or as “tandem in space” when analysis of tandem mass spectra is performed in different mass analyzers in parallel [144]. The recording of tandem mass spectra from selected precursor ions requires time and not all of the precursor ions can be selected to record a tandem mass spectrum. Hence, acquisition of tandem mass spectra is data dependent and only precursors with a high intensity are selected for fragmentation. In data dependent acquisition (DDA) experiments the maximal number of tandem mass spectra that are generated of an MS1 spectrum can be defined but only a certain number is reasonable at a given speed of the mass spectrometer. The shortcomings of DDA experiments are the incomplete identification of eluting features, the stochastic nature of precursor selection and the resulting lack of reproducibility in peptide identifications [145-147].

Peptide fragmentation

Tandem mass spectrometry is the basis to gain information of the composition of a peptide. To record fragment spectra of precursors, different fragmentation principles were developed and can be applied or combined to achieve a good characterization of the sample. The most often used fragmentation techniques include collision induced dissociation (CID) [148], higher energy C-trap dissociation (HCD) [141] and electron transfer dissociation (ETD) [149]. Common to all fragmentation techniques is the generation of different peptide fragments by bond breakage along the peptide backbone. According to the nomenclature of Roepstorff and Fohlman [150] peptides containing an intact N-terminus are termed a-, b- and c-ions and peptides containing an intact C-terminus are termed x-, y- and z-ions. The bond breakage between carbonyl residue and C_α-atom is designated as a- or x-ion, in the peptide bond as b or y ion and between amino group and C_α-atom as c- or z-ion (Fig. 9). The two fragmentation techniques CID and HCD are conceptually relatively similar. The peptides acquire vibrational energy by collision with inert gas molecules (He, Ar, N_2), which leads to breakage of the chemical bond. CID and HCD preferentially generate b- and y-ions and therefore generate sequence informative MS/MS spectra with the characteristic mass difference of one amino acid (Fig. 9). One difference between CID and HCD fragmentation is the energy that is applied to induce the bond breakage. The lower energy CID is performed in ion traps (trap-type CID). Application of radio frequencies (RF) accelerates ions and their kinetic energy while multiple collisions with gas molecules induce the fragmentation at the weakest bonds. Readout of MS/MS spectra after CID is usually very fast as fragments can be directly analyzed in the ion trap, but inefficient trapping of ions at al low m/z is a common drawback of trap-type CID [151].

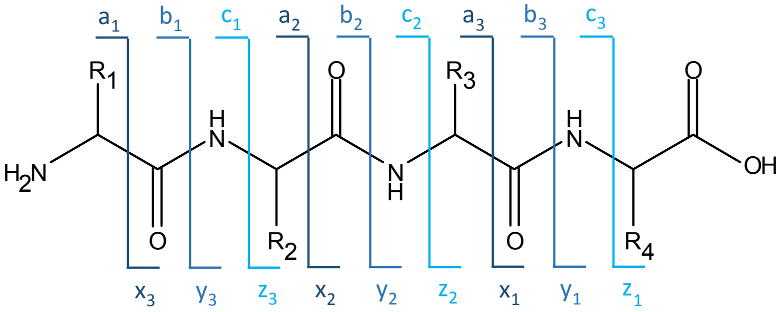

Figure 9: Fragmentation of peptides according to the nomenclature of Roepstorff and Fohlman [150]. Peptides generate a-, b- and c-ions, if the N-terminal residue remains at the fragment and x-, y-, and z-ions, if the C-terminal residue remains at the fragment. The mass difference between two of the same ions corresponds to the residue mass of the amino acid.

HCD fragmentation, also known as beam type fragmentation, applies high energies to the precursor ions, leading to an almost instantaneous breakage of the chemical bonds. Fragmentation is performed in a dedicated collision cell allowing acquisition of high resolution spectra in the orbitrap mass analyzer. HCD does not suffer from a low molecular weight cutoff which enables the identification of informative reporter ions [152] or isobaric tags for quantification [153].

Electron transfer dissociation (ETD) is different to CID type fragmentations and uses an electron donor for induction of fragmentation. The anionic electron donor (e.g. anthracene or fluoranthene) transfers an electron to the analyte leading to an instable transition state that ends up in rapid bond breakage and charge reduction. Fragmentation along the peptide backbone occurs preferentially between the Cα and amino bond and generates c- and z-ions [154]. The mechanism of ETD better preserves post translational modifications that are cleaved in CID and HCD before backbone fragmentation occurs [155]. However, ETD spectra often lack sufficient backbone fragmentation as consequence of charge reduction. The introduction of EThcD, a combination of ETD and HCD fragmentation combines beneficial information of both technologies resulting in better sequence identification and PTM site localization [156].

Protein identification by mass spectrometry

The generation of tandem mass spectra enables the identification of proteins from sequence databases. These approaches are very common, however it is important to mention that they cannot de-novo identify proteins, only a protein which sequence is in the database can be identified. This approach is consequently also known as database searching and was comprehensively reviewed by Nesvizhskii et al. [157]. Different search algorithms as Mascot [158] or Andromeda [159] were developed and work on the same principle.

First, peptide spectra and MS/MS spectra are derived from high resolution mass spectrometry. Experimental spectra are then correlated to theoretical spectra that are generated from an in-silico digest of all proteins in the sequence database (e.g. all protein entries from the human genome) (Fig. 10A). A search algorithm can consider protease specificity, missed cleavage sites, fixed modifications or variable modifications of PTMs to assign as many peaks as possible. It also takes different metrics like the length of consecutive ion series, overlap of the ion series, number of matching precursor and peptide fragments and their mass deviations into account. Based on these metrics peptide matches are scored and ranked according to this score in a list and the peptide is assigned to the best match. Often also an expectation value is calculated that reflects the probability that a peptide is matched to a wrong spectrum (Fig. 10A). Identified peptides in the database search can be assigned to proteins and thereby result in protein identifications, which is not a trivial task. Peptides often match to more than one protein, especially if the sequence is not long and hence not protein specific. This protein inference problem [160] is often the reason that only the identification of protein groups can be reported, where peptides are unique to a group of proteins that are sequentially conserved.

False peptide assignments are a common shortcoming of database search algorithms and occur from chimeric spectra (selection and co-fragmentation of two peptides), low signal spectra and assignments to signal noise, incorrect charge state determination or sequence variants that are not present in the sequence database [157]. As the data generated in proteomics experiments are too large to check spectra quality manually, essentially two techniques were developed to control for the number of false positive assignments (Fig. 10A). One is the target decoy approach where the database contains the real existing protein sequences in the target space and reversed or scrambled sequences in the decoy space. Peptide sequences that match to the decoy space are per definition false positive matches because this sequence is randomly generated.

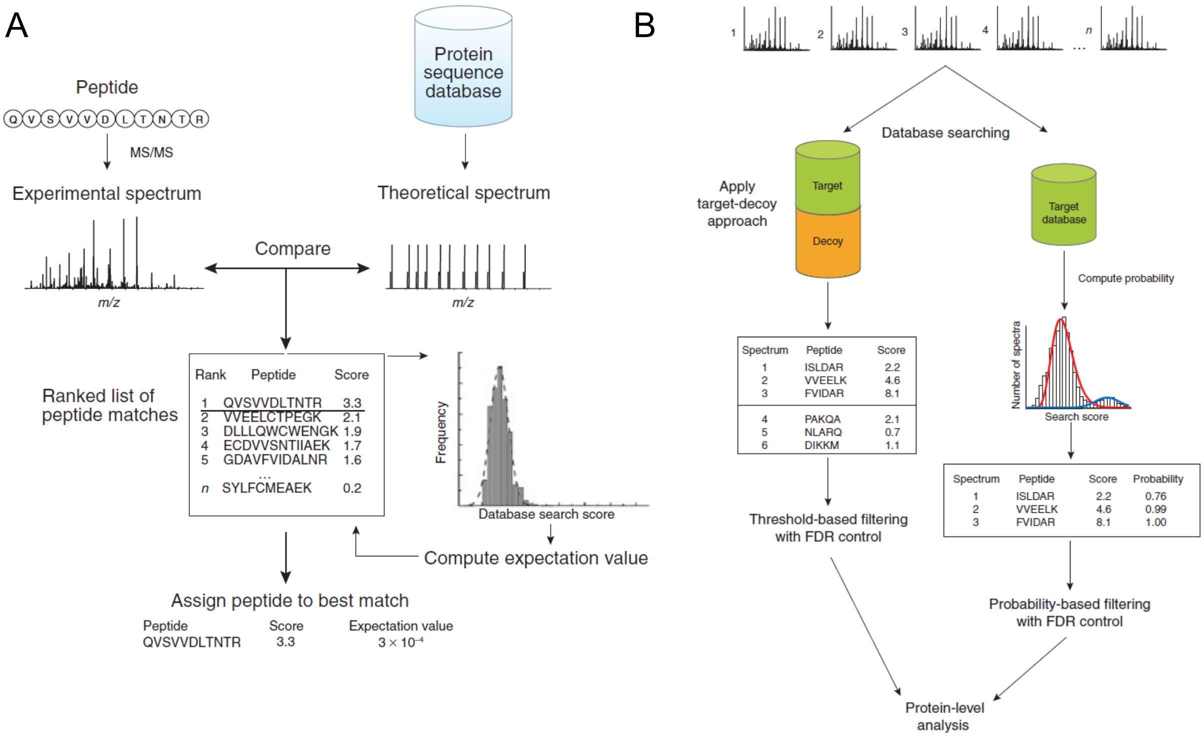
A
Peptide
Q V S V V D L T N T R
MS/MS
Experimental spectrum
m/z
Protein sequence database
Theoretical spectrum
m/z
Compare
Ranked list of peptide matches
Rank Peptide Score
1 QVSVVDLTNTR 3.3
2 VVEELCTPEGK 2.1
3 DLLLQWCWENGK 1.9
4 ECDVVSNTIIAEK 1.7
5 GDAVFVIDALNR 1.6
...
n SYLFCMEAEK 0.2
Frequency
Database search score
Compute expectation value
Assign peptide to best match
Peptide QVSVVDLTNTR
Score 3.3
Expectation value 3 × 10⁻⁴
B
1 2 3 4 ... n
Database searching
Apply target-decoy approach
Target
Decoy
Target database
Compute probability
Number of spectra
Search score
Spectrum Peptide Score
1 ISLDAR 2.2
2 VVEELK 4.6
3 FVIDAR 8.1
4 PAKQA 2.1
5 NLARQ 0.7
6 DIKKM 1.1
Spectrum Peptide Score Probability
1 ISLDAR 2.2 0.76
2 VVEELK 4.6 0.99
3 FVIDAR 8.1 1.00
Threshold-based filtering with FDR control
Probability-based filtering with FDR control
Protein-level analysis

Figure 10: Identification of peptides from tandem mass spectra and quality assignment in database searches. A) Correlation of experimental and theoretical spectra from in-silico digestion of protein sequences. Peptides are scored and ranked to filter for the best peptide spectrum match. B) Control for false positive peptide spectrum assignments with a target-decoy approach or Bayesian statistics (Adapted from [157]).

It can be expected that the number of hits in the decoy space is equal to the wrong assigned hits in the target space and a false discovery rate (FDR) can be calculated to control the number of wrong assignments in the dataset. This filtering is usually applied at the level of peptide spectrum matches and the protein level. The use of bayesian statistics represents an alternative approach and models the peptide distribution of false and true assignments to generate a local peptide probability (Fig. 10B) [157].

Quantitative Proteomics

The qualitative information that a protein is present in a sample is sometimes not very informative. Instead it is often of interest how proteins change in abundance over time or how a certain molecule influences the proteome abundance in cells or tissues. Mass spectrometers can measure the abundance of an analyte, as the signal detected in the mass analyzer is dependent on the amount of ions. The quantification of proteins by spectrum counting or integration of the signal intensity became easier with the development of software tools, and nowadays the quantification of thousands of proteins is routine [161, 162]. Quantification in proteomics can be divided into label based quantification techniques and label free quantification. Label based quantification techniques use stable isotopes that induce a mass shift into labeled peptides. The incremental mass difference is resolved by the mass spectrometer and can be used for multiplexing of quantitative information in the same spectrum. In contrast, label free quantification relies on the quantification between different MS runs which is accompanied with a high measurement time. On the other side an unlimited amount of samples can be easily compared by label free quantification which renders this technique ideal for large proteomics studies [1, 163]. The earlier samples are combined in the proteomics workflow the lower is the accumulation of technical variation and the higher the precision to quantify biological changes (Fig. 11A and B). Label based quantification techniques are described in the following in more detail.

A

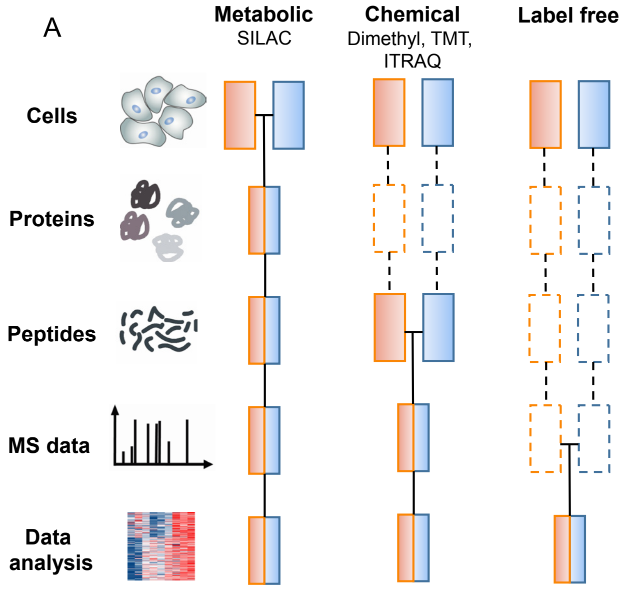

B

	Metabolic	Chemical	Label free
Quantitative precision	+++	++	+
Dynamic range	+++	MS1:+++ MS2:+ MS3:++	+++
Multiplexing	++	+++	+

High: +++ Intermediate: ++ low: +

Figure 11: Quantitative proteomics by metabolic- or chemical labeling and label free approaches. A) Metabolic labeling is performed in the cells, chemical labeling most often on the peptide level. Dashed lines indicate steps that are prone to experimental variation due to sample handling and analysis (adapted from [161]). B) Characteristics of metabolic-, chemical labeling and label free quantification. Metabolic labeling (SILAC) has the highest quantitative precision due to early combination of the samples. Dynamic range for quantification is reduced, if chemical labels are quantified in MS2 or MS3 (iTRAQ, TMT). Chemical labeling techniques allow the highest degree of multiplexing (iTRAQ, TMT).

Metabolic labeling

The most common technique for metabolic labeling is stable isotope labeling by amino acids in cell culture (SILAC). The isotopic labels are introduced at the earliest possible time point, in living cells. For this purpose, media can be supplemented with a maximum of three labels: (I) the natural amino acids of lysine and arginine, (II) $^{2}H_{4}$-lysine and ^{13}C-arginine or (III) $^{15}N_{2}{}^{13}C_{6}$-lysine and $^{15}N_{4}{}^{13}C_{6}$-arginine [164]. The cells than directly incorporate the amino acids into the proteins during protein biosynthesis and samples can be directly combined after this step (Fig. 11A). This makes this technique the most accurate of all quantification techniques. The quantification of intensity differences in isotopic clusters at the MS1 level furthermore enables the coverage of a high dynamic range when compared to MS2 based quantification (discussed later). However, major shortcomings of this technique include the increase in sample complexity in MS1, the restriction to cell culture or small animals [165, 166], long incorporation times of the labels and restricted number of multiplexing (Fig. 11B). Some of these issues could be partially addressed. For example, SILAC can be applied to quantification of proteins in higher complex organisms by spike-in and super-SILAC approaches [167, 168]. For this approach a mix of heavy SILAC labeled peptides, that represents the biology of the sample (e.g. cell mix) is spiked into peptide digests from complex organisms (e.g. human tissues). Also higher multiplexing has been shown in principle [169] but is not at a level to be applied in further studies.

Chemical labeling

The introduction of stable isotopes by modification of amino acids of proteins or peptides after biosynthesis is termed chemical labeling. Compared to metabolic labeling, chemical labeling introduces the stable isotopes at a later time point in the sample preparation workflow, resulting in increased technical variation (Fig. 11A). While labeling on the protein level is possible, most techniques aim to the chemical derivatization of primary amine residues at the ε-amino group of lysine or the peptide N-terminus [162].

One very cheap technique for incorporation of stable isotopes into peptides is dimethyl labeling of amines on lysine and the peptide N-termini. This technique uses different isotopomers of formaldehyde and cyanoborohydride for reductive amidation. Afterwards, corresponding dimethyl labeled peptides have a mass difference of 4 Da between light, intermediate and heavy label. Dimethyl labeling is restricted to three labels, as higher multiplexing would result in mass differences smaller than 4 Da and overlap of isotopic patterns [170, 171]. As the SILAC approach, dimethyl labeling leads to higher MS1 complexity, resulting in lower peptide identifications. However, it can be simply applied for the labeling tissues of complex organisms [170].

The perhaps most prominent and powerful chemical labeling techniques are based on the complete incorporation of an isobaric chemical tag. Tandem mass tags (TMT) [172] and isobaric tags for relative and absolute quantification (iTRAQ) [173] can be considered most popular and have the same functional principle. Both labels contain an activated NHS-ester as amine reactive group, a balancer and a mass reporter that contain stable isotopes. The reporter group and the balancer group together always have exactly the same weight, if the reporter contains a ^{13}C or ^{15}N isotope more the balancer contains one ^{13}C or ^{15}N isotope less. Labels have the same mass (they are isobaric) and different labels are therefore not visible in MS1. Peptide intensities are not derived from the intensity of intact peptides directly. Instead the intensity of differently labeled mass reporter ions is measured in MS2 fragment spectra at the low molecular weight region. TMT labeling was a long time only available for six tags [174] and iTRAQ for 8 tags [175]. However, because the high resolution of modern orbitrap mass spectrometers can be used to visualize mDa differences in molecular weight, the small mass difference for the exchange of one ^{15}N by a ^{13}C isotope became technically usable. The small difference in the mass of a neutron in nitrogen and the mass of a neutron in carbon is caused by binding energy differences in the nucleus. This so called mass defect leads to a 6.32 mDa difference of the reporter ions that can be resolved with high resolution mass spectrometers. The use of these neutron encoded mass differences allowed the extension of the multiplexing capacity of the TMT reporter ions from 6plex to 10plex when 127N, 127C, 128N, 128C, 129N, 129C, 130N, 130C isotopic reporter ions were used [176]. TMT 10plex is therefore the technology that allows highest multiplexing of proteomics quantification to date and MS2 based quantification does not suffer from shortcomings of MS1 based quantification mentioned above. A disadvantage of MS2 based quantification is the compressed dynamic range (ratio compression) that results from co-eluting and co-isolation and hence, co-fragmented peptides that do not reflect the change of the identified peptide [177-180]. MS2 based quantifications therefore show only small changes, even if the true changes are much higher or changes are not visible (false negative change in abundance). A solution to regain the ratios that are compressed in MS2 was presented recently. Multiple isolation waveforms with multiple sequencing notches were used for synchronous selection of precursors from MS2. The read out of reporter ions is then performed on MS3 spectra, that do not suffer from compressed ratios due to the two steps selection process [181] (Fig. 11B).

Objectives

There is a continuous and growing interest in the development of agents for targeted cancer therapies, which is reflected by an increase of approved small molecule kinase inhibitors in recent years. The major drawback of targeted cancer therapies is the fast development of treatment resistance that results in clinical relapse. Even if there is an intensive effort to develop more effective agents and combination treatments there is still lacking knowledge of underlying molecular mechanisms that render tumor cells resistant. The application of mass spectrometry-based proteomics enables the global study of proteome and sub-proteome compositions and post-translational modifications. Hence, the prime objective of this thesis was to apply current proteomic, chemical proteomic and phosphoproteomic techniques for the system-wide analysis of molecular mechanisms of treatment resistance.

Long term treatment with kinase inhibitors over 6 months results in drug resistance which can be observed clinically and in cell line models. In the second chapter I apply kinase affinity enrichment (chemical proteomics) to identify adaptive molecular changes that appear after long term EGFR inhibition. Upregulated kinases in the resistant cells are then specifically inhibited in combination with the EGFR inhibitor gefitinib.

In the third chapter I address the question how microenvironment secreted growth factors can render anti-cancer agents ineffective. I apply phosphoproteomics for a systems wide quantification of phosphorylation changes upon kinase inhibition and growth factor mediated rescue and will use tandem mass tagging for sample multiplexing and improved quantitative precision. Information from phosphoproteomics experiments will be used to prioritize signaling nodes for more effective treatments to overcome growth factor mediated resistance.

Adaptations to kinase inhibitor treatment arise within days after treatment and result in proteome reprogramming and network rewiring. In the fourth chapter I will apply tandem mass tagging for time-dependent quantification of changes in the proteome and phosphoproteome after EGFR and FGFR inhibition. Results will provide more insights into time dependent adaptation and potential fast occurring resistance mechanisms.

Abbreviations:

ATP	Adenosine triphosphate
CAF	Cancer associated fibroblast
CID	Collision induced dissociation
DDA	Data dependent acquisition
DFG	Asp-Phe-Gly motif
ESI	Electrospray ionization
ETD	Electron transfer dissociation
FDA	Food and Drug Administration
FDR	False discovery rate
HCD	Beam type fragmentation
HILIC	Hydrophilic liquid interaction chromatography
HPLC	High pressure liquid chromatography
IC	Immune inflammatory cells
IMAC	Immobilized metal affinity chromatography
iTRAQ	Isobaric Tags for Relative and Absolute Quantitation
LC-MS/MS	Liquid chromatography tandem mass spectrometry
LTQ	Linear trap quadrupole
MOAC	Metal oxide affinity chromatography
MS1	Mass spectrum of intact peptides
MS2	Fragment mass spectrum from MS1 precursor
MS3	Isolated fragment ion spectrum from MS2 precursors
nano-LC	Nanoliter liquid chromatography
NHS	N-hydroxysuccinimide
ppm	Parts per million
PTM	Post-translational modification
PTP	Protein tyrosine phosphatase
RF	Radio frequency
RP	Reversed phase
SAX	Strong anion exchange
SCX	Strong cation exchange
SH2	SRC homology 2

SILAC	Stable isotope labeling by amino acids in cell culture
TMT	Tandem mass tags
UHPLC	Ultra high pressure liquid chromatography

References

1. Wilhelm M, Schlegl J, Hahne H, Moghaddas Gholami A, Lieberenz M, Savitski MM, Ziegler E*, et al.* Mass-spectrometry-based draft of the human proteome. Nature 2014, 509: 582-587

2. Kim M-S, Pinto SM, Getnet D, Nirujogi RS, Manda SS, Chaerkady R, Madugundu AK*, et al.* A draft map of the human proteome. Nature 2014, 509: 575-581

3. Smith LM, Kelleher NL. Proteoform: a single term describing protein complexity. Nat Meth 2013, 10: 186-187

4. Manning G, Whyte DB, Martinez R, Hunter T, Sudarsanam S. The Protein Kinase Complement of the Human Genome. Science 2002, 298: 1912-1934

5. Taylor SS, Kornev AP. Protein Kinases: Evolution of Dynamic Regulatory Proteins. Trends in biochemical sciences 2011, 36: 65-77

6. Sebolt-Leopold JS, English JM. Mechanisms of drug inhibition of signalling molecules. Nature 2006, 441: 457-462

7. Ubersax JA, Ferrell Jr JE. Mechanisms of specificity in protein phosphorylation. Nature reviews Molecular cell biology 2007, 8: 530-541

8. Beltrao P, Albanèse V, Kenner Lillian R, Swaney Danielle L, Burlingame A, Villén J, Lim Wendell A*, et al.* Systematic Functional Prioritization of Protein Posttranslational Modifications. Cell 2012, 150: 413-425

9. Sharma K, D'Souza RC, Tyanova S, Schaab C, Wisniewski JR, Cox J, Mann M. Ultradeep human phosphoproteome reveals a distinct regulatory nature of Tyr and Ser/Thr-based signaling. Cell reports 2014, 8: 1583-1594

10. Hunter T, Sefton BM. Transforming gene product of Rous sarcoma virus phosphorylates tyrosine. Proceedings of the National Academy of Sciences of the United States of America 1980, 77: 1311-1315

11. Olsen JV, Vermeulen M, Santamaria A, Kumar C, Miller ML, Jensen LJ, Gnad F*, et al.* Quantitative phosphoproteomics reveals widespread full phosphorylation site occupancy during mitosis. Science signaling 2010, 3: ra3

12. Ptacek J, Devgan G, Michaud G, Zhu H, Zhu X, Fasolo J, Guo H*, et al.* Global analysis of protein phosphorylation in yeast. Nature 2005, 438: 679-684

13. Pearson RB, Kemp BE. [3] Protein kinase phosphorylation site sequences and consensus specificity motifs: Tabulations. Methods in Enzymology: Academic Press 1991: 62-81

14. Tanoue T, Adachi M, Moriguchi T, Nishida E. A conserved docking motif in MAP kinases common to substrates, activators and regulators. Nature cell biology 2000, 2: 110-116

15. Sharrocks AD, Yang S-H, Galanis A. Docking domains and substrate-specificity determination for MAP kinases. Trends in Biochemical Sciences 2000, 25: 448-453

16. Lim WA, Pawson T. Phosphotyrosine signaling: evolving a new cellular communication system. Cell 2010, 142: 661-667

17. Ciardiello F, Tortora G. EGFR Antagonists in Cancer Treatment. New England Journal of Medicine 2008, 358: 1160-1174

18. Li S, Schmitz KR, Jeffrey PD, Wiltzius JJW, Kussie P, Ferguson KM. Structural basis for inhibition of the epidermal growth factor receptor by cetuximab. Cancer cell 2005, 7: 301-311

19. Liu Q, Sabnis Y, Zhao Z, Zhang T, Buhrlage SJ, Jones LH, Gray NS. Developing irreversible inhibitors of the protein kinase cysteinome. Chemistry & biology 2013, 20: 146-159

20. Tong M, Seeliger MA. Targeting Conformational Plasticity of Protein Kinases. ACS chemical biology 2015, 10: 190-200

21. Wu P, Nielsen TE, Clausen MH. FDA-approved small-molecule kinase inhibitors. Trends in Pharmacological Sciences 2015, 36: 422-439

22. Zhang J, Yang PL, Gray NS. Targeting cancer with small molecule kinase inhibitors. Nature reviews Cancer 2009, 9: 28-39

23. Cox KJ, Shomin CD, Ghosh I. Tinkering outside the kinase ATP box: allosteric (type IV) and bivalent (type V) inhibitors of protein kinases. Future Medicinal Chemistry 2010, 3: 29-43

24. Morita S, Okamoto I, Kobayashi K, Yamazaki K, Asahina H, Inoue A, Hagiwara K*, et al.* Combined survival analysis of prospective clinical trials of gefitinib for non-small cell lung cancer with EGFR mutations. Clinical cancer research 2009, 15: 4493-4498

25. Maemondo M, Inoue A, Kobayashi K, Sugawara S, Oizumi S, Isobe H, Gemma A*, et al.* Gefitinib or chemotherapy for non-small-cell lung cancer with mutated EGFR. The New England journal of medicine 2010, 362: 2380-2388

26. Wang Y, Schmid-Bindert G, Zhou C. Erlotinib in the treatment of advanced non-small cell lung cancer: an update for clinicians. Therapeutic Advances in Medical Oncology 2012, 4: 19-29

27. Park Jin H, Liu Y, Lemmon Mark A, Radhakrishnan R. Erlotinib binds both inactive and active conformations of the EGFR tyrosine kinase domain. Biochemical Journal 2012, 448: 417-423

28. Gajiwala Ketan S, Feng J, Ferre R, Ryan K, Brodsky O, Weinrich S, Kath John C*, et al.* Insights into the Aberrant Activity of Mutant EGFR Kinase Domain and Drug Recognition. Structure, 21: 209-219

29. Bilancia D, Rosati G, Dinota A, Germano D, Romano R, Manzione L. Lapatinib in breast cancer. Annals of Oncology 2007, 18: vi26-vi30

30. Wood ER, Truesdale AT, McDonald OB, Yuan D, Hassell A, Dickerson SH, Ellis B*, et al.* A Unique Structure for Epidermal Growth Factor Receptor Bound to GW572016 (Lapatinib): Relationships among Protein Conformation, Inhibitor Off-Rate, and Receptor Activity in Tumor Cells. Cancer research 2004, 64: 6652-6659

31. Ramos P, Bentires-Alj M. Mechanism-based cancer therapy: resistance to therapy, therapy for resistance. Oncogene 2015, 34: 3617-3626

32. Karvela M, Helgason GV, Holyoake TL. Mechanisms and novel approaches in overriding tyrosine kinase inhibitor resistance in chronic myeloid leukemia. Expert Review of Anticancer Therapy 2012, 12: 381-392

33. Jabbour E, Kantarjian H, Jones D, Talpaz M, Bekele N, O'Brien S, Zhou X*, et al.* Frequency and clinical significance of BCR-ABL mutations in patients with chronic myeloid leukemia treated with imatinib mesylate. Leukemia 2006, 20: 1767-1773

34. Emery CM, Vijayendran KG, Zipser MC, Sawyer AM, Niu L, Kim JJ, Hatton C*, et al.* MEK1 mutations confer resistance to MEK and B-RAF inhibition. Proceedings of the National Academy of Sciences 2009, 106: 20411-20416

35. Cools J, Mentens N, Furet P, Fabbro D, Clark JJ, Griffin JD, Marynen P*, et al.* Prediction of Resistance to Small Molecule FLT3 Inhibitors: Implications for Molecularly Targeted Therapy of Acute Leukemia. Cancer research 2004, 64: 6385-6389

36. Suda K, Onozato R, Yatabe Y, Mitsudomi T. EGFR T790M Mutation: A Double Role in Lung Cancer Cell Survival? Journal of Thoracic Oncology 2009, 4: 1-4

37. Yun CH, Mengwasser KE, Toms AV, Woo MS, Greulich H, Wong KK, Meyerson M*, et al.* The T790M mutation in EGFR kinase causes drug resistance by increasing the affinity for ATP. Proceedings of the National Academy of Sciences of the United States of America 2008, 105: 2070-2075

38. Balak MN, Gong Y, Riely GJ, Somwar R, Li AR, Zakowski MF, Chiang A*, et al.* Novel D761Y and Common Secondary T790M Mutations in Epidermal Growth Factor Receptor–Mutant Lung Adenocarcinomas with Acquired Resistance to Kinase Inhibitors. Clinical cancer research 2006, 12: 6494-6501

39. Kosaka T, Yatabe Y, Endoh H, Yoshida K, Hida T, Tsuboi M, Tada H*, et al.* Analysis of Epidermal Growth Factor Receptor Gene Mutation in Patients with Non–Small Cell Lung Cancer and Acquired Resistance to Gefitinib. Clinical cancer research 2006, 12: 5764-5769

40. Solca F, Dahl G, Zoephel A, Bader G, Sanderson M, Klein C, Kraemer O*, et al.* Target Binding Properties and Cellular Activity of Afatinib (BIBW 2992), an Irreversible ErbB Family Blocker. Journal of Pharmacology and Experimental Therapeutics 2012, 343: 342-350

41. Corcoran RB, Dias-Santagata D, Bergethon K, Iafrate AJ, Settleman J, Engelman JA. BRAF Gene Amplification Can Promote Acquired Resistance to MEK Inhibitors in Cancer Cells Harboring the BRAF V600E Mutation. Science signaling 2010, 3: ra84-ra84

42. Paplomata E, O'Regan R. The PI3K/AKT/mTOR pathway in breast cancer: targets, trials and biomarkers. Therapeutic Advances in Medical Oncology 2014, 6: 154-166

43. Nagata Y, Lan K-H, Zhou X, Tan M, Esteva FJ, Sahin AA, Klos KS*, et al.* PTEN activation contributes to tumor inhibition by trastuzumab, and loss of PTEN predicts trastuzumab resistance in patients. Cancer cell, 6: 117-127

44. Berns K, Horlings HM, Hennessy BT, Madiredjo M, Hijmans EM, Beelen K, Linn SC*, et al.* A Functional Genetic Approach Identifies the PI3K Pathway as a Major Determinant of Trastuzumab Resistance in Breast Cancer. Cancer cell, 12: 395-402

45. Eichhorn PJA, Gili M, Scaltriti M, Serra V, Guzman M, Nijkamp W, Beijersbergen RL*, et al.* Phosphatidylinositol 3-Kinase Hyperactivation Results in Lapatinib Resistance that Is Reversed by the mTOR/Phosphatidylinositol 3-Kinase Inhibitor NVP-BEZ235. Cancer research 2008, 68: 9221-9230

46. Wang L, Zhang Q, Zhang J, Sun S, Guo H, Jia Z, Wang B*, et al.* PI3K pathway activation results in low efficacy of both trastuzumab and lapatinib. BMC cancer 2011, 11: 248-248

47. Engelman JA, Zejnullahu K, Mitsudomi T, Song Y, Hyland C, Park JO, Lindeman N*, et al.* MET amplification leads to gefitinib resistance in lung cancer by activating ERBB3 signaling. Science 2007, 316: 1039-1043

48. Chen C-T, Kim H, Liska D, Gao S, Christensen JG, Weiser MR. MET Activation Mediates Resistance to Lapatinib Inhibition of HER2-Amplified Gastric Cancer Cells. Molecular cancer therapeutics 2012, 11: 660-669

49. Tang MKS, Zhou HY, Yam JWP, Wong AST. c-Met Overexpression Contributes to the Acquired Apoptotic Resistance of Nonadherent Ovarian Cancer Cells through a Cross Talk Mediated by Phosphatidylinositol 3-Kinase and Extracellular Signal-Regulated Kinase 1/2. Neoplasia 2010, 12: 128-IN125

50. Bardelli A, Corso S, Bertotti A, Hobor S, Valtorta E, Siravegna G, Sartore-Bianchi A*, et al.* Amplification of the MET Receptor Drives Resistance to Anti-EGFR Therapies in Colorectal Cancer. Cancer discovery 2013, 3: 658-673

51. Zhou L, Liu XD, Sun M, Zhang X, German P, Bai S, Ding Z*, et al.* Targeting MET and AXL overcomes resistance to sunitinib therapy in renal cell carcinoma. Oncogene 2015: 1-11

52. Zhang Z, Lee JC, Lin L, Olivas V, Au V, LaFramboise T, Abdel-Rahman M*, et al.* Activation of the AXL kinase causes resistance to EGFR-targeted therapy in lung cancer. Nature genetics 2012, 44: 852-860

53. Liu L, Greger J, Shi H, Liu Y, Greshock J, Annan R, Halsey W*, et al.* Novel Mechanism of Lapatinib Resistance in HER2-Positive Breast Tumor Cells: Activation of AXL. Cancer research 2009, 69: 6871-6878

54. Suda K, Mizuuchi H, Sato K, Takemoto T, Iwasaki T, Mitsudomi T. The insulin-like growth factor 1 receptor causes acquired resistance to erlotinib in lung cancer cells with the wild-type epidermal growth factor receptor. International journal of cancer Journal international du cancer 2014, 135: 1002-1006

55. Ware KE, Hinz TK, Kleczko E, Singleton KR, Marek LA, Helfrich BA, Cummings CT*, et al.* A mechanism of resistance to gefitinib mediated by cellular reprogramming and the acquisition of an FGF2-FGFR1 autocrine growth loop. Oncogenesis 2013, 2: e39

56. Sergina NV, Rausch M, Wang D, Blair J, Hann B, Shokat KM, Moasser MM. Escape from HER-family tyrosine kinase inhibitor therapy by the kinase-inactive HER3. Nature 2007, 445: 437-441

57. Lee H-J, Zhuang G, Cao Y, Du P, Kim H-J, Settleman J. Drug Resistance via Feedback Activation of Stat3 in Oncogene-Addicted Cancer Cells. Cancer cell 2014, 26: 207-221

58. Carracedo A, Ma L, Teruya-Feldstein J, Rojo F, Salmena L, Alimonti A, Egia A*, et al.* Inhibition of mTORC1 leads to MAPK pathway activation through a PI3K-dependent feedback loop in human cancer. The Journal of clinical investigation 2008, 118: 3065-3074

59. Serra V, Scaltriti M, Prudkin L, Eichhorn PJA, Ibrahim YH, Chandarlapaty S, Markman B*, et al.* PI3K inhibition results in enhanced HER signaling and acquired ERK dependency in HER2-overexpressing breast cancer. Oncogene 2011, 30: 2547-2557

60. Wee S, Jagani Z, Xiang KX, Loo A, Dorsch M, Yao Y-M, Sellers WR*, et al.* PI3K Pathway Activation Mediates Resistance to MEK Inhibitors in KRAS Mutant Cancers. Cancer research 2009, 69: 4286-4293

61. Hoeflich KP, O'Brien C, Boyd Z, Cavet G, Guerrero S, Jung K, Januario T*, et al.* In vivo Antitumor Activity of MEK and Phosphatidylinositol 3-Kinase Inhibitors in Basal-Like Breast Cancer Models. Clinical cancer research 2009, 15: 4649-4664

62. Yu K, Toral-Barza L, Shi C, Zhang WG, Zask A. Response and determinants of cancer cell susceptibility to PI3K inhibitors: combined targeting of PI3K and Mek1 as an effective anticancer strategy. Cancer biology & therapy 2008, 7: 307-315

63. Hanahan D, Weinberg Robert A. Hallmarks of Cancer: The Next Generation. Cell 2011, 144: 646-674

64. Damiano JS, Hazlehurst LA, Dalton WS. Cell adhesion-mediated drug resistance (CAM-DR) protects the K562 chronic myelogenous leukemia cell line from apoptosis induced by BCR/ABL inhibition, cytotoxic drugs, and gamma-irradiation. Leukemia 2001, 15: 1232-1239

65. Huang C, Park CC, Hilsenbeck SG, Ward R, Rimawi MF, Wang Y-c, Shou J*, et al.* β1 integrin mediates an alternative survival pathway in breast cancer cells resistant to lapatinib. Breast Cancer Research 2011, 13: 1-15

66. Muranen T, Selfors Laura M, Worster Devin T, Iwanicki Marcin P, Song L, Morales Fabiana C, Gao S*, et al.* Inhibition of PI3K/mTOR Leads to Adaptive Resistance in Matrix-Attached Cancer Cells. Cancer cell, 21: 227-239

67. Manshouri T, Estrov Z, Quintás-Cardama A, Burger J, Zhang Y, Livun A, Knez L*, et al.* Bone Marrow Stroma–Secreted Cytokines Protect JAK2V617F-Mutated Cells from the Effects of a JAK2 Inhibitor. Cancer research 2011, 71: 3831-3840

68. Wilson TR, Fridlyand J, Yan Y, Penuel E, Burton L, Chan E, Peng J*, et al.* Widespread potential for growth-factor-driven resistance to anticancer kinase inhibitors. Nature 2012, 487: 505-509

69. Straussman R, Morikawa T, Shee K, Barzily-Rokni M, Qian ZR, Du J, Davis A*, et al.* Tumour micro-environment elicits innate resistance to RAF inhibitors through HGF secretion. Nature 2012, 487: 500-504

70. Mueller KL, Madden JM, Zoratti GL, Kuperwasser C, List K, Boerner JL. Fibroblast-secreted hepatocyte growth factor mediates epidermal growth factor receptor tyrosine kinase inhibitor resistance in triple-negative breast cancers through paracrine activation of Met. Breast cancer research : BCR 2012, 14: R104-R104

71. Yano S, Takeuchi S, Nakagawa T, Yamada T. Ligand-triggered resistance to molecular targeted drugs in lung cancer: roles of hepatocyte growth factor and epidermal growth factor receptor ligands. Cancer science 2012, 103: 1189-1194

72. Terai H, Soejima K, Yasuda H, Nakayama S, Hamamoto J, Arai D, Ishioka K*, et al.* Activation of the FGF2-FGFR1 autocrine pathway: a novel mechanism of acquired resistance to gefitinib in NSCLC. Molecular cancer research 2013, 11: 759-767

73. Tovar V, Cornella H, Moeini A, Vidal S, Hoshida Y, Sia D, Peix J*, et al.* Tumour initiating cells and IGF/FGF signalling contribute to sorafenib resistance in hepatocellular carcinoma. Gut 2015,

74. Eliuk S, Makarov A. Evolution of Orbitrap Mass Spectrometry Instrumentation. Annual Review of Analytical Chemistry 2015, 8: 61-80

75. Human Genome Sequencing C. Finishing the euchromatic sequence of the human genome. Nature 2004, 431: 931-945

76. Genome Sequence of the Nematode C. elegans: A Platform for Investigating Biology. Science 1998, 282: 2012-2018

77. Analysis of the genome sequence of the flowering plant Arabidopsis thaliana. Nature 2000, 408: 796-815

78. Wasinger VC, Cordwell SJ, Cerpa-Poljak A, Yan JX, Gooley AA, Wilkins MR, Duncan MW*, et al.* Progress with gene-product mapping of the Mollicutes: Mycoplasma genitalium. Electrophoresis 1995, 16: 1090-1094

79. Tran JC, Zamdborg L, Ahlf DR, Lee JE, Catherman AD, Durbin KR, Tipton JD*, et al.* Mapping intact protein isoforms in discovery mode using top-down proteomics. Nature 2011, 480: 254-258

80. Hein Marco Y, Hubner Nina C, Poser I, Cox J, Nagaraj N, Toyoda Y, Gak Igor A*, et al.* A Human Interactome in Three Quantitative Dimensions Organized by Stoichiometries and Abundances. Cell, 163: 712-723

81. Mann M, Jensen ON. Proteomic analysis of post-translational modifications. Nat Biotech 2003, 21: 255-261

82. Garcia BA. What Does the Future Hold for Top Down Mass Spectrometry? Journal of the American Society for Mass Spectrometry 2010, 21: 193-202

83. Moradian A, Kalli A, Sweredoski MJ, Hess S. The top-down, middle-down, and bottom-up mass spectrometry approaches for characterization of histone variants and their post-translational modifications. Proteomics 2014, 14: 489-497

84. Chait BT. Mass Spectrometry: Bottom-Up or Top-Down? Science 2006, 314: 65-66

85. Olsen JV, Ong S-E, Mann M. Trypsin Cleaves Exclusively C-terminal to Arginine and Lysine Residues. Molecular & Cellular Proteomics 2004, 3: 608-614

86. Tsiatsiani L, Heck AJR. Proteomics beyond trypsin. FEBS Journal 2015, 282: 2612-2626

87. Choudhary G, Wu S-L, Shieh P, Hancock WS. Multiple Enzymatic Digestion for Enhanced Sequence Coverage of Proteins in Complex Proteomic Mixtures Using Capillary LC with Ion Trap MS/MS. Journal of proteome research 2003, 2: 59-67

88. Swaney DL, Wenger CD, Coon JJ. Value of Using Multiple Proteases for Large-Scale Mass Spectrometry-Based Proteomics. Journal of proteome research 2010, 9: 1323-1329

89. Guo X, Trudgian DC, Lemoff A, Yadavalli S, Mirzaei H. Confetti: A Multiprotease Map of the HeLa Proteome for Comprehensive Proteomics. Molecular & Cellular Proteomics 2014, 13: 1573-1584

90. Giansanti P, Aye TT, van den Toorn H, Peng M, van Breukelen B, Heck AJ. An Augmented Multiple-Protease-Based Human Phosphopeptide Atlas. Cell reports 2015, 11: 1834-1843

91. Steen H, Mann M. The abc's (and xyz's) of peptide sequencing. Nature reviews Molecular cell biology 2004, 5: 699-711

92. Neverova I, Van Eyk JE. Role of chromatographic techniques in proteomic analysis. Journal of Chromatography B 2005, 815: 51-63

93. Köcher T, Swart R, Mechtler K. Ultra-High-Pressure RPLC Hyphenated to an LTQ-Orbitrap Velos Reveals a Linear Relation between Peak Capacity and Number of Identified Peptides. Analytical chemistry 2011, 83: 2699-2704

94. Wang X, Barber WE, Carr PW. A practical approach to maximizing peak capacity by using long columns packed with pellicular stationary phases for proteomic research. Journal of Chromatography A 2006, 1107: 139-151

95. Ritorto MS, Cook K, Tyagi K, Pedrioli PG, Trost M. Hydrophilic strong anion exchange (hSAX) chromatography for highly orthogonal peptide separation of complex proteomes. Journal of proteome research 2013, 12: 2449-2457

96. Yang F, Shen Y, Camp DG, Smith RD. High pH reversed-phase chromatography with fraction concatenation as an alternative to strong-cation exchange chromatography for two-dimensional proteomic analysis. Expert Review of Proteomics 2012, 9: 129-134

97. Washburn MP, Wolters D, Yates JR. Large-scale analysis of the yeast proteome by multidimensional protein identification technology. Nat Biotech 2001, 19: 242-247

98. Taylor P, Nielsen PA, Trelle MB, Hørning OB, Andersen MB, Vorm O, Moran MF*, et al.* Automated 2D Peptide Separation on a 1D Nano-LC-MS System. Journal of proteome research 2009, 8: 1610-1616

99. Zhou F, Sikorski TW, Ficarro SB, Webber JT, Marto JA. Online Nanoflow Reversed Phase-Strong Anion Exchange-Reversed Phase Liquid Chromatography–Tandem Mass Spectrometry Platform for Efficient and In-Depth Proteome Sequence Analysis of Complex Organisms. Analytical chemistry 2011, 83: 6996-7005

100. Lau E, Lam MPY, Siu SO, Kong RPW, Chan WL, Zhou Z, Huang J*, et al.* Combinatorial use of offline SCX and online RP-RP liquid chromatography for iTRAQ-based quantitative proteomics applications. Molecular BioSystems 2011, 7: 1399-1408

101. Boersema PJ, Mohammed S, Heck AJR. Hydrophilic interaction liquid chromatography (HILIC) in proteomics. Analytical and Bioanalytical Chemistry 2008, 391: 151-159

102. Batth TS, Francavilla C, Olsen JV. Off-Line High-pH Reversed-Phase Fractionation for In-Depth Phosphoproteomics. Journal of proteome research 2014, 13: 6176-6186

103. Dunham WH, Mullin M, Gingras A-C. Affinity-purification coupled to mass spectrometry: Basic principles and strategies. Proteomics 2012, 12: 1576-1590

104. Mohammed H, Taylor C, Brown GD, Papachristou EK, Carroll JS, D'Santos CS. Rapid immunoprecipitation mass spectrometry of endogenous proteins (RIME) for analysis of chromatin complexes. Nat Protocols 2016, 11: 316-326

105. Rolland T, Taşan M, Charloteaux B, Pevzner Samuel J, Zhong Q, Sahni N, Yi S*, et al.* A Proteome-Scale Map of the Human Interactome Network. Cell 2014, 159: 1212-1226

106. Bantscheff M, Eberhard D, Abraham Y, Bastuck S, Boesche M, Hobson S, Mathieson T*, et al.* Quantitative chemical proteomics reveals mechanisms of action of clinical ABL kinase inhibitors. Nature biotechnology 2007, 25: 1035-1044

107. Medard G, Pachl F, Ruprecht B, Klaeger S, Heinzlmeir S, Helm D, Qiao H*, et al.* Optimized chemical proteomics assay for kinase inhibitor profiling. Journal of proteome research 2015,

108. Bantscheff M, Hopf C, Savitski MM, Dittmann A, Grandi P, Michon A-M, Schlegl J*, et al.* Chemoproteomics profiling of HDAC inhibitors reveals selective targeting of HDAC complexes. Nat Biotech 2011, 29: 255-265

109. Graves PR, Kwiek JJ, Fadden P, Ray R, Hardeman K, Coley AM, Foley M*, et al.* Discovery of novel targets of quinoline drugs in the human purine binding proteome. Molecular pharmacology 2002, 62: 1364-1372

110. Hanke SE, Bertinetti D, Badel A, Schweinsberg S, Genieser H-G, Herberg FW. Cyclic nucleotides as affinity tools: Phosphorothioate cAMP analogues address specific PKA subproteomes. New Biotechnology 2011, 28: 294-301

111. Huang S-MA, Mishina YM, Liu S, Cheung A, Stegmeier F, Michaud GA, Charlat O*, et al.* Tankyrase inhibition stabilizes axin and antagonizes Wnt signalling. Nature 2009, 461: 614-620

112. Schirle M, Petrella EC, Brittain SM, Schwalb D, Harrington E, Cornella-Taracido I, Tallarico JA. Kinase inhibitor profiling using chemoproteomics. Methods in molecular biology 2012, 795: 161-177

113. Choudhary C, Kumar C, Gnad F, Nielsen ML, Rehman M, Walther TC, Olsen JV*, et al.* Lysine Acetylation Targets Protein Complexes and Co-Regulates Major Cellular Functions. Science 2009, 325: 834-840

114. Swaney DL, Villen J. Enrichment of Modified Peptides via Immunoaffinity Precipitation with Modification-Specific Antibodies. Cold Spring Harbor protocols 2016, 2016: pdb prot088013

115. Mertins P, Qiao JW, Patel J, Udeshi ND, Clauser KR, Mani DR, Burgess MW*, et al.* Integrated proteomic analysis of post-translational modifications by serial enrichment. Nature methods 2013, 10: 634-637

116. Olsen JV, Mann M. Status of large-scale analysis of post-translational modifications by mass spectrometry. Molecular & cellular proteomics : MCP 2013, 12: 3444-3452

117. Humphrey SJ, Azimifar SB, Mann M. High-throughput phosphoproteomics reveals in vivo insulin signaling dynamics. Nature biotechnology 2015, 33: 990-995

118. Tsai C-F, Wang Y-T, Chen Y-R, Lai C-Y, Lin P-Y, Pan K-T, Chen J-Y*, et al.* Immobilized Metal Affinity Chromatography Revisited: pH/Acid Control toward High Selectivity in Phosphoproteomics. Journal of proteome research 2008, 7: 4058-4069

119. Bodenmiller B, Mueller LN, Mueller M, Domon B, Aebersold R. Reproducible isolation of distinct, overlapping segments of the phosphoproteome. Nat Meth 2007, 4: 231-237

120. Tsai C-F, Hsu C-C, Hung J-N, Wang Y-T, Choong W-K, Zeng M-Y, Lin P-Y*, et al.* Sequential Phosphoproteomic Enrichment through Complementary Metal-Directed Immobilized Metal Ion Affinity Chromatography. Analytical chemistry 2014, 86: 685-693

121. Ruprecht B, Koch H, Medard G, Mundt M, Kuster B, Lemeer S. Comprehensive and reproducible phosphopeptide enrichment using iron immobilized metal ion affinity chromatography (Fe-IMAC) columns. Molecular & cellular proteomics : MCP 2015, 14: 205-215

122. Wilm M. Principles of Electrospray Ionization. Molecular & Cellular Proteomics 2011, 10

123. Fenn J, Mann M, Meng C, Wong S, Whitehouse C. Electrospray ionization for mass spectrometry of large biomolecules. Science 1989, 246: 64-71

124. Meng CK, Mann M, Fenn JB. Of protons or proteins. Zeitschrift für Physik D Atoms, Molecules and Clusters, 10: 361-368

125. Wilm MS, Mann M. Electrospray and Taylor-Cone theory, Dole's beam of macromolecules at last? International Journal of Mass Spectrometry and Ion Processes 1994, 136: 167-180

126. Iribarne JV, Thomson BA. On the evaporation of small ions from charged droplets. The Journal of Chemical Physics 1976, 64: 2287-2294

127. Thomson BA, Iribarne JV. Field induced ion evaporation from liquid surfaces at atmospheric pressure. The Journal of Chemical Physics 1979, 71: 4451-4463

128. Wilm M, Mann M. Analytical Properties of the Nanoelectrospray Ion Source. Analytical chemistry 1996, 68: 1-8

129. Hahne H, Pachl F, Ruprecht B, Maier SK, Klaeger S, Helm D, Medard G*, et al.* DMSO enhances electrospray response, boosting sensitivity of proteomic experiments. Nat Meth 2013, 10: 989-991

130. Han X, Aslanian A, Yates JR. Mass Spectrometry for Proteomics. Current opinion in chemical biology 2008, 12: 483-490

131. Beck S, Michalski A, Raether O, Lubeck M, Kaspar S, Goedecke N, Baessmann C*, et al.* The Impact II, a Very High-Resolution Quadrupole Time-of-Flight Instrument (QTOF) for Deep Shotgun Proteomics. Molecular & Cellular Proteomics 2015, 14: 2014-2029

132. B.A. Mamyrin VIK, D.V. Shmikk, V.A. Zagulin. The mass-reflectron, a new nonmagnetic time-of-flight mass spectrometer with high resolution. Journal of Experimental and Theoretical Physics 1973, 37: 45

133. Jonscher KR, Yates JR, 3rd. The quadrupole ion trap mass spectrometer--a small solution to a big challenge. Anal Biochem 1997, 244: 1-15

134. Douglas DJ, Frank AJ, Mao D. Linear ion traps in mass spectrometry. Mass spectrometry reviews 2005, 24: 1-29

135. Scigelova M, Makarov A. Orbitrap Mass Analyzer – Overview and Applications in Proteomics. Proteomics 2006, 6: 16-21

136. Zubarev RA, Makarov A. Orbitrap Mass Spectrometry. Analytical chemistry 2013, 85: 5288-5296

137. Makarov A, Denisov E, Kholomeev A, Balschun W, Lange O, Strupat K, Horning S. Performance Evaluation of a Hybrid Linear Ion Trap/Orbitrap Mass Spectrometer. Analytical chemistry 2006, 78: 2113-2120

138. Clauser KR, Baker P, Burlingame AL. Role of Accurate Mass Measurement (±10 ppm) in Protein Identification Strategies Employing MS or MS/MS and Database Searching. Analytical chemistry 1999, 71: 2871-2882

139. Pekar Second T, Blethrow JD, Schwartz JC, Merrihew GE, MacCoss MJ, Swaney DL, Russell JD*, et al.* Dual-Pressure Linear Ion Trap Mass Spectrometer Improving the Analysis of Complex Protein Mixtures. Analytical chemistry 2009, 81: 7757-7765

140. Makarov A, Denisov E, Lange O. Performance Evaluation of a High-field Orbitrap Mass Analyzer. Journal of the American Society for Mass Spectrometry 2009, 20: 1391-1396

141. Olsen JV, Macek B, Lange O, Makarov A, Horning S, Mann M. Higher-energy C-trap dissociation for peptide modification analysis. Nat Meth 2007, 4: 709-712

142. Michalski A, Damoc E, Hauschild J-P, Lange O, Wieghaus A, Makarov A, Nagaraj N*, et al.* Mass Spectrometry-based Proteomics Using Q Exactive, a High-performance Benchtop Quadrupole Orbitrap Mass Spectrometer. Molecular & Cellular Proteomics 2011, 10

143. Hebert AS, Richards AL, Bailey DJ, Ulbrich A, Coughlin EE, Westphall MS, Coon JJ. The One Hour Yeast Proteome. Molecular & cellular proteomics : MCP 2014, 13: 339-347

144. Louris JN, Cooks RG, Syka JEP, Kelley PE, Stafford GC, Todd JFJ. Instrumentation, applications, and energy deposition in quadrupole ion-trap tandem mass spectrometry. Analytical chemistry 1987, 59: 1677-1685

145. Michalski A, Cox J, Mann M. More than 100,000 Detectable Peptide Species Elute in Single Shotgun Proteomics Runs but the Majority is Inaccessible to Data-Dependent LC−MS/MS. Journal of proteome research 2011, 10: 1785-1793

146. Wenner BR, Lynn BC. Factors that affect ion trap data-dependent MS/MS in proteomics. Journal of the American Society for Mass Spectrometry, 15: 150-157

147. Geromanos SJ, Vissers JPC, Silva JC, Dorschel CA, Li G-Z, Gorenstein MV, Bateman RH*, et al.* The detection, correlation, and comparison of peptide precursor and product ions from data independent LC-MS with data dependant LC-MS/MS. Proteomics 2009, 9: 1683-1695

148. Hunt DF, Yates JR, Shabanowitz J, Winston S, Hauer CR. Protein sequencing by tandem mass spectrometry. Proceedings of the National Academy of Sciences of the United States of America 1986, 83: 6233-6237

149. Syka JEP, Coon JJ, Schroeder MJ, Shabanowitz J, Hunt DF. Peptide and protein sequence analysis by electron transfer dissociation mass spectrometry. Proceedings of the National Academy of Sciences of the United States of America 2004, 101: 9528-9533

150. Roepstorff P, Fohlman J. Proposal for a common nomenclature for sequence ions in mass spectra of peptides. Biomed Mass Spectrom 1984, 11: 601

151. Yang Y-H, Lee K, Jang K-S, Kim Y-G, Park S-H, Lee C-S, Kim B-G. Low mass cutoff evasion with qz value optimization in ion trap. Analytical Biochemistry 2009, 387: 133-135

152. Michalski A, Neuhauser N, Cox J, Mann M. A Systematic Investigation into the Nature of Tryptic HCD Spectra. Journal of proteome research 2012, 11: 5479-5491

153. Köcher T, Pichler P, Schutzbier M, Stingl C, Kaul A, Teucher N, Hasenfuss G*, et al.* High Precision Quantitative Proteomics Using iTRAQ on an LTQ Orbitrap: A New Mass Spectrometric Method Combining the Benefits of All. Journal of proteome research 2009, 8: 4743-4752

154. McAlister GC, Phanstiel D, Good DM, Berggren WT, Coon JJ. Implementation of Electron-Transfer Dissociation on a Hybrid Linear Ion Trap–Orbitrap Mass Spectrometer. Analytical chemistry 2007, 79: 3525-3534

155. Mikesh LM, Ueberheide B, Chi A, Coon JJ, Syka JEP, Shabanowitz J, Hunt DF. The Utility of ETD Mass Spectrometry in Proteomic Analysis: BIOCHIMICA ET BIOPHYSICA ACTA Proteins and Proteomics Posttranslational Modifications in Proteomics Special Issue. Biochimica et biophysica acta 2006, 1764: 1811-1822

156. Frese CK, Zhou H, Taus T, Altelaar AFM, Mechtler K, Heck AJR, Mohammed S. Unambiguous Phosphosite Localization using Electron-Transfer/Higher-Energy Collision Dissociation (EThcD). Journal of proteome research 2013, 12: 1520-1525

157. Nesvizhskii AI, Vitek O, Aebersold R. Analysis and validation of proteomic data generated by tandem mass spectrometry. Nat Meth 2007, 4: 787-797

158. Eng JK, McCormack AL, Yates JR. An approach to correlate tandem mass spectral data of peptides with amino acid sequences in a protein database. Journal of the American Society for Mass Spectrometry 1994, 5: 976-989

159. Cox J, Neuhauser N, Michalski A, Scheltema RA, Olsen JV, Mann M. Andromeda: a peptide search engine integrated into the MaxQuant environment. Journal of proteome research 2011, 10: 1794-1805

160. Nesvizhskii AI, Aebersold R. Interpretation of Shotgun Proteomic Data: The Protein Inference Problem. Molecular & Cellular Proteomics 2005, 4: 1419-1440

161. Bantscheff M, Schirle M, Sweetman G, Rick J, Kuster B. Quantitative mass spectrometry in proteomics: a critical review. Analytical and Bioanalytical Chemistry 2007, 389: 1017-1031

162. Bantscheff M, Lemeer S, Savitski MM, Kuster B. Quantitative mass spectrometry in proteomics: critical review update from 2007 to the present. Analytical and Bioanalytical Chemistry 2012, 404: 939-965

163. Moghaddas Gholami A, Hahne H, Wu Z, Auer FJ, Meng C, Wilhelm M, Kuster B. Global proteome analysis of the NCI-60 cell line panel. Cell reports 2013, 4: 609-620

164. Ong S-E, Blagoev B, Kratchmarova I, Kristensen DB, Steen H, Pandey A, Mann M. Stable Isotope Labeling by Amino Acids in Cell Culture, SILAC, as a Simple and Accurate Approach to Expression Proteomics. Molecular & Cellular Proteomics 2002, 1: 376-386

165. Krüger M, Moser M, Ussar S, Thievessen I, Luber CA, Forner F, Schmidt S*, et al.* SILAC Mouse for Quantitative Proteomics Uncovers Kindlin-3 as an Essential Factor for Red Blood Cell Function. Cell, 134: 353-364

166. Geiger T, Velic A, Macek B, Lundberg E, Kampf C, Nagaraj N, Uhlen M*, et al.* Initial quantitative proteomic map of 28 mouse tissues using the SILAC mouse. Molecular & cellular proteomics : MCP 2013, 12: 1709-1722

167. Geiger T, Wisniewski JR, Cox J, Zanivan S, Kruger M, Ishihama Y, Mann M. Use of stable isotope labeling by amino acids in cell culture as a spike-in standard in quantitative proteomics. Nat Protocols 2011, 6: 147-157

168. Geiger T, Cox J, Ostasiewicz P, Wisniewski JR, Mann M. Super-SILAC mix for quantitative proteomics of human tumor tissue. Nat Meth 2010, 7: 383-385

169. Hebert AS, Merrill AE, Bailey DJ, Still AJ, Westphall MS, Strieter ER, Pagliarini DJ*, et al.* Neutron-encoded mass signatures for multiplexed proteome quantification. Nat Meth 2013, 10: 332-334

170. Boersema PJ, Aye TT, van Veen TAB, Heck AJR, Mohammed S. Triplex protein quantification based on stable isotope labeling by peptide dimethylation applied to cell and tissue lysates. Proteomics 2008, 8: 4624-4632

171. Boersema PJ, Raijmakers R, Lemeer S, Mohammed S, Heck AJR. Multiplex peptide stable isotope dimethyl labeling for quantitative proteomics. Nat Protocols 2009, 4: 484-494

172. Thompson A, Schafer J, Kuhn K, Kienle S, Schwarz J, Schmidt G, Neumann T*, et al.* Tandem mass tags: a novel quantification strategy for comparative analysis of complex protein mixtures by MS/MS. Analytical chemistry 2003, 75: 1895-1904

173. Wiese S, Reidegeld KA, Meyer HE, Warscheid B. Protein labeling by iTRAQ: A new tool for quantitative mass spectrometry in proteome research. Proteomics 2007, 7: 340-350

174. Dayon L, Hainard A, Licker V, Turck N, Kuhn K, Hochstrasser DF, Burkhard PR*, et al.* Relative Quantification of Proteins in Human Cerebrospinal Fluids by MS/MS Using 6-Plex Isobaric Tags. Analytical chemistry 2008, 80: 2921-2931

175. Pottiez G, Wiederin J, Fox HS, Ciborowski P. Comparison of 4-plex to 8-plex iTRAQ Quantitative Measurements of Proteins in Human Plasma Samples. Journal of proteome research 2012, 11: 3774-3781

176. McAlister GC, Huttlin EL, Haas W, Ting L, Jedrychowski MP, Rogers JC, Kuhn K*, et al.* Increasing the multiplexing capacity of TMTs using reporter ion isotopologues with isobaric masses. Analytical chemistry 2012, 84: 7469-7478

177. Savitski MM, Mathieson T, Zinn N, Sweetman G, Doce C, Becher I, Pachl F*, et al.* Measuring and Managing Ratio Compression for Accurate iTRAQ/TMT Quantification. Journal of proteome research 2013, 12: 3586-3598

178. Ow SY, Salim M, Noirel J, Evans C, Rehman I, Wright PC. iTRAQ Underestimation in Simple and Complex Mixtures: “The Good, the Bad and the Ugly”. Journal of proteome research 2009, 8: 5347-5355

179. Sandberg A, Branca RMM, Lehtiö J, Forshed J. Quantitative accuracy in mass spectrometry based proteomics of complex samples: The impact of labeling and precursor interference. Journal of proteomics 2014, 96: 133-144

180. Karp NA, Huber W, Sadowski PG, Charles PD, Hester SV, Lilley KS. Addressing Accuracy and Precision Issues in iTRAQ Quantitation. Molecular & Cellular Proteomics 2010, 9: 1885-1897

181. McAlister GC, Nusinow DP, Jedrychowski MP, Wühr M, Huttlin EL, Erickson BK, Rad R*, et al.* MultiNotch MS3 Enables Accurate, Sensitive, and Multiplexed Detection of Differential Expression across Cancer Cell Line Proteomes. Analytical chemistry 2014, 86: 7150-7158

Chapter II

Chemical proteomics uncovers EPHA2 as a mechanism of acquired resistance to small molecule EGFR kinase inhibition

Summary

Tyrosine kinase inhibitors (TKIs) have become an important therapeutic option for treating several forms of cancer. Gefitinib, an inhibitor of the epidermal growth factor receptor (EGFR), is in clinical use for treating non-small cell lung cancer (NSCLC) harboring activating EGFR mutations. However, despite high initial response rates, many patients develop resistance to gefitinib. The molecular mechanisms of TKI resistance often remain unclear. Here, a chemical proteomic approach comprising kinase affinity purification (Kinobeads) and quantitative mass spectrometry for the identification of kinase inhibitor resistance mechanisms in cancer cells is described. The previously described amplification of MET was found together with a more than 10-fold overexpression of EPHA2 ($p<0.001$) in gefitinib resistant HCC827 cells suggesting a potential role in development of resistance. siRNA mediated EPHA2 knockdown or treating cells with the multi-kinase inhibitor dasatinib restored sensitivity to gefitinib. Of all dasatinib targets, EPHA2 exhibited the most drastic effect ($p<0.001$). In addition, EPHA2 knockdown or Ephrin-A1 treatment of resistant cells decreased FAK phosphorylation and cell migration. These findings confirm EPHA2 as an actionable drug target, provide a rational basis for drug combination approaches and indicate that chemical proteomics is broadly applicable for the discovery of kinase inhibitor resistance.

Introduction

Protein kinases are involved in regulating signaling networks important for cell growth, proliferation and survival [1]. Over the past 15 years, drug development in oncology has become increasingly focused on molecularly targeted therapies using e.g. kinase inhibitors to modulate deregulated signaling pathways. The number of small molecule kinase inhibitors in clinical trials has increased rapidly with more than 150 such drugs under investigation to date. About two dozen kinase inhibitors have by now been approved for use in humans and some of them have reached blockbuster status with sales of more than one billion dollars per year [2].However, acquired drug resistance has been observed in a wide variety of indications and is one of main reasons for tumor progression after initial response. Several molecular mechanisms have been found that allow the tumor to evade drug mediated cell death such as drug efflux via ABC transporters [3], deregulation of apoptosis [4], epithelial-to-mesenchymal transition (EMT) [5], secondary mutations leading to decreased drug binding [6] or activation of alternative pro-survival pathways. The latter may take the form of ‘kinome reprogramming’ [7-9] which could be caused either by intrinsic or extrinsic cellular factors. For example, kinase upregulation has been described as an intrinsic mechanism [7] while e. g. growth factors provided by the tumor microenvironment constitute an extrinsic signal, both of which can result in activation of alternative pro-survival pathways [10].

Small molecule inhibitors of the epidermal growth factor receptor (EGFR) such as gefitinib often show a good (up to 75%) overall initial response in patients with activating EGFR mutations. Disappointingly, the median progression free survival is typically less than one year [11] because the vast majority of patients eventually develop acquired drug resistance constituting a major drawback in the management of the disease [12]. The so-called T790M gatekeeper mutation in EGFR often occurs in response to gefitinib and erlotinib [13, 14] for which second and third generation molecules have been developed [15, 16]. Amplification of wild type EGFR [17] or activation of bypass pathways in response to EGFR inhibition are further well-known acquired resistance mechanisms. Examples for the latter include upregulation of the receptor tyrosine kinases and proto-oncogenes hepatocyte growth factor receptor MET [18, 19], insulin-like growth factor-1 receptor (IGF1R) [20] and fibroblast growth factor receptor 1 (FGFR1) [8, 21]. In addition, MET activation by endogenous hepatocyte growth factor (HGF) has been described as a potential rapidly occurring and short term resistance mechanism [22].

While assessing the mutational status of EGFR has proven to be powerful [23-25] and has led to the development of next generation drugs with demonstrated clinical benefit [26], less systematic effort has been expended to identify resistance mechanisms caused by reprogramming of the kinome [7]. This is however attractive as kinases represent actionable targets with rich chemical matter suitable to address these. Therefore, a chemical proteomics approach was undertaken to employ kinome affinity enrichment using the kinobead technology [27, 28] in conjunction with quantitative mass spectrometry to profile the expression of kinases on the protein level in three distinct gefitinib sensitive and corresponding resistant cell lines. The approach confirmed previous findings and enabled the identification of ephrin receptor A2 (EPHA2) as a novel kinase conferring gefitinib resistance in non-small cell lung cancer (NSCLC). This finding enabled a rational drug combination treatment using pharmacological inhibition of EPHA2 which in turn restored gefitinib sensitivity of the cells. Collectively, the data further suggests that the kinobead approach is broadly applicable and may be of generic utility for the identification of kinase driven resistance mechanisms.

Experimental procedures

Cell culture and lysate preparation

The EGFR mutant (del E746_A750) NSCLC cell lines HCC827 and HCC827 GR (GR for gefitinib resistant) were kindly provided by Dr. P. Jäne and have been previously characterized [18]. The human epidermoid carcinoma cell lines A431 and A431 GR (gefitinib resistant) as well as the head and neck carcinoma cell lines HN11 and HN11 GR (gefitinib resistant) were a gift from Dr. J. Engelman and have been previously described [29]. All cells were maintained in RPMI-1640 medium supplemented with 10% (v/v) heat-inactivated fetal bovine serum (FBS) (PAA) in a humidified incubator under 10% CO_2 at 37 °C. Cells were grown to 80-90% confluency, washed twice with ice-cold PBS and lysed with 1 x compound pulldown (CP) buffer (50 mM Tris/HCl pH 7.5, 5% Glycerol, 1.5 mM $MgCl_2$, 150 mM NaCl, 1 mM Na_3VO_4, 25 mM NaF, 0.8% NP-40) containing protease (Roche Applied Science, Mannheim, Germany) and phosphatase inhibitors (Phosphatase Inhibitor Cocktail 1, 2, 3, Sigma-Aldrich). Lysates were then clarified by centrifugation at 6,000 x g at 4 °C for 15 min. Protein concentration was determined by the Coomassie (Bradford) protein assay kit (Thermo Scientific). All samples were stored at -80 °C until further analysis.

Affinity purification and protein digestion

Kinobead pulldowns from control and resistant cell lysates were performed in triplicate as previously described [27, 30]. Briefly, cell lysates were diluted with equal volumes of 1 x CP buffer to reduce detergent concentration to 0.4% NP-40 and cleared by ultracentrifugation at 52,000 x g and 4 °C for 20 min. For pulldown experiments, 100 µl of in house synthesized Kinobeads were incubated with 5 mg cleared lysates on an end-over-end tube rotator for 1 h at 4 °C. After washing the beads in CP buffer, bound proteins were eluted with 2 x NuPAGE LDS sample buffer (Invitrogen) containing 50 mM DTT, boiled for 30 min at 50 °C and subsequently alkylated with 55 mM IAA for 30 min in the dark. Then, samples were run about 1 cm into a 4–12% Bis-Tris NuPAGE gel (Invitrogen). Gels were stained with colloidal Coomassie blue (Sigma-Aldrich) and bands were excised and subjected to in-gel digestion using trypsin (Promega). Finally, tryptic peptides were dried in a vacuum concentrator and stored at -20 °C prior to LC-MS/MS analysis.

LC-MS/MS analysis

LC-ESI-MS/MS was performed on a LTQ-Orbitrap XL (Thermo Scientific) mass spectrometer coupled to a nanoLC-Ultra (Eksigent) chromatography system. Peptide digest (10 µl in 0.1% formic acid, FA) was loaded on a trap column (ReproSil-PUR C18-AQ, 5 µm 20 mm x 100 µm ID, Dr. Maisch) at 5 µL/min using solvent A (0.1% FA in HPLC grade water). Chromatographic separation was performed using an analytical column (ReproSil-PUR C18-AQ, 3 µm 40 mm x 75 µm ID, Dr. Maisch) at 300 nL/min using a linear gradient from 2-35% solvent B (0.1% FA in acetonitrile) over 210 min. The eluent was introduced into the mass spectrometer via emitter tips (PicoTip) using a nano-electrospray ion source (Proxeon Biosystems). The mass spectrometer was operated in positive ion mode and programmed to acquire in data dependent mode, automatically switching between MS and MS/MS. Full scan spectra were acquired in the Orbitrap recording a window between 300 and 1500 m/z at a resolution of 60,000 (at m/z 400) after ion accumulation to a target value of 500,000. The five most intense precursor ions were selected for collision-induced dissociation (CID) in the linear ion trap (LTQ) at a normalized collision energy of 35% following precursor ion accumulation to a target value of 10,000 for max. 500 ms. Internal calibration was enabled for MS mode using the ion signal of $(Si(CH_3)_2O)_6$ as a lock mass.

Data analysis

For intensity-based label free protein quantification, the Maxquant software (v.1.4.0.5) was used [31]. Briefly, raw data files of biological replicates were searched against a concatenated forward-decoy protein sequence database (Uniprot, version 2013_07_22, 88,354 sequences) and modified to contain PFAM annotations for each entry. The parameters used for database search were as follows: a precursor ion tolerance of ±20 ppm was used for the first search and a tolerance of ±4.5 ppm was allowed for the main search, MS/MS tolerance was set to ±0,5 Da. The search included cysteine carbamidomethylation as a fixed modification and oxidation of methionine and N-terminal protein acetylation as variable modifications. Enzyme specificity was set to trypsin and up to two missed cleavage sites were allowed. The match between runs option was enabled and unique and razor peptides were used for protein quantification with at least two peptides to count a protein ratio. A false discovery rate of 1% was applied to peptides and proteins and the minimum peptide length was seven amino acids. Protein intensities were log transformed and proteins that did not contain three valid values in the resistance or control group were removed. Remaining missing values were imputed using values derived from the intensity distribution close to the detection limit of the mass spectrometer. To simulate this distribution, mean and standard deviation of the actual intensities were used and a down shift of 1.8 standard deviations and a width of 0.3 standard deviations was applied in the in the Perseus software. From the resulting list of protein identifications, only protein kinases were further considered in two sample t-tests to identify significantly regulated kinases.

Cell viability assays

Gefitinib (Iressa) and dasatinib (Sprycel) were purchased from LC Laboratories and the c-MET inhibitor PHA665752 was obtained from Tocris Bioscience. Stock solutions of all drugs were prepared in DMSO and stored at -20 °C. Cells were seeded in 96-well plates at a concentration of $5x10^3$ cells/well with complete culture medium and allowed to adhere to the plate overnight. At the next day, cells were exposed to TKIs (10 nM to 10 µM) or 0.1% DMSO (vehicle control) for 72 h at 37 °C in 10% CO_2. Cell proliferation assays were performed using the XTT Cell Proliferation Kit II (Roche) according to the manufacturer's instructions. Each combination of cell line and drug concentration was set up in four replicates and repeated at least three times. Data were visualized using GraphPad Prism v.5.01 and EC_{50} curves were fitted using a non-linear regression model with a sigmoidal dose response characteristic.

Western blotting

EGFR, p-EGFR (Y1068), MET, p-MET (Y1234/1235), FAK and AURORA antibodies were purchased from Cell Signaling Technology (provided by New England Biolabs) and EPHA2, IGF1R, DDR1, SCR, p-FAK (Y576) and α-tubulin antibodies were obtained from Santa Cruz. For immunoblot analysis, cell lysates were boiled in LDS buffer containing 100 mM DTT for 10 min at 95 ˚C, resolved on 4–12% Bis-Tris NuPAGE gels, and transferred to PVDF membranes (Invitrogen, Darmstadt, Germany). Membranes were blocked in 2% BSA in TBS for 1 h and incubated with primary antibodies overnight at 4 °C. After incubation with secondary antibodies (IRDye 800 goat anti-rabbit or anti-mouse, LI-COR), proteins were visualized and quantified using the LI-COR Odyssey Infrared Imaging Scanner and the Imaging software v.3.0 (LI-COR Biosciences).

Transfection of small interfering RNA

The small interfering RNA (siRNA) reagents were purchased from Qiagen. Interferin in vitro siRNA transfection protocol was performed (Polyplus Tranfection) following manufacturer instructions. Briefly, one day before the transfection, HCC827-C and GR cells were seeded in 96 well plates at a density of $9x10^3$ cells/ml. Next day, siRNA was diluted in serum-free medium and combined with Interferin transfection reagent, and applied to the cells along with fresh medium. Controls included cells that were mock transfected (i.e., no siRNA). Cell viability assays or cell lysis was performed after four days as described above. For western blot analysis, 10^5 cells were seeded in 6-well plates. The siRNA concentrations used in the described experiments were twice the values recommended by the manufacturer.

Ephrin-A1-Fc treatment

For Ephrin stimulation experiments, cells grown in 10% FBS were stimulated with Ephrin-A1-Fc or Fc alone for control cells (R&D Systems). For cell viability, cells were exposed to Ephrin-A1-Fc (0.01-1.0 µg/ml) or 1.0 µg/ml Fc (control) for 72 h at 37 °C in 10% CO_2. For western blots, cells were stimulated either with 1.0 µg/ml Ephrin-A1-Fc or Fc for 2 h.

Cell migration and invasion assay

ThinCert cell culture inserts (8 µm pore size, Greiner Bio-One GmbH) were used for cell migration and invasion assays following manufacturer instructions. For invasion assays, the bottom side of the filter inserts was coated with 0,5 mg/ml collagen A (Biochrom) and was dried overnight under laminar air flow. Parental and resistant HCC827 cells were seeded at $1x10^5$ cells/ml in T25 flasks. Next day, cells were transfected with EPHA2 siRNA, Ephrin-A1-Fc stimulated (as described above) or left untreated. After four days, cells were starved in serum-free culture medium overnight. Next day, cells ($8x10^4$ cells/well) in serum-free medium were plated into the upper chamber and 10% FBS was added as a chemoattractant in the lower chambers. Four replicates for each condition were performed. After 20 h of incubation, cells remaining in the upper chamber were removed by a cotton swab. Fixed cells were stained with the fluorescein derivative calcein-AM (Invitrogen) for 45 min and detached from the insert membrane with Accutase (PAA). Cell migration was quantified by measuring the fluorescence of the stained cells at excitation wavelength of 485 nm and an emission wavelength of 520 nm using a FLUO star Omega (BMG Labtech) fluorimeter.

Results

Chemical proteomic strategy for the identification of kinome reprogramming

In order to identify kinome reprogramming processes in gefitinib resistant cells, I used the approach depicted in Fig. 1. Gefitinib sensitive cells were grown in culture over an extended period of time (6-8 months) in the presence of increasing concentrations of the EGFR inhibitor gefitinib until the cells were entirely resistant to the drug. Kinases from lysates of sensitive and resistant cells were affinity purified using Kinobeads and subsequently identified by tandem mass spectrometry and quantified by intensity based label free quantification.

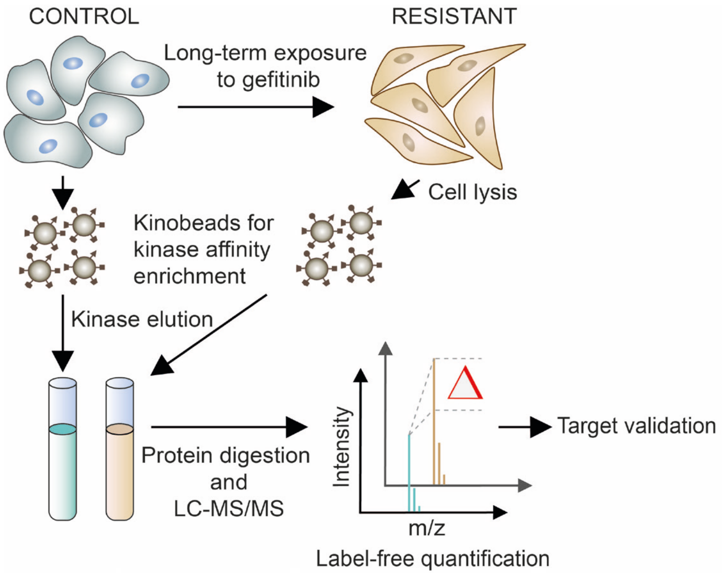
CONTROL
RESISTANT
Long-term exposure to gefitinib
Cell lysis
Kinobeads for kinase affinity enrichment
Kinase elution
Protein digestion and LC-MS/MS
Intensity
m/z
Δ
Target validation
Label-free quantification

Figure 1: Workflow for the elucidation of kinome reprogramming events driving acquired drug resistance mechanisms. Gefitinib resistant cells were generated by long term exposure to the drug. Lysates of parental and resistant cells were then subjected to a kinase affinity enrichment using Kinobeads. Subsequently, kinase expression profiles were obtained by label free quantitative mass spectrometry.

To exemplify the approach three different EGFR dependent cell lines that have been previously used were selected to identify resistance mechanisms to EGFR inhibition [18, 29]. The choice of cell lines further aimed to reflect the variance in EGFR expression and mutational status found in patients with EGFR driven tumors irrespective of the tumor entity. First, the NSCLC cell line HCC827 that harbors the EGFR activating mutation E746_A750del; second, the epidermoid carcinoma cell line A431 which expresses very high levels of wild type EGFR and third, the head and neck cancer cell line HN11 that moderately overexpresses wild type EGFR. Long term exposure of HCC827 cells to gefitinib led to complete resistance. While the control cell line HCC827-C was killed at an effective concentration (EC_{50}) of 20 nM, the gefitinib resistant cell line, HCC827-GR was viable at 10 µM of the drug (Fig. 2A). The results of the measurement of kinase protein expression changes using Kinobeads and LC-MS/MS (performed in biological triplicate) are represented as volcano plots in figure 2. Volcano plots show the magnitude of a change (on the x-axis) and the statistical significance of that change (expressed as a p-value on the y-axis). It is evident that numerous changes in kinase expression take place in gefitinib resistant cells and that the types of kinases and the magnitude of the expression changes vary between the cell lines. Both mass spectrometry of proteins captured on Kinobeads (Fig. 3A) as well as western blot analysis from lysates of HCC827-GR cells (Fig. 3B) showed a five-fold increase in MET expression which is a known resistance mechanism in this cell line [18]. Levels of EGFR itself were virtually unchanged but EPHA2 expression was massively upregulated (16-fold, $p<<0.01$). As shown below this is a novel mechanism by which HCC827 cells become gefitinib resistant. Further significantly regulated kinases include the cell cycle kinase AURKA, the SRC familiy kinases SRC and CSK (up) as well as the tyrosine kinases FYN and several members of different kinase families (down). Gefitinib resistant A431 cells (Fig. 3C, D) showed a 40-fold reduction in responsiveness to gefitinib in comparison to their sensitive counterpart (A431-C, EC_{50}=0.13 µM; A431-GR, EC_{50}=5.78 µM; Fig. 2B). Here, a robust upregulation of EGFR, PRKCD and IGF1R was observed while other kinases including EPHA2, PTK2B, DDR1 and SRC were found to be down regulated.

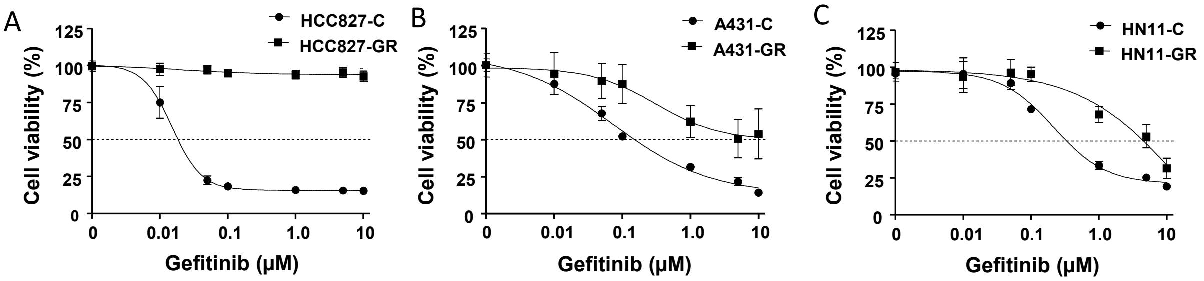

Figure 2: Cell viability assays of the parental and resistant cell line models. A) EGFR overexpressing cell line A431. B) Head and neck cell line HN11 and C) HCC827 cell line expressing EGFR activating mutation del E746_A750.

The gefitinib resistant head and neck cancer cell line HN11 exhibited an almost ten-fold reduction in sensitivity to gefitinib (HN11-C, EC_{50}=0.51µM; HN11-GR, EC_{50}=4.26µM; Fig. 2C) and its kinome profile showed increased CIT, IGF1R, DDR1, PRKC1 and MARK2 expression while EPHA2 and EPHB2 expression is significantly reduced in this cell line and no change was detected for EGFR (Fig. 3E, F).

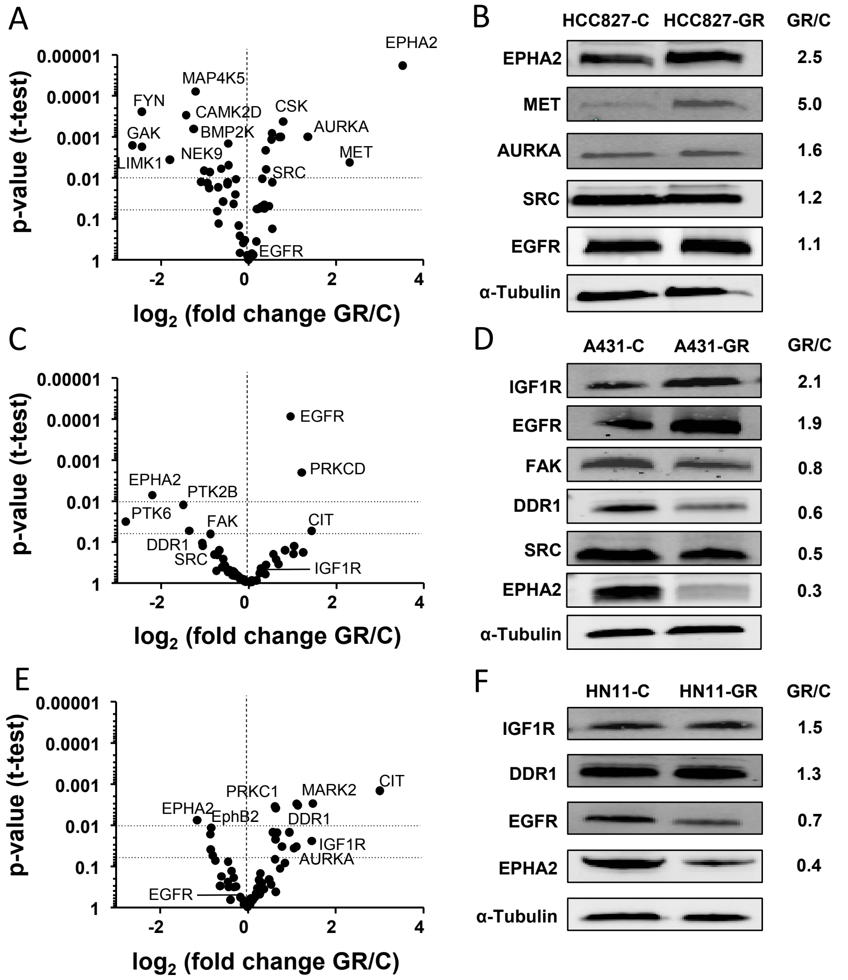

Figure 3: Kinase expression analysis in gefitinib sensitive and resistant cell line models. A) Differentially regulated kinases found in HCC827 control (C) and gefitinib resistant (GR) cells using kinobead enrichment and quantitative mass spectrometry. B) Western blot analysis of regulated kinases in lysates of HCC827 cells. C, D) Same as in panel A, B but for A431 cells. E, F) Same as in panel A, B but for HN11 cells.

HCC827 cells are a well-accepted in-vitro cell line model for studying the effects of EGFR activating mutations in NSCLC. In addition, gefitinib and erlotinib are first line treatments in patients with such genetic lesions. Based on the striking upregulation of EPHA2 in the gefitinib resistant HCC827 cell line, it can be hypothesized that EPHA2 may be directly involved in creating gefitinib resistance in these cells.

Pharmacological inhibition of EPHA2 restores sensitivity of HCC827-GR cells to gefitinib

To test the hypothesis that EPHA2 overexpression is driving the proliferation of HCC82-GR cells, cells were treated with the potent but unselective EPHA2 inhibitor dasatinib [32]. Control cells (HCC827-C) responded to dasatinib treatment with an EC_{50} of 109 nM and to gefitinib with an EC_{50} of 22 nM (Fig.4A) demonstrating that these cells are sensitive to both drugs.

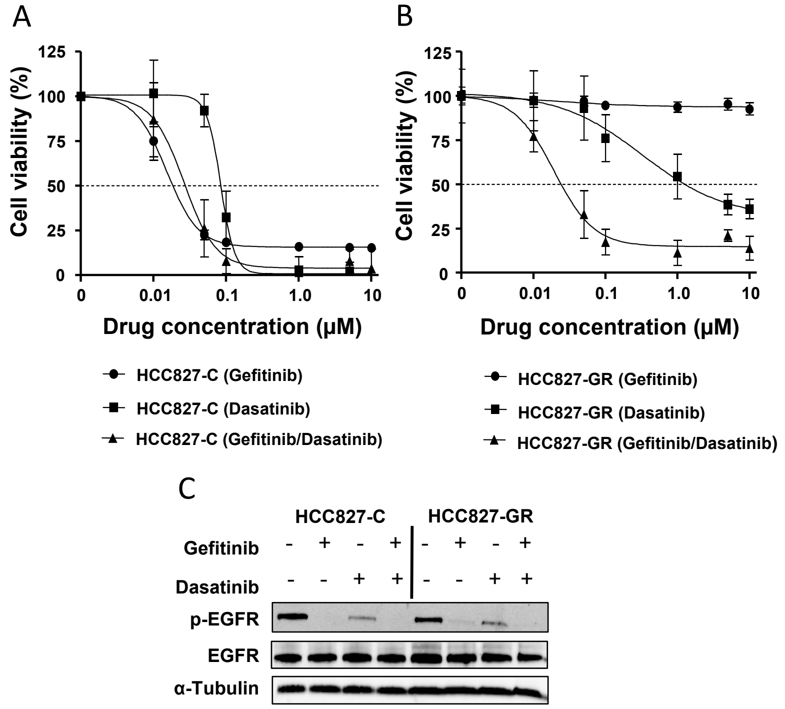

Figure 4: Combination treatment of gefitinib and dasatinib restores gefitinib sensitivity in HCC827-GR cells. A) HCC827-C cells are responsive to gefitinib and dasatinib in the low nanomolar range. B) HCC827-GR cells are not at all responsive to gefitinib and only poorly responsive to the multi kinase inhibitor dasatinib which is a potent inhibitor of EPHA2. Dasatinib does however completely restore the sensitivity to gefitinib in HCC827-GR cells. C) EGFR activation is fully blocked by gefitinib in HCC827-C and in HCC827-GR cells. Dasatinib only leads to a partial block of EGFR activity and the combination of gefitinib and dasatinib fully blocks EGFR activity.

Combining both compounds had no additive effect in these cells (EC_{50}= 25 nM). In contrast, dasatinib treatment of HCC827-GR cells was only weakly effective in inhibiting cell viability (EC_{50}= 2.3 µM) and gefitinib was entirely ineffective at 10 µM. However, the combination of both drugs effectively killed the cells with an EC_{50} value of 27 nM strongly indicating that inhibition of a dasatinib target is driving resistance and is responsible for restoring gefitinib sensitivity in these cells (Fig.4B).This is supported by immunoblot analysis showing that gefitinib alone completely abrogated EGFR autophosphorylation (pY1068) in both HCC827-C and HCC827-GR cells. Dasatinib alone showed a partial block of Tyr-1068 phosphorylation and the drug combination again completely blocked pY1068 phoshporylation (Fig. 4C).

Silencing EPHA2 expression in HCC827 GR cells restores gefitinib sensitivity

The strong overexpression of EPHA2 in HCC827-GR and the ability of dasatinib to restore gefitinib sensitivity suggested EPHA2 to be responsible for the observed effect. This interpretation is however not entirely conclusive as no selective EPHA2 inhibitor is available and dasatinib has many targets. To assure that resistance in HCC827-GR cells is indeed mediated by EPHA2, the expression of EPHA2 and other dasatinib targets was silenced using siRNA (Fig. 5A). EPHA2 and EGFR protein knockdown was efficient in HCC827 cells (Fig. 5A) and EPHA2 knockdown in HCC827-GR cells resulted in the reduction of cell viability by more than 50%. In contrast, EPHA2 knockdown in HCC827-C cells had no influence on cell viability ($p<0.001$; Fig. 5B). Knockdown of nine other dasatinib targets including EGFR, SRC and ephrin receptor familiy members did not result in strong differences in cell viability between HCC827-C and HCC827-GR cells, indicating that EPHA2 rather than other dasatinib targets is responsible for driving gefitinib resistance (Fig.5 B). This was confirmed by data showing that knocking down EPHA2 in HCC827-GR cells restored gefitinib sensitivity to levels similar to those of the parental HCC827-C cells (EC_{50}= 37 nM; Fig. 5C). Apparently, HCC827-GR could not be killed completely in this setting suggesting the presence of an additional growth signal. Further experiments similar to the ones above showed that this signal is provided by MET overexpression. Treatment of HCC827-GR cells with the potent MET inhibitor PHA665752 had no effect on EGFR phosphorylation or cell viability but the combination with gefitinib killed cells with an EC_{50}= 79 nM (Fig. 5D). Similarly, siRNA knockdown of MET expression also restored gefitinib sensitivity (EC_{50}= 39 nM, Fig. 5E). These data suggest that MET and EPHA2 are parallel drivers of gefitinib resistance. Unfortunately, no additive effects could be detected when simultaneously knocking down EPHA2 and MET or any combination of

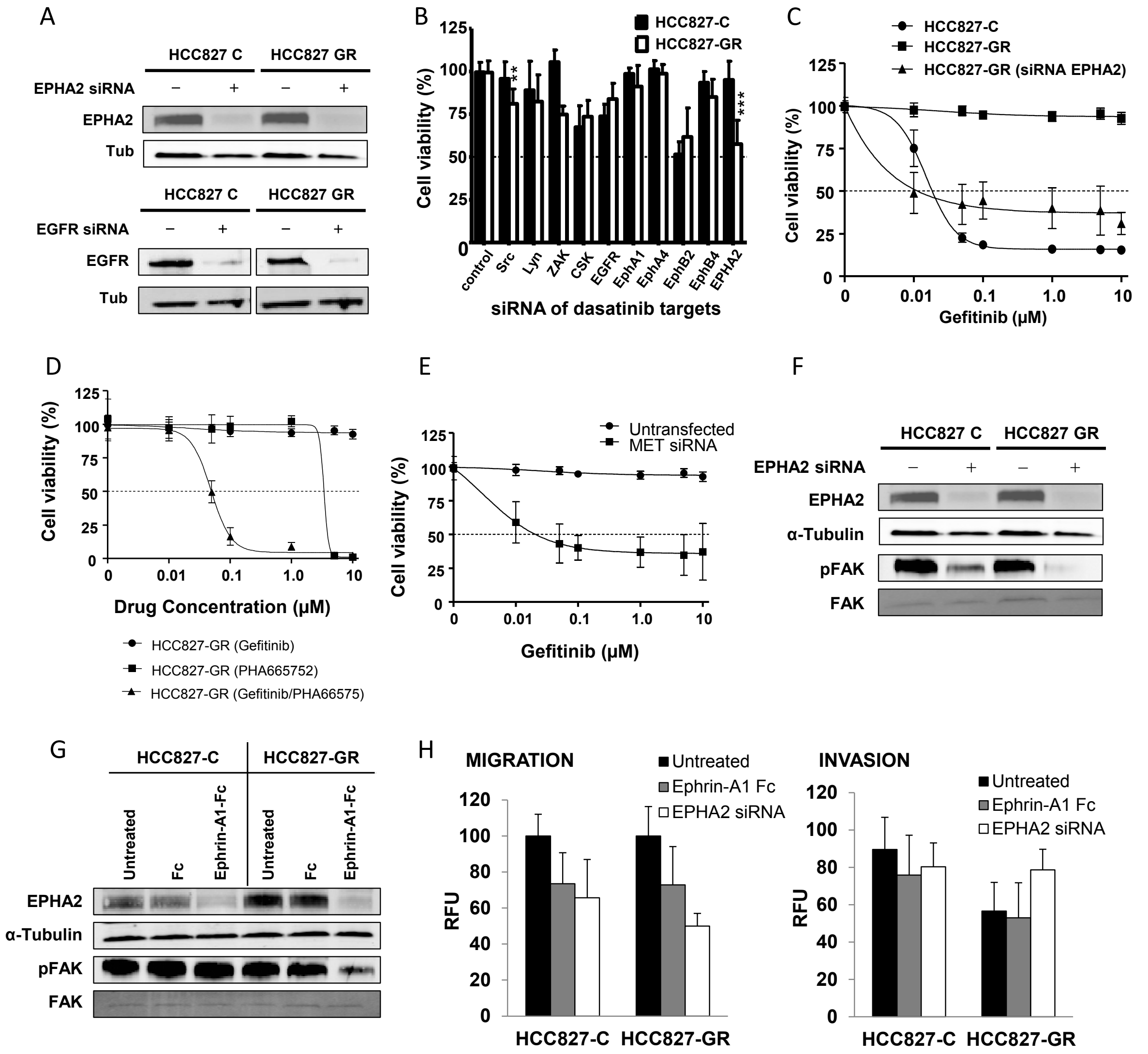

Figure 5: Silencing of EPHA2 expression in HCC827-GR cells restores gefitinib sensitivity. A) Knockdown of EPHA2 and EGFR by siRNA in HCC827-C and HCC827-GR cells. B) Knockdown of EPHA2 shows the most significant effect on cell viability among all known dasatinib targets in HCC827-GR cells ($p<0.001$). C) EPHA2 knockdown substantially restores sensitivity of HCC827-GR cells to gefitinib. D) Gefitinib responsive HCC827 cells only respond to the MET inhibitor in high concentrations. E) Gefitinib dose response after MET siRNA knockdown. F) EPHA2 knockdown decreases FAK phosphorylation but has a more pronounced effect in HCC827-GR. G) Ligand stimulation using Ephrin-A1 Fc has only effects on FAK phosphorylation in HCC827-GR. H) Knockdown and Ephrin-A1 ligand stimulation of EphA2 decreases cellular motility without a difference between HCC827-C and HCC827-GR cells. Invasion is not influenced by EphA2 knockdown or Ephrin-A1 ligand stimulation.

EGFR, MET and EPHA2 because it was impossible to achieve simultaneous full knockdown of the proteins. As a result, sufficient residual kinase activity remained in the system to allow a part of the cell population to survive. Apart from events occurring at the cell surface, the data also indicates widespread changes in the intracellular kinome. Activation of the protein focal adhesion kinase FAK often promotes tumor survival [33] and controls migration and the invasiveness of tumor cells [34]. EPHA2 forms a complex with FAK in resting cells and Ephrin-A1 ligand binding results in dephosphorylation of FAK and subsequent dissociation of the FAK-EPHA2 complex in Ephrin forward signaling [35]. It was therefore investigated if FAK signaling is also involved in gefitinib resistant cells. FAK was phosphorylated at Y576 in both untransfected HCC827-C and HCC827-GR cells (Fig. 5F). Upon EPHA2 knockdown, pFAK 576 was diminished in HCC827-C and almost undetectable in HCC827-GR cells. Stimulating EPHA2 with its endogenous ligand Ephrin-A1-Fc did not decrease pFAK in gefitinib sensitive cells but markedly decreased pFAK in HCC827-GR cells (Fig. 5G). This reduced signaling via FAK is consistent with the observation that the migration (but not invasion) of HCC827 cells was reduced when knocking down EPHA2 or treating cells with Ephrin-A1-Fc (Fig. 5H). The reduced migration phenotype was somewhat more pronounced in HCC827-GR cells but likely is a consequence of the very high EPHA2 expression in these cells rather than contributing gefitinib resistance itself.

Discussion

Using kinase affinity enrichment coupled to label free quantitative mass spectrometry, overexpression of known EGFR resistance markers including MET [18, 36] and IGFR-1 [20] in gefitinib resistant cell line models could be confirmed. These findings validate that the approach can be used to uncover kinase reprogramming events that drive drug resistance. In addition, EPHA2 overexpression as a novel mechanism that triggers resistance to gefitinib in NSCLC cells with EGFR activating mutations was found. The EPHA2 overexpression in the resistant cell line models HN11 and A431 that overexpress moderate and high amounts of wild type EGFR respectively could not be detected. This leads to the conclusion that EPHA2 is not a mechanism of resistance in these cells. However, EPHA2 is increasingly emerging as a drug target in solid tumors not only in cells with EGFR activating mutations. Wu et al. reported differential expression of EPHA2 in a panel of head and neck cancer cell lines in which EPHA2 overexpressing cells could be killed by pharmacological inhibition or siRNA knockdown of EPHA2 [30]. It has also been found that inhibition of EPHA2 expression can induce apoptosis in NSCLC cells and tumor regression in human NSCLC xenografts [37]. Other reports show that there are significant correlations between EPHA2 expression and (reduced) overall survival in patients with breast cancer and NSCLC [38, 39]. EPHA2 has previously also been linked to cancer resistance. Zhuang et al. found EPHA2 overexpression in trastuzumab resistant epidermal growth factor receptor-2 (HER2) expressing breast cancer cells. They could further show that antibody mediated inhibition of EPHA2 restored sensitivity towards trastuzumab [40]. The results now show that this is not an isolated case but that EPHA2 overexpression in NSCLC cells can drive resistance formation and that inhibition of this growth signal results in restoring sensitivity to EGFR inhibition. Combination treatment with gefitinib and dasatinib in resistant cells restored the EC_{50} of around 20 nM observed for the treatment of the gefitinib sensitive cells. The serum concentration of dasatinib in patients is between 20-200 nM [41], and for gefitinib between 100-600 nM and even up to 16 μM in the tumor tissue [42, 43]. The concentrations of drug used for combination treatment are therefore fully within the normal therapeutic range. Besides EPHA2, the study also recapitulated the previous observation that MET expression can lead to gefitinib resistance [44] and the data presented in this report indeed suggest that both mechanisms are at work in parallel in HCC827-GR cells. Gusenbauer et al. showed that EPHA2 is upregulated upon HGF mediated MET stimulation indicating a possible interdependence of EPHA2 and MET expression [44]. Irrespective of this possibility, the data showed that knocking down or pharmacologically inhibiting

EPHA2 in cells that massively overexpress the protein strongly reduces cell viability, indicating oncogene addiction of these cells to EPHA2.

The results obtained here and elsewhere can be summarized in a model (Fig. 6) in which the three receptor tyrosine kinases EGFR, MET and EPHA2 functionally interact to mediate gefitinib resistance in HCC827 cells. In the sensitive cell line, EGFR is the only growth promoting signal which can be abrogated by gefitinib. In the resistant cells, the kinase domain of EGFR is blocked by the drug (no phosphorylation rendering EGFR inactive; Fig. 4C). In this situation, one (or both) of the other two RTKs provides the kinase activity to signal cell survival. Given that neither the EPHA2 drug dasatinib nor the MET inhibitor PHA66575 alone have the ability to kill gefitinib resistant cells, it can be postulated that heterodimers of EGFR/MET and EGFR/EPHA2 are the signaling competent units in the resistant cell line. This notion is supported by literature showing that EGFR and EPHA2 [44, 45] as well as EGFR and MET can physically interact [46, 47].

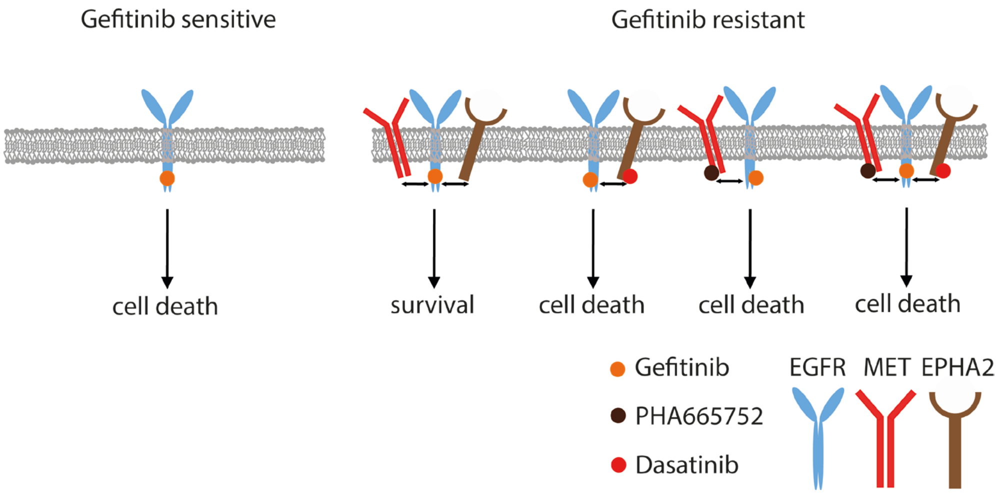

Figure 6: Proposed simplified model for gefitinib resistance in HCC827GR cells. Gefitinib induces cell death in sensitive cells. Inhibition of EGFR alone has no effect on the viability of resistant cells because EGFR may form signaling competent heterodimers or multimers with EPHA2 or MET. Co-inhibition of EGFR and EPHA2 or MET therefore restores gefitinib sensitivity.

There are further RTKs that show upregulation in resistant cell lines investigated in this and other studies. IGF1R [21] and AXL [48] are known cases and DDR1 overexpression has been observed as part of this study (Fig 2E, F). In addition, overexpression of many RTKs has been found associated with poor prognosis [20, 49] [38, 39, 50]. It is therefore tempting to speculate that RTKs can generally mediate resistance to RTK drugs. This would offer opportunities for personalized medicine approaches that stratify patients according to their RTK profile and, in turn, lead to the selection of drug combinations that may be effective in breaking, delaying, circumventing or preventing acquired drug resistance.

Acknowledgments

I am indebted to Estela Del Castillo Busto for conduction of experiments, Andreas Klaus for preparation of in-gel digestions and Karl Kramer for discussions.

Abbreviations

-C	Gefitinib sensitive
CID	Collision induced dissociation
Da	Dalton
DTT	Dithiothreitol
EMT	Epithelial-to-mesenchymal transition
-GR	Gefitinib resistant
IAA	Iodo acetamide
LTQ	Linear ion trap
MS/MS	Fragment mass spectrum from MS1 precursor
NSCLC	Non-small cell lung cancer
PFAM	Protein Families
ppm	Parts per million
RTK	Receptor tyrosine kinase
siRNA	Small interfering RNA

References

1. Lemmon MA, Schlessinger J. Cell signaling by receptor tyrosine kinases. Cell 2010, 141: 1117-1134
2. Cohen P, Alessi DR. Kinase drug discovery--what's next in the field? ACS chemical biology 2013, 8: 96-104
3. Shukla S, Chen ZS, Ambudkar SV. Tyrosine kinase inhibitors as modulators of ABC transporter-mediated drug resistance. Drug resistance updates : reviews and commentaries in antimicrobial and anticancer chemotherapy 2012, 15: 70-80
4. Miyashita T, Reed JC. bcl-2 gene transfer increases relative resistance of S49.1 and WEHI7.2 lymphoid cells to cell death and DNA fragmentation induced by glucocorticoids and multiple chemotherapeutic drugs. Cancer research 1992, 52: 5407-5411
5. Yao Z, Fenoglio S, Gao DC, Camiolo M, Stiles B, Lindsted T, Schlederer M*, et al.* TGF-beta IL-6 axis mediates selective and adaptive mechanisms of resistance to molecular targeted therapy in lung cancer. Proceedings of the National Academy of Sciences of the United States of America 2010, 107: 15535-15540
6. Bresler SC, Wood AC, Haglund EA, Courtright J, Belcastro LT, Plegaria JS, Cole K*, et al.* Differential inhibitor sensitivity of anaplastic lymphoma kinase variants found in neuroblastoma. Science translational medicine 2011, 3: 108ra114
7. Duncan JS, Whittle MC, Nakamura K, Abell AN, Midland AA, Zawistowski JS, Johnson NL*, et al.* Dynamic reprogramming of the kinome in response to targeted MEK inhibition in triple-negative breast cancer. Cell 2012, 149: 307-321
8. Ware KE, Hinz TK, Kleczko E, Singleton KR, Marek LA, Helfrich BA, Cummings CT*, et al.* A mechanism of resistance to gefitinib mediated by cellular reprogramming and the acquisition of an FGF2-FGFR1 autocrine growth loop. Oncogenesis 2013, 2: e39
9. Kampen KR, Ter Elst A, Mahmud H, Scherpen FJ, Diks SH, Peppelenbosch MP, de Haas V*, et al.* Insights in dynamic kinome reprogramming as a consequence of MEK inhibition in MLL-rearranged AML. Leukemia 2014, 28: 589-599
10. Wilson TR, Fridlyand J, Yan Y, Penuel E, Burton L, Chan E, Peng J*, et al.* Widespread potential for growth-factor-driven resistance to anticancer kinase inhibitors. Nature 2012, 487: 505-509
11. Morita S, Okamoto I, Kobayashi K, Yamazaki K, Asahina H, Inoue A, Hagiwara K*, et al.* Combined survival analysis of prospective clinical trials of gefitinib for non-small cell lung cancer with EGFR mutations. Clinical cancer research 2009, 15: 4493-4498
12. Wagle N, Emery C, Berger MF, Davis MJ, Sawyer A, Pochanard P, Kehoe SM*, et al.* Dissecting therapeutic resistance to RAF inhibition in melanoma by tumor genomic profiling. Journal of clinical oncology : official journal of the American Society of Clinical Oncology 2011, 29: 3085-3096
13. Kobayashi S, Boggon TJ, Dayaram T, Janne PA, Kocher O, Meyerson M, Johnson BE*, et al.* EGFR mutation and resistance of non-small-cell lung cancer to gefitinib. The New England journal of medicine 2005, 352: 786-792
14. Pao W, Miller VA, Politi KA, Riely GJ, Somwar R, Zakowski MF, Kris MG*, et al.* Acquired resistance of lung adenocarcinomas to gefitinib or erlotinib is associated with a second mutation in the EGFR kinase domain. PLoS medicine 2005, 2: e73
15. Li D, Ambrogio L, Shimamura T, Kubo S, Takahashi M, Chirieac LR, Padera RF*, et al.* BIBW2992, an irreversible EGFR/HER2 inhibitor highly effective in preclinical lung cancer models. Oncogene 2008, 27: 4702-4711

16. Cross DA, Ashton SE, Ghiorghiu S, Eberlein C, Nebhan CA, Spitzler PJ, Orme JP*, et al.* AZD9291, an irreversible EGFR TKI, overcomes T790M-mediated resistance to EGFR inhibitors in lung cancer. Cancer discovery 2014, 4: 1046-1061

17. Sequist LV, Waltman BA, Dias-Santagata D, Digumarthy S, Turke AB, Fidias P, Bergethon K*, et al.* Genotypic and histological evolution of lung cancers acquiring resistance to EGFR inhibitors. Science translational medicine 2011, 3: 75ra26

18. Engelman JA, Zejnullahu K, Mitsudomi T, Song Y, Hyland C, Park JO, Lindeman N*, et al.* MET amplification leads to gefitinib resistance in lung cancer by activating ERBB3 signaling. Science 2007, 316: 1039-1043

19. Turke AB, Zejnullahu K, Wu YL, Song Y, Dias-Santagata D, Lifshits E, Toschi L*, et al.* Preexistence and clonal selection of MET amplification in EGFR mutant NSCLC. Cancer cell 2010, 17: 77-88

20. Peled N, Wynes MW, Ikeda N, Ohira T, Yoshida K, Qian J, Ilouze M*, et al.* Insulin-like growth factor-1 receptor (IGF-1R) as a biomarker for resistance to the tyrosine kinase inhibitor gefitinib in non-small cell lung cancer. Cellular oncology 2013,

21. Terai H, Soejima K, Yasuda H, Nakayama S, Hamamoto J, Arai D, Ishioka K*, et al.* Activation of the FGF2-FGFR1 autocrine pathway: a novel mechanism of acquired resistance to gefitinib in NSCLC. Molecular cancer research 2013, 11: 759-767

22. Wang W, Li Q, Yamada T, Matsumoto K, Matsumoto I, Oda M, Watanabe G*, et al.* Crosstalk to stromal fibroblasts induces resistance of lung cancer to epidermal growth factor receptor tyrosine kinase inhibitors. Clinical cancer research : an official journal of the American Association for Cancer Research 2009, 15: 6630-6638

23. Sorensen BS, Wu L, Wei W, Tsai J, Weber B, Nexo E, Meldgaard P. Monitoring of epidermal growth factor receptor tyrosine kinase inhibitor-sensitizing and resistance mutations in the plasma DNA of patients with advanced non-small cell lung cancer during treatment with erlotinib. Cancer 2014,

24. Janjigian YY, Smit EF, Groen HJ, Horn L, Gettinger S, Camidge DR, Riely GJ*, et al.* Dual Inhibition of EGFR with Afatinib and Cetuximab in Kinase Inhibitor-Resistant EGFR-Mutant Lung Cancer with and without T790M Mutations. Cancer discovery 2014, 4: 1036-1045

25. Boeckx C, Weyn C, Vanden Bempt I, Deschoolmeester V, Wouters A, Specenier P, Van Laer C*, et al.* Mutation analysis of genes in the EGFR pathway in Head and Neck cancer patients: implications for anti-EGFR treatment response. BMC research notes 2014, 7: 337

26. Sequist LV, Yang JC, Yamamoto N, O'Byrne K, Hirsh V, Mok T, Geater SL*, et al.* Phase III study of afatinib or cisplatin plus pemetrexed in patients with metastatic lung adenocarcinoma with EGFR mutations. Journal of clinical oncology : official journal of the American Society of Clinical Oncology 2013, 31: 3327-3334

27. Bantscheff M, Eberhard D, Abraham Y, Bastuck S, Boesche M, Hobson S, Mathieson T*, et al.* Quantitative chemical proteomics reveals mechanisms of action of clinical ABL kinase inhibitors. Nature biotechnology 2007, 25: 1035-1044

28. Medard G, Pachl F, Ruprecht B, Klaeger S, Heinzlmeir S, Helm D, Qiao H*, et al.* Optimized chemical proteomics assay for kinase inhibitor profiling. Journal of proteome research 2015,

29. Guix M, Faber AC, Wang SE, Olivares MG, Song Y, Qu S, Rinehart C*, et al.* Acquired resistance to EGFR tyrosine kinase inhibitors in cancer cells is mediated by loss of IGF-binding proteins. The Journal of clinical investigation 2008, 118: 2609-2619

30. Wu Z, Doondeea JB, Gholami AM, Janning MC, Lemeer S, Kramer K, Eccles SA*, et al.* Quantitative chemical proteomics reveals new potential drug targets in head and neck cancer. Molecular & cellular proteomics : MCP 2011, 10: M111 011635

31. Cox J, Mann M. MaxQuant enables high peptide identification rates, individualized p.p.b.-range mass accuracies and proteome-wide protein quantification. Nature biotechnology 2008, 26: 1367-1372

32. Chang Q, Jorgensen C, Pawson T, Hedley DW. Effects of dasatinib on EphA2 receptor tyrosine kinase activity and downstream signalling in pancreatic cancer. British journal of cancer 2008, 99: 1074-1082

33. Zhao J, Guan JL. Signal transduction by focal adhesion kinase in cancer. Cancer metastasis reviews 2009, 28: 35-49

34. Mitra SK, Hanson DA, Schlaepfer DD. Focal adhesion kinase: in command and control of cell motility. Nature reviews Molecular cell biology 2005, 6: 56-68

35. Miao H, Burnett E, Kinch M, Simon E, Wang B. Activation of EphA2 kinase suppresses integrin function and causes focal-adhesion-kinase dephosphorylation. Nature cell biology 2000, 2: 62-69

36. Bean J, Brennan C, Shih JY, Riely G, Viale A, Wang L, Chitale D*, et al.* MET amplification occurs with or without T790M mutations in EGFR mutant lung tumors with acquired resistance to gefitinib or erlotinib. Proceedings of the National Academy of Sciences of the United States of America 2007, 104: 20932-20937

37. Amato KR, Wang S, Hastings AK, Youngblood VM, Santapuram PR, Chen H, Cates JM*, et al.* Genetic and pharmacologic inhibition of EPHA2 promotes apoptosis in NSCLC. The Journal of clinical investigation 2014, 124: 2037-2049

38. Brantley-Sieders DM, Jiang A, Sarma K, Badu-Nkansah A, Walter DL, Shyr Y, Chen J. Eph/ephrin profiling in human breast cancer reveals significant associations between expression level and clinical outcome. PloS one 2011, 6: e24426

39. Brannan JM, Dong W, Prudkin L, Behrens C, Lotan R, Bekele BN, Wistuba I*, et al.* Expression of the receptor tyrosine kinase EphA2 is increased in smokers and predicts poor survival in non-small cell lung cancer. Clinical cancer research : an official journal of the American Association for Cancer Research 2009, 15: 4423-4430

40. Zhuang G, Brantley-Sieders DM, Vaught D, Yu J, Xie L, Wells S, Jackson D*, et al.* Elevation of receptor tyrosine kinase EphA2 mediates resistance to trastuzumab therapy. Cancer research 2010, 70: 299-308

41. Demetri GD, Lo Russo P, MacPherson IR, Wang D, Morgan JA, Brunton VG, Paliwal P*, et al.* Phase I dose-escalation and pharmacokinetic study of dasatinib in patients with advanced solid tumors. Clinical cancer research : an official journal of the American Association for Cancer Research 2009, 15: 6232-6240

42. Swaisland HC, Smith RP, Laight A, Kerr DJ, Ranson M, Wilder-Smith CH, Duvauchelle T. Single-dose clinical pharmacokinetic studies of gefitinib. Clinical pharmacokinetics 2005, 44: 1165-1177

43. McKillop D, Partridge EA, Kemp JV, Spence MP, Kendrew J, Barnett S, Wood PG*, et al.* Tumor penetration of gefitinib (Iressa), an epidermal growth factor receptor tyrosine kinase inhibitor. Molecular cancer therapeutics 2005, 4: 641-649

44. Gusenbauer S, Vlaicu P, Ullrich A. HGF induces novel EGFR functions involved in resistance formation to tyrosine kinase inhibitors. Oncogene 2013, 32: 3846-3856

45. Larsen AB, Pedersen MW, Stockhausen MT, Grandal MV, van Deurs B, Poulsen HS. Activation of the EGFR gene target EphA2 inhibits epidermal growth factor-induced cancer cell motility. Molecular cancer research 2007, 5: 283-293

46. Mueller KL, Yang ZQ, Haddad R, Ethier SP, Boerner JL. EGFR/Met association regulates EGFR TKI resistance in breast cancer. Journal of molecular signaling 2010, 5: 8

47. Li L, Puliyappadamba VT, Chakraborty S, Rehman A, Vemireddy V, Saha D, Souza RF*, et al.* EGFR wild type antagonizes EGFRvIII-mediated activation of Met in glioblastoma. Oncogene 2015, 34: 129-134

48. Zhang Z, Lee JC, Lin L, Olivas V, Au V, LaFramboise T, Abdel-Rahman M*, et al.* Activation of the AXL kinase causes resistance to EGFR-targeted therapy in lung cancer. Nature genetics 2012, 44: 852-860

49. Miao L, Zhu S, Wang Y, Li Y, Ding J, Dai J, Cai H*, et al.* Discoidin domain receptor 1 is associated with poor prognosis of non-small cell lung cancer and promotes cell invasion via epithelial-to-mesenchymal transition. Medical oncology 2013, 30: 626

50. Strimpakos A, Pentheroudakis G, Kotoula V, De Roock W, Kouvatseas G, Papakostas P, Makatsoris T*, et al.* The prognostic role of ephrin A2 and endothelial growth factor receptor pathway mediators in patients with advanced colorectal cancer treated with cetuximab. Clinical colorectal cancer 2013, 12: 267-274 e262

Chapter III

Phosphoproteome profiling reveals molecular mechanisms of growth factor mediated kinase inhibitor resistance in EGFR overexpressing cancer cells

Summary

Although substantial progress has been made regarding the use of molecularly targeted cancer therapies, resistance almost invariably develops and presents a major clinical challenge. To evade the selective pressure of kinase inhibitors, cells often activate bypass signaling tracks and become intrinsically resistant. Apart from intrinsic cellular adaptation, the tumor microenvironment can rescue cancer cells by growth factor mediated induction of pro-survival signaling. In this study, I show that EGFR inhibition by gefitinib is counteracted by several growth factors notably FGF2 and I assessed the global molecular consequences of FGF2 mediated gefitinib resistance at the proteome and phosphoproteome level. Multiplexed tandem mass tag (TMT) peptide labeling in conjunction with high resolution tandem mass spectrometry allowed the identification and quantification of ~22,000 phosphopeptides and ~8,800 proteins in biological triplicates without missing values. The data shows that gefitinib treated cells are forced into developing intrinsic resistance by reprogramming of the proteome and phosphoproteome, whereas co-treatment with FGF2 largely reverts these changes to resemble the molecular composition of untreated cells. Simultaneous small molecule EGFR and FGFR inhibition overcomes FGF2 induced gefitinib resistance and the phosphoproteomic experiments further prioritized the RAS/MEK/ERK axis as well as the PI3K/mTOR axis for combination treatment. Consequently, the MEK inhibitor trametinib prevented FGF2 mediated survival of EGFR inhibitor resistant cells when used in combination with gefitinib. Surprisingly, the phase II PI3K/mTOR inhibitor GSK2126458/omipalisib reversed resistance mediated by all four growth factors tested, making it an interesting candidate for targeting the survival signals provided by the tumor microenvironment.

Introduction

The epidermal growth factor receptor (EGFR, ERBB1) is a member of the ERBB family of receptor tyrosine kinases (RTKs). It is expressed in many cell types and is important for cell proliferation and differentiation [1]. Ligand induced dimerization of EGFR monomers or heterodimerization with other members of the ERBB family results in autophosphorylation and activated downstream signaling [2, 3]. The EGFR assumes a central role in the tumorigenesis of many solid tumor types and is often highly expressed [4, 5]. In fact, treatment with selective EGFR inhibitors has become an important strategy for treating non-small cell lung cancer (NSCLC) patients [6] harboring activating mutations in EGFR and approved therapies for NSCLC include first line treatment with the EGFR inhibitors gefitinib and erlotinib as monotherapy [7, 8]. The utility of EGFR inhibitors for treating other tumor entities has been intensively investigated but the treatment often lacks clinical benefits [9-11]. This is because EGFR activating mutations are often absent in other tumor entities and result in only partial or no dependency on this particular oncogenic pathway. Furthermore, tumor cells are often intrinsically resistant or acquire resistance to kinase inhibitors by adaptive reprogramming of the proteome and/or their cellular signaling pathways. Multiple kinases have previously been shown to be adaptively upregulated in response to EGFR kinase inhibition leading to a resistant phenotype. These proteins include the EGFR dimerization partners ERBB2 and ERBB3 [12], hepatocyte growth factor receptor (MET) [13, 14], insulin like growth factor receptor (IGF1R) [15], ephrin receptor A2 (EPHA2) [16] or fibroblast growth factor receptor (FGFR1) [17, 18]. Kinome reprogramming in response to MEK and ERBB2 inhibition has been characterized by proteomics in some detail and has also revealed a large heterogeneity of adaptive changes [19, 20]. Beside these intrinsic adaptive changes, it is well known that cellular survival signaling can be reactivated by stimulation of RTKs by factors present in the tumor microenvironment or secreted by tumor cells as an autocrine mechanism [17, 21, 22]. These factors can activate bypass signaling pathways and thereby lead to resistance to the original drug. The extent to which growth factors can drive tumor resistance to kinase inhibitors was recently impressively demonstrated and revealed an extensive molecular redundancy in both RTK signaling and resistance mechanisms to targeted oncogene inhibition [23].

To improve the molecular understanding of adaptive response and growth factor mediated resistance mechanisms to EGFR inhibition, I investigated the global changes occurring at the protein expression and protein phosphorylation level in response to EGFR inhibition and/or growth factor stimulation. By using multiplexed tandem mass tag (TMT) labeling of peptides [24] and quantification by high resolution tandem mass spectrometry, I obtained a detailed map of alterations occurring under circumstances of kinase inhibition and growth factor mediated resistance formation. I found multiple kinases and transcription factors among the upregulated proteins in response to EGFR inhibition. Changes in protein phosphorylation partially reflect the changes in protein abundance, but there is extensive additional adaptation at the level of protein activity that is not discernable from the protein abundance level measurements. The phenotypically observed rescue from EGFR inhibition by FGF2 treatment was mirrored at the molecular level by rapid restoration of protein phosphorylation abundance (and thus signaling capacity) to base line for many proteins. The data confirms the widely accepted view that bypass signaling constitutes a common resistance mechanism and the date set provides a valuable resource of molecular information for this process. In addition, the data also prioritized signaling nodes as targets for drug combination treatments and highlights how simultaneous targeting of EGFR/FGFR, EGFR/MEK or PI3K can break FGF2 mediated resistance to EGFR inhibition.

Experimental procedures

Cell viability and proliferation assays

Assays were performed in 96-well plates with each well containing 3,000 cells. On day 0, A431 epidermoid cancer cells were seeded in RPMI-1640, supplemented with 4% heat-inactivated fetal bovine serum (FBS, Biochrom). The next day, FBS was diluted to 2% with RPMI-1640 before the cells were exposed to different drugs and growth factors. Gefitinib (LC Laboratories), saracatinib, trametinib, AZD5364, AZD4547, OSI906, NVP-BEZ235 and GSK2126458 (all from Selleckchem) were used in concentrations ranging from 10 nM to 5 μM, while IGF1, HGF, FGF2 and EGF (all from Peprotech) were added at 50 ng/ml. The cells were then incubated for 72 h at 37 °C and 5% CO_2. Subsequently, cell viability and proliferation assays were performed using the XTT cell proliferation kit II (Roche) according to the manufacturer instructions. The XTT assay measures the quantity of formazan salt that is generated by metabolically active cells from the XTT reagent using colorimetry. Accordingly, this assay does not distinguish between viability and proliferation. For simplicity, I refer to viability throughout this thesis, acknowledging that this may also mean proliferation.

Cell culture and cell lysis

Epidermoid A431 cancer cells were cultivated in RPMI-1640, supplemented with 10% (v/v) heat-inactivated FBS (Biochrom) in a humidified atmosphere at 5% CO_2 and 37 °C. For stimulation and inhibition experiments, the cells were plated onto 150 mm cell culture dishes in RPMI-1640 containing only 4% FBS (day 0). The next day, FBS was diluted to 2% with RPMI-1640 and the cells were treated with 0.1% DMSO, 1 μM gefitinib or 1 μM gefitinib together with 50 ng/ml IGF1, HGF, FGF2 or EGF (Peprotech), respectively. At the end of day 3, the cells were washed two times with PBS (Sigma Aldrich) and were subsequently lysed by scraping in the presence of 400 μl lysis buffer (40 mM Tris/HCl pH 7.6, 8 M urea, EDTA-free protease inhibitor complete mini from Roche, phosphatase inhibitor cocktail 1, 2 and 3 from Sigma Aldrich at 1 x final concentration according to the manufacturer instructions). Afterwards, the lysate was transferred into reaction vessels and homogenized for one minute using a sonotrode (Branson) set to 50% amplitude and 30 pulses per minute at 4 °C. The protein concentration was determined with a Bradford assay (Pierce).

Protein digestion and peptide purification

A total of 200 µg of protein per experimental condition was used for digestion. Disulfide bonds were reduced with DTT at a final concentration of 10 mM for 45 min at 37 °C. Cysteine residues were alkylated using 55 mM chloroacetamide for 30 min at room temperature in the dark. The sample was diluted with three volumes of 40 mM Tris/HCl pH 7.6 to decrease the urea concentration to 1.5 M. Trypsin was added to a protease-to-protein ratio of 1:50 (w/w) and digestion was performed for 4 h at 37 °C and 700 rpm using a thermoshaker. A second aliquot of trypsin was added, again at a ratio of 1:50 (w/w) and the samples were incubated at 37 °C overnight. The following day, the samples were cooled to room temperature and acidified using 0.5% TFA. Following the precipitation of insoluble debris at 5000 x g, the supernatant was desalted using 50 mg Sep-Pak columns (Waters) and a vacuum manifold. Columns were primed with 1 ml of solvent B (0.07% TFA, 50% ACN) and equilibrated with 2 ml solvent A (0.07% TFA in deionized water). The sample was then slowly passed through the column to allow proper peptide binding. Peptides were washed three times with 1 ml solvent A and then eluted into a reaction vessel using 2 times 150 µl solvent B. Finally, the samples were frozen at -80 °C and dried to completeness in a speed vac.

Peptide labeling using tandem mass tags (TMT10)

Lyophilized peptides (200 µg) were dissolved for 10 min at 700 rpm in 62 µl of 50 mM TEAB buffer (Sigma Aldrich). TMT reagents (Thermo Scientific) were dissolved in water-free ACN at a concentration of 60 mM. Afterwards, 12.5 µl TMT solution was added to each of the 9 samples, resulting in a final concentration of 10 mM TMT. The samples were incubated at 700 rpm for 1 h at room temperature before the labeling reaction was stopped by adding hydroxylamine to a concentration of 0.4%. Following 15 min incubation at room temperature, the samples were acidified and diluted with 0.07% TFA in deionized water to dilute the ACN concentration to below 1%. The samples were then desalted according to the procedure described above. In order to correct for potential sample loss and varying labeling efficiency, a labeling test was performed by measuring defined sample mixtures by LC-MS/MS. Peptides were then mixed in equimolar ratios for proteomic and phosphoproteomic analysis.

Phosphopeptide enrichment using Fe-IMAC columns

Phosphopeptide enrichment was essentially performed as previously described [25]. Briefly, a Fe-IMAC column (ProPac IMAC-10 column, 4 x 50 mm, Thermo Scientific) was charged with Fe^{3+} ions using 3 ml $FeCl_3$ (Sigma Aldrich). Next, the column was equilibrated with solvent A (30%

ACN, 0.07% TFA) and connected to an Aekta FPLC system (GE Healthcare). Subsequently, 1.5 mg TMT-labeled peptides were reconstituted in 500 µl solvent A and loaded onto the column (5 min, 0.2 ml/min). Peptides were eluted with solvent B (0.3% NH_4OH) in a stepwise gradient of 0-16% (5-6.72 min, 3 ml/min), 16-26.25% (6.7-11.7 min, 0.55 ml/min), 26.25-50% (11.7-12.35 min, 3 ml/min), and 12.35-15 min 0% (3 ml/min). The phosphopeptide-containing fraction (UV) was collected in a reaction vessel (1 ml) and was evaporated to dryness in a speed vac.

High pH reversed-phase micro-column fractionation for phosphopeptides

High pH reversed-phase micro-columns were prepared in 200 µl pipette tips. Five discs (Ø 1.5 mm) of C18 material (3M Empore) per micro-column were squeezed into a 200 µl pipette tip that was fixed in a 1.5 ml reaction vessel. All solvents were passed through the columns by centrifugation. Columns were primed with 40 µl 50% ACN, 25 mM NH_4COOH (pH 10) and equilibrated with two times 40 µl 25 mM NH_4COOH (pH 10). The sample was then slowly passed through the column and the flow-through was collected and applied to a low pH micro-column for desalting as described previously [26]. Peptides were fractionated using solvents with increasing ACN concentrations (5%, 7.5%, 10%, 12.5%, 15%, 17.5% and 50% ACN in 25 mM NH_4COOH, pH10 respectively). The desalted flow-through was combined with the 17.5% fraction and the 50% fraction was combined with the 5% fraction, leading to a total of six fractions. The fractionated samples were dried down prior to mass spectrometric analysis.

Hydrophilic strong anion exchange chromatography (hSAX) for peptide fractionation

For full proteome analysis, peptides were fractionated using hydroxide-selective anion-exchange chromatography as described previously [27]. Briefly, an IonPac AS24, analytical column and IonPac AG24 guard column (2 x 250 mm and 2 x 50 mm, Thermo Scientific) were connected to a Dionex Ultimate 3000 HPLC system (Thermo Scientific). A total amount of 300 µg TMT-labeled peptides was loaded onto the column in solvent A (5 mM Tris/HCl pH 8.5) and was eluted at a flow rate of 0.25 ml/min using solvent B (5 mM Tris/HCl pH 8.5, 1 M NaCl) in a two-step gradient (0-3 min 0% B, 3-27 min 27% B, 27-40 min 100% B). Fraction collection was initiated after two minutes and was continued for 36 minutes. The UV-trace was used to estimate the amount of peptides and neighboring fractions with low intensity were pooled, resulting in 24 fractions. Fractions were acidified by adding 0.5% FA and were transferred to pre-equilibrated micro-columns for desalting as previously described [26].

LC-MS/MS

Peptides were reconstituted in 0.1% FA and phosphopeptides were reconstituted in 0.1% FA and 50 mM citric acid, in order to chelate residual Fe^{3+}-ions. LC-MS/MS measurements were performed by coupling an Eksigent NanoLC-Ultra $1D^+$ to a Q-Exactive Plus mass spectrometer. Peptides were delivered to a trap column (ID 75 µm, ReproSil-Gold 120 C18 3 µm, Dr. Maisch) for 10 min at a flow rate of 5 µl/min in loading solvent (0.1% FA in water). Peptides were then separated on the analytical column using a 110 min gradient (solvent A: 0.1% FA, 5% DMSO; solvent B: 0.1% FA, 5% DMSO in ACN) at a flow rate of 300 nl/min (0 - 2 min: 2 - 4% B; 102 min: 32% B; 103 min - 106 min: 80% B, 107 min: 2%). For phosphopeptides, we used a shallower two-step gradient as follows: 0 - 2 min: 2 - 4% B; 70 min 15% B, 102 min: 27% B, 103-106 min 80% B, 107 min: 0% B. The Q-Exactive Plus was operated in data-dependent mode, automatically switching between MS1 and MS2. Full-scan MS1 spectra were acquired at 360 to 1300 m/z, 70,000 resolution, automatic gain control (AGC) target value of 3×10^6 charges and a maximum injection time of 100 ms. Up to 20 precursor ions were selected for fragmentation. MS2 spectra were acquired at 200 to 2000 m/z at 35,000 resolution to enable resolution of all TMT labels, AGC target value of 2×10^5 charges and maximum injection time of 50 ms. Precursor ion isolation width was fixed at 1.3 Th and dynamic exclusion was set to 20 s.

Experimental design and statistical rational

Proteomic experiments were performed in three biological replicates per experimental condition (DMSO control, gefitinib treatment and gefitinib treatment plus FGF2 stimulation), allowing analysis in a single TMT9-plex experiment. Under the assumption that the total sum of all protein and phosphopeptide intensities per TMT channel is the same across all channels, we used total-sum normalization to correct these intensities for systematic experimental bias. Since the data were log-normally distributed, we used a one-way ANOVA test on log2-transformed intensities to identify proteins and phosphopeptides with differential abundance at an FDR of 1% (Benjamini-Hochberg correction was applied).

Data analysis

MaxQuant [28] version 1.5.2.8 was used together with its integrated search engine Andromeda [29] for the analysis of LC-MS/MS data. Raw files were searched against the UniProtKB database (v.22.07.13, containing 88,381 entries). Carbamidomethylated cysteine was set as a fixed modification. For raw files of phosphopeptide fractions, phosphorylation of serine, threonine and tyrosine, as well as oxidation of methionine and N-terminal protein acetylation were allowed as variable modifications. For raw files of full proteome fractions, only oxidation of methionine and N-terminal protein acetylation were allowed as variable modifications. Enzyme specificity was set to trypsin/P, allowing for cleavage after proline to account for in-source fragmentation. The minimum peptide length was set to seven amino acids and a maximum of two missed-cleavages were allowed. Quantification was performed on TMT reporter ions for protein and phosphopeptide analysis. All tandem mass tags were corrected for their isotopic impurities. The mass tolerance was set to 4.5 ppm for precursor ions and to 20 ppm for fragment ions. The dataset was adjusted to 1% FDR on the level of proteins and peptide spectrum matches (PSMs). Data were further processed using Perseus (v. 1.5.1.6, Max Plank Institute of Biochemistry, Munich), Microsoft Excel, GraphPad Prism and the R statistical programming environment. Known potential contaminants were excluded from analysis. Phosphopeptides identified with Andromeda scores below 40 and site-localization probabilities of less than 0.75 (class I sites) were not considered for further analysis. Significantly differentially regulated proteins and phosphopeptides were used to perform GO-term and KEGG pathway enrichment analysis using DAVID [30]. Regulated sites were analyzed for phosphoprotein interactions using the gene identifiers and STRING (combined score >0.4) [31]. Networks were exported and visualized with Cytoscape (v 3.1). Large networks were further characterized using the Cytoscape plugin clustermaker [32] and GLay community clustering [33]. Networkin was used to predict kinases substrate relationships (min. score = 3) [34]. Data of cell viability assays were analyzed using GraphPad Prism v.5.01. Four parameter logistic models and nonlinear regression analysis were applied to fit dose-response curves and calculate EC_{50} values.

Results and Discussion

Growth factors can mediate resistance to EGFR inhibition

The EGFR overexpressing cell line A431 was treated with increasing concentrations of the EGFR inhibitor gefitinib resulting in a clear inhibition of cell growth and viability (Fig. 1). Addition of growth factors to the cell culture medium (50 ng/ml) mitigated the inhibitory effect of gefitinib. While the effect was weak for IGF1 (Fig. 1A), treatment with HGF (Fig. 1B) clearly improved cell viability and treatment with FGF2 (Fig. 1C) led to complete gefitinib resistance. In contrast, treatment with EGF sensitized cells for killing by gefitinib (Fig. 1D), an observation that has been made before in EGFR overexpressing cells [35]. Although the underlying mechanisms are not fully understood, the effect can at least in part be attributed to an induction of apoptosis potentially via suppression of the DNA damage repair [36].

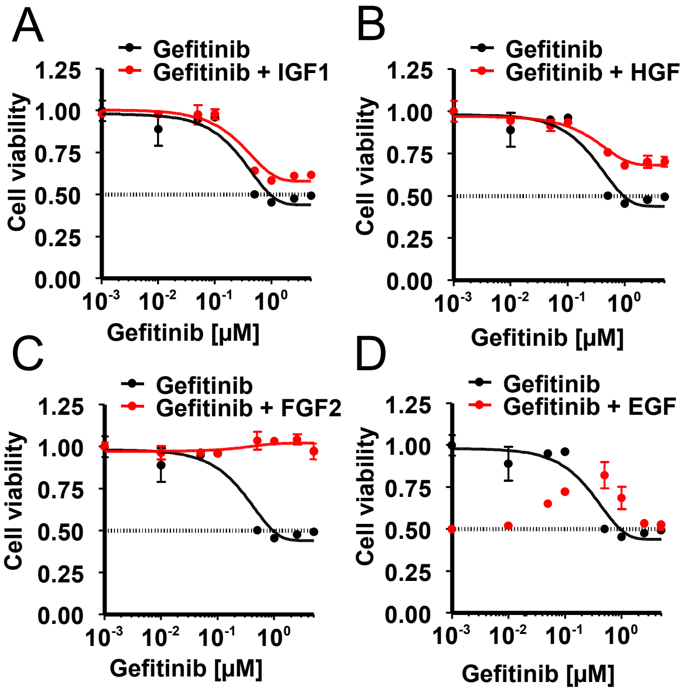

Figure 1: Cell viability as a function of gefitinib and growth factor treatment. A431 cells were treated with increasing concentrations of gefitinib alone or in combination with 50 ng/ml each of IGF1 (panel A), HGF (panel B), FGF2 (panel C) or EGF (panel D). While FGF2 completely prevented cell death by gefitinib, EGF treatment sensitized cells to the kinase inhibitor. Error bars represent the standard deviation (SD) of triplicate experiments.

The above data clearly shows that FGF2 provides a strong survival signal to the cells that is independent of EGFR possibly involving FGF receptors and/or further pro-survival pathways. This cellular system may therefore provide a simplified model for studying bypass signaling routes induced by soluble growth factors present in tumor microenvironments [21, 37]. To shed light on the molecular mechanisms involved, I set up an experiment in which I performed a three way comparison of the proteomes and phosphoproteomes of human epidermoid A431 cancer cells treated for three days with vehicle (DMSO), gefitinib and gefitinib plus FGF2 (Fig. 2A). Each experiment was performed in biological triplicates. Following protein extraction and digestion, each of the nine resulting peptide pools (corresponding to 200 µg protein per experiment) was labeled with a different stable isotope encoded TMT reagent and all peptides were pooled. TMT labeled peptides were separated into 24 fractions by hydrophilic strong anion exchange chromatography [27] and each fraction was analyzed by a 2 h LC-MS/MS experiment on a Q-Exactive Plus mass spectrometer. In parallel, phosphopeptides were enriched using an Fe-IMAC HPLC column [25] and the isolated phosphopeptides were separated into six fractions using high pH reversed-phase stage tips [26] and analyzed in a technical duplicate by the aforementioned LC-MS/MS setup. Principal component analysis of both data sets indicated good overall quality as biological replicates clustered tightly together and the three different experiments were well separated from each other. The analysis also showed that the molecular signatures of DMSO treated cells and FGF2/gefitinib treated cells are much closer to each other (~15%, PC1) than to the gefitinib treated cells (~60%, PC2). The PCA analysis clearly mirrored the phenotypic data in that FGF2 can protect cells from gefitinib mediated effects and that it largely restores protein abundance and protein activity levels. However, there are also differences between the untreated cells (DMSO control) and FGF2/gefitinib treated cells (PC1 axis), indicating that the molecular changes induced by gefitinib are not fully reverted by the growth factor treatment (Fig. 2B). In the proteomics workflow, ~8,800 proteins and in the phosphoproteomics workflow ~23,309 phosphopeptides corresponding to ~16,306 phosphorylation sites (~13,410 class I sites and 133 pY sites, Fig. 2C) were quantified across all experimental conditions (i. e. no missing values).

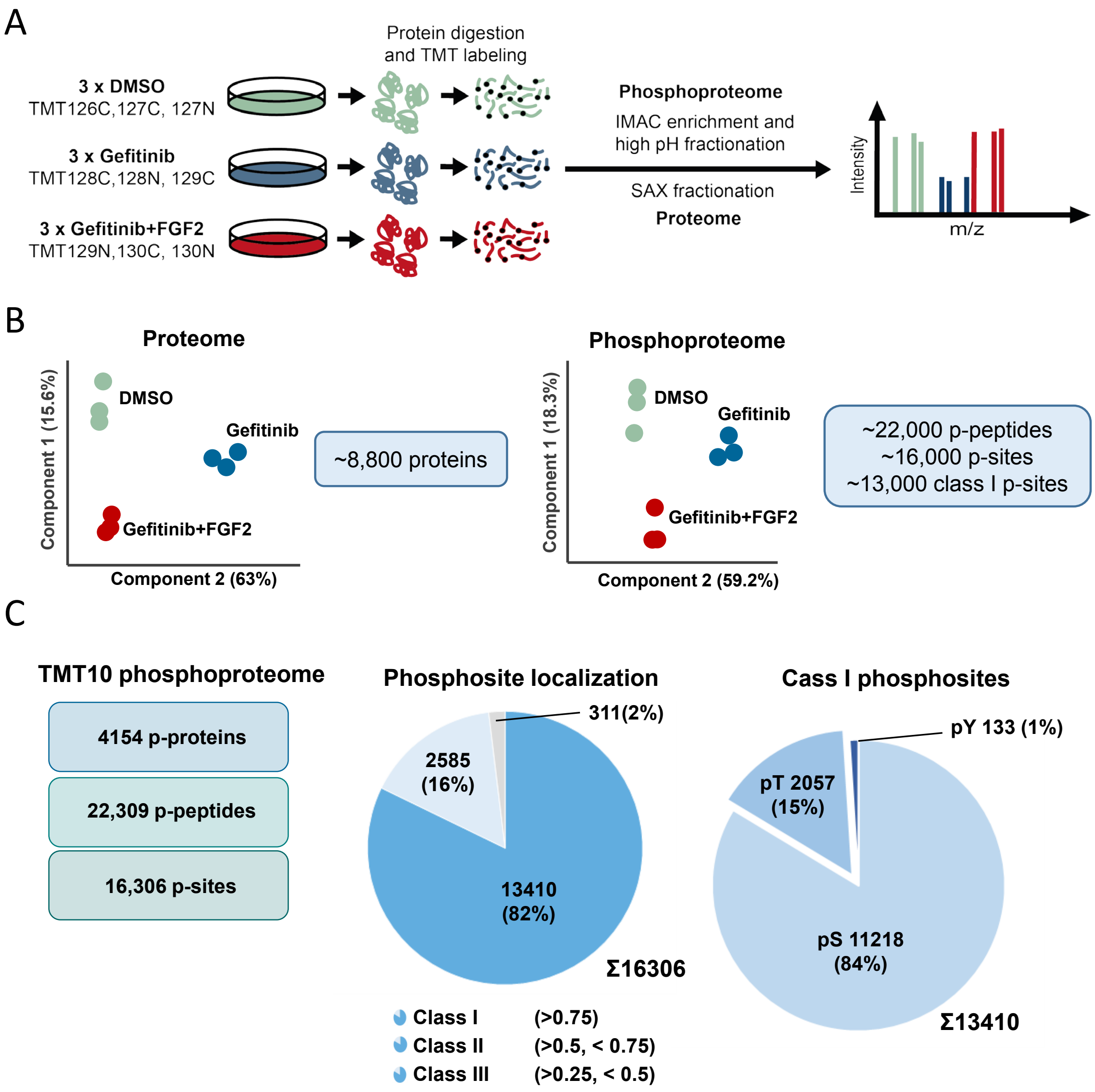

Figure 2: Quantitative proteomic and phosphoproteomic workflow for the molecular analysis of EGFR inhibition and FGF2 mediated resistance. A) Cells were grown in three biological replicates over three days in the presence of DMSO, gefitinib or gefitinib + FGF2. Proteins were extracted, digested and labeled with tandem mass tags (TMT) and samples were combined. For proteomic analysis, mixed peptides were separated by strong anion exchange chromatography (SAX) prior to LC-MS/MS analysis. For phosphoproteomic analysis, TMT labeled phosphopeptides were enriched by Fe-IMAC and the phosphopeptide pool was separated by high pH reversed-phase stage tips prior to LC-MS/MS analysis. B) Principle component analysis (PCA) of the ~8,800 proteins identified and quantified across all conditions showing distinct molecular phenotypes for the different treatments but also that that FGF2 treatment largely reverts the effects of gefitinib. PCA of the ~13,000 confidently localized phosphorylation sites across all conditions resulting in molecular phenotypes similar to the ones for proteins. C) Composition of the phosphoproteome.

Gefitinib and FGF2 induced proteome rewiring reveals adaptive resistance mechanisms

I assessed protein abundance changes following three days of gefitinib or gefitinib/FGF2 treatment compared to untreated cells in more detail and found that a large proportion of all detected proteins (~3,800 out of ~8,800) displayed statistically significant expression differences ($p<0.01$, Benjamini-Hochberg corrected) including 134 protein kinases. Many of the observed changes were small which can in part be attributed to the well-known phenomenon of ratio compression in isobaric labeling [38]. Still, the precision of the TMT quantification clearly allowed recognizing distinct cellular states (see the PCA in Fig. 2B). Figure 3A illustrates the global changes for the three-way comparison on the protein abundance level. Interestingly, proteome expression changes were much larger for gefitinib *vs.* DMSO and gefitinib/FGF2 *vs.* gefitinib alone (σ of 0.352 and 0.335 of the respective distributions) compared to DMSO *vs.* gefitinib/FGF2 treated cells (σ of 0.188) showing that the co-addition of the growth factor to the drug treated cells, reverses many of the proteome changes induced by gefitinib. Unsupervised hierarchical clustering of the 3,805 proteins associated with the most significant expression differences ($p<0.01$; Fig. 3B) identified groups of proteins enriched in certain cellular and molecular functions. For example, cluster 1 contains metabolic enzymes including those involved in glycolysis that remain downregulated following gefitinib plus FGF2 treatment indicating that the cells did not required a full metabolic recovery to achieve the same level of cell viability as untreated cells. Processes downregulated by gefitinib but reverted by FGF2 treatment include RNA processing mechanisms, proteins involved in cell cycle progression, mitosis and cell division (Fig. 3B, cluster 2). This is consistent with numerous reports in the literature showing that gefitinib can inhibit cell cycle progression, induce G0/G1 cell cycle arrest and block G2/M transition [39-41]. It is evident, that FGF2 addition partially or even fully restored protein abundance levels to that of the DMSO control thus releasing cell cycle arrest and allowing normal cell cycle progression to proceed.

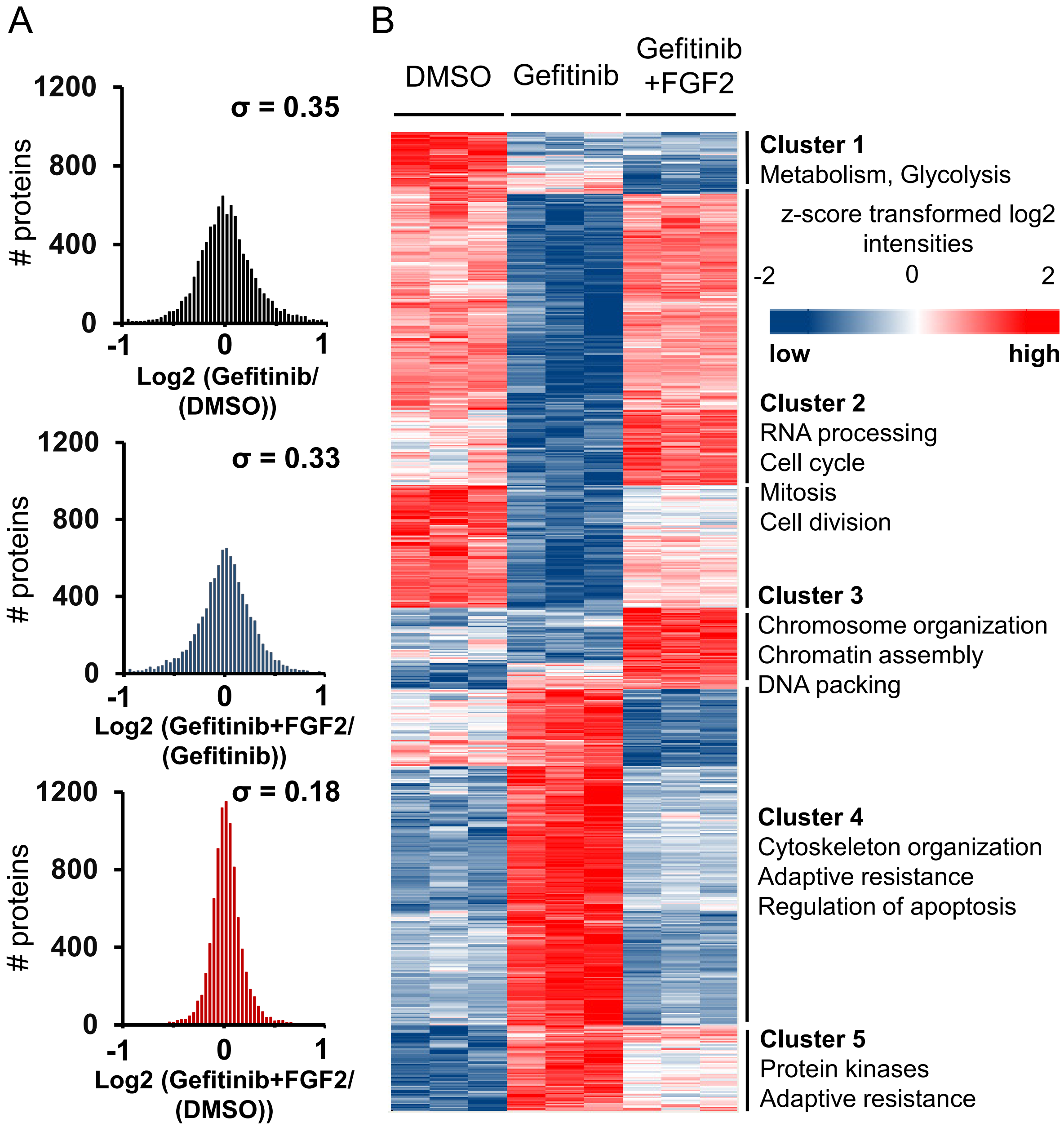

Figure 3: Widespread changes of the proteome in response to gefitinib and substantial reversal in the presence of FGF2. A) The distribution of quantitative protein expression changes showed larger differences for gefitinib vs. DMSO and gefitinib vs. gefitinib + FGF2 treated cells (δ = 0.352 and δ = 0.335 respectively) compared to DMSO and gefitinib + FGF2 treated cells (δ = 0.188) indicating that the effects of gefitinib can be largely reverted by the growth factor. B) Unsupervised hierarchical clustering of significantly regulated proteins (n=3,805; p<0.01, Benjamini-Hochberg corrected) of all replicates highlights clusters of co-regulated proteins and gene ontology analysis reveals enrichment of the underlying biological process for the proteins involved.

Interestingly, FGF2/gefitinib co-treatment led to upregulation of some proteins that are not influenced by gefitinib treatment alone (cluster 3). Most of these proteins are involved in DNA organization and include, for example, a substantial number of histones, transcription factors, group box proteins and other DNA binders. It is quite likely that this is a direct consequence of FGF2 acting as a mitogen, thus improving cell viability by the induction of genes that are transcribed within this transcriptional framework. A large number of 1,309 proteins was upregulated by gefitinib and downregulated by FGF2 (cluster 4). Many of these proteins are involved in cytoskeleton organization, notably actin filament organization and in the regulation of apoptosis. The latter is not surprising as apoptosis induction is one of the mechanisms by which gefitinib kills cancer cells. Apoptosis was, however, not apparent from microscopic inspection of gefitinib treated cells. Instead of the anticipated morphological changes associated with apoptosis (e.g. blebbing), the cells showed a more spindle shaped morphology and showed fewer cell-cell contacts than control cells. The bottom section of the heat map (cluster 5) contains protein kinases and other proteins that were upregulated upon gefitinib treatment and partially downregulated again in the presence of FGF2. Interestingly, this cluster includes kinases known to be involved in resistance formation following small molecule tyrosine kinase inhibition. Prominent examples are depicted in figure 4A. The receptor tyrosine kinases ERBB2 and its kinase dead interaction partner ERBB3 were upregulated upon gefitinib treatment and can compensate EGFR inhibition by the drug via the formation of kinase active heterodimers [12]. Interestingly, both proteins return to almost baseline levels in the presence of FGF2 (the dose or treatment time may not have been sufficient for a full reversal). Another well described resistance mechanism is the upregulation of hepatocyte growth factor receptor (c-MET) [13] which bypasses the EGF receptor and leads to the activation of pro-survival pathways. Further examples from the data include the PI3K subunit PIK3CB [42], AKT1 and the SRC-like kinase FYN that itself physically and functionally interacts with ERBB2 [43]. Overexpression of PI3K and AKT1 can activate the PI3K/AKT/mTOR pathway and thereby prevent apoptosis. There is growing evidence for important roles of PI3K subunits in cancer [44]. Apart from PIK3CB, the subunits PIK3CA, PIK3C2A and PIK3CD were also differential expressed suggesting that PI3K subunit composition is also important for adaptation of cellular signaling in the model cell line.

Figure 4B summarize the expression changes of protein kinases in response to gefitinib and gefitinib/FGF2 respectively. It is plausible that pro-survival kinases are upregulated to counter adverse effects elicited by gefitinib, but they may not be required in case a mitogenic signal is provided by FGF2 as an external stimulus. The most strongly downregulated kinase in the data set following gefitinib treatment was STK17A (Fig. 4B). This protein is a p53 target gene [45] and downregulation was recently found to be associated with decreased proliferation, migration and invasion [46]. At the other end of the spectrum, unc-51 like kinase 4 (ULK4) and myotonin-protein kinase (DMPK) were the most upregulated kinases following gefitinib treatment. DMPK regulates cell shape, remodels the actomyosin cytoskeleton and mediates protein oligomerization and localization [47, 48]. In light of these described functions, the protein may play a lesser role for cellular survival in the experiment but may contribute to the observed morphological changes of the cells. The role of myosin light chain kinase (MYLK) is discussed further below as phosphorylation sites on this kinase were also significantly upregulated in response to gefitinib. The protein kinase ABL2 is strongly linked to survival and cell growth and was also upregulated after gefitinib treatment (but not in the presence of FGF2) possibly indicating an early cellular response leading to eventual gefitinib resistance. FGFR2 was weakly upregulated following gefitinib treatment and serves as another example that cells adapt to negative selective pressure by the upregulation of bypass signaling kinases. Interestingly, it was recently shown that FGFR2 promotes ERBB2 shedding and that intracellular accumulation of the truncated fragment results in enhanced ERBB signaling [49]. In this regard, upregulation of FGFR2 could also serve as an adaptive mechanism to recover ERBB signaling even in the presence of an EGFR inhibitor. Stimulation by FGF2 resulted in downregulation of FGFR2 likely because overexpression was no longer necessary for bypass activation of ERBB signaling. The protein kinase GSG2 (Haspin) was the most strongly upregulated kinase in the gefitinib/FGF2 treated cells compared to untreated cells, whereas its expression was unaffected by gefitinib alone (Fig. 4C). Interestingly, this kinase phosphorylates histone H3 at Thr-3 during mitosis and thereby targets the chromosomal passenger complex (CPC) to the inner centromere [50]. The FGF2 induced upregulation of GSG2 may, therefore, play a role in breaking gefitinib induced cell cycle arrest and apoptosis.

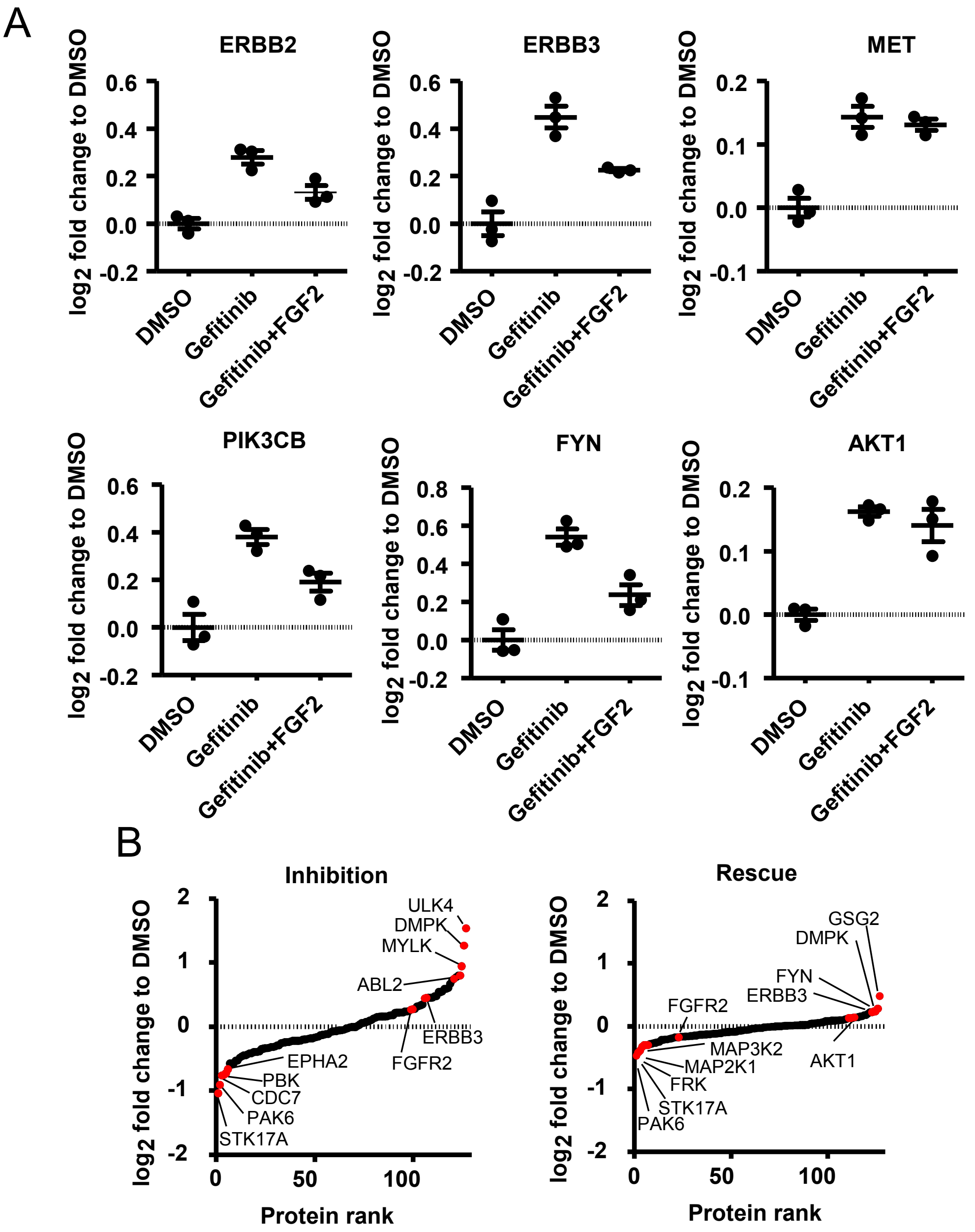

Figure 4: Kinases potentially involved in intrinsic gefitinib or FGF2 mediated resistance. A) Examples for protein kinases upregulated in response to gefitinib and partially downregulated by co-treatment by FGF2. Upregulation of these proteins by gefitinib may represent kinome reprogramming events leading to intrinsic resistance. The addition of the growth factor may relieve cells from the selective pressure of the drug and thereby leading to reduced levels of these pro-survival kinases. Error bars represent the SEM of triplicate experiments. B) Full range of expression regulation for protein kinases. Dots indicate the mean fold change of three biological replicates.

Quantitative phosphorylation profiling reveals widespread changes in kinase mediated cellular processes

In order to complement proteome expression information with more direct functional molecular data, I generated quantitative phosphoproteome profiles of the same samples (in triplicate). This resulted in the identification of ~22,000 phosphopeptides in all nine experiments (i.e. no missing values) corresponding to ~16,000 different phosphorylation sites that were further filtered to 13,410 class I sites (i.e. phosphorylation site localization probability of >0.75; Andromeda score of >40. As observed for the proteome, the phosphoproteome also showed extensive differences between the three cellular conditions (5,465 differential sites; $p<0.01$, Benjamini-Hochberg corrected). Unsupervised hierarchical clustering of this data provided a picture much akin to that obtained for the proteome: extensive changes in response to gefitinib that were largely (albeit not always completely) reverted by the simultaneous presence of the growth factor FGF2 (Fig. 5A).

About 10% (571 sites) of all regulated phosphorylation sites were repressed by gefitinib and were not restored in abundance by FGF2 treatment (Fig. 5 cluster 1). These presumably result from direct or indirect inhibition of kinase activity by the drug in cellular pathways that are not part of FGF2 signaling. Biological processes in this cluster are diverse but include RNA processing and cytoskeleton organization. Given that RNA processing is highly represented in all clusters, it seems likely that this reflects the adaptation to a new steady state that goes along with changes in gene transcription and translation. Downregulated phosphorylation was observed for kinases such as MAP2K2 (MEK2) (pS295, pT394), a component of the RAS/MEK/ERK cascade that activates MAPK1/3 in an EGFR activity dependent manner [51] or MAP4K4 (pS781, pS882), which is involved in the Hippo pathway [52]. Considering that MAPK's are downstream targets of EGFR, the downregulation of their respective phosphorylation sites in response to gefitinib treatment is plausible. A similar number of phosphorylation sites (14%; 787 sites) was moderately repressed by gefitinib but strongly upregulated in the presence of FGF2 (Fig. 5 cluster 2). In keeping with the above argument, these phosphorylation sites may reflect kinase activity that is primarily governed by FGF2 stimulation but largely independent of gefitinib affected pathways. Regulated biological processes in this cluster include DNA replication and cell cycle progression. Prominent examples here are histones, e.g. HIST2H3A (pS29) which can be phosphorylated by AURKB, AURKC and GSG2 [53]. Given that GSG2 was found to be the most upregulated protein after FGF2 treatment (Fig. 4C), the phosphorylation changes on the histones are likely a direct consequence of GSG2 protein expression change. Moreover, FGF2 induced phosphorylation of the proto-oncogene c-MYC (pS293, pS347) was observed, which is consistent with the fact that c-MYC is a known transducer of cell proliferation in response to extracellular stimulation [54] and was found to be stabilized by FGF2 [55]. Also a number of further kinase phosphorylation sites were observed, including MET_pS977, MET_pY1234 and several CDK12/13 sites that are discussed further below.

The vast majority of all significantly regulated phosphorylation site levels (64%, 3,502 sites) were, however, largely restored to base line by co-treating cells with gefitinib and FGF2 (Fig. 5 cluster 3 and 4), implying that both drugs and growth factor affect a lot of common biology and that FGF2 can act as a direct antagonist to gefitinib. As mentioned earlier, the fact that FGF2 did not always fully restore protein activity to baseline levels may simply be related to an insufficient dose or time of treatment in the set of experiments. Further characterization of proteins in clusters 3 and 4 was performed by community clustering using the GLay clustering algorithm [33] that allows structuring and visualizing similar protein functions in a Cytoscape network structure. Here, GLay Nodes represent phosphoproteins and edges are known interactions between proteins based on the combined STRING score [31]. The obtained results are in line with the interpretation of common biology affected by drug and growth factor. Proteins involved in processing of RNA and mRNA are strongly represented in both clusters. Cluster 3 contains many phosphorylation sites in proteins that are part of signal transduction cascades (e.g. EGFR, ERBB2, EPHA2, PTK2, IRS1, SRC, RAF1, MAPK's) and proteins involved in the cell cycle and in mitosis (e.g. RB1, RBPP8, CDCA3, CHEK1). More specifically, a large number of differentially regulated phosphorylation sites were found on protein kinases indicating that signal transduction cascades are (re-)activated following FGF2 treatment (further discussed below). This is entirely in line with the phenotypic starting point of this study that shows that cells were fully viable in the presence of gefitinib and FGF2 (Fig. 1). Somewhat unexpectedly, a large number of phosphorylation sites (2,105) was upregulated by gefitinib treatment, implying the strong activation of at least some kinases (Fig. 5 cluster 4) that may drive the strong representation of cytoskeletal organization and transcription regulation in the GLay networks (also discussed further below). As mentioned above, cells showed a more spindle like shape after treatment with gefitinib and a reduction of cell-cell contacts, which confirms, at the phenotypic level, the network analysis results indicating cytoskeleton reorganization. A small but statistically significant number of phosphorylation sites in cluster 5 point to cell death and apoptosis processes which can most likely be attributed to the known and therapeutically desired induction of cell death by the drug.

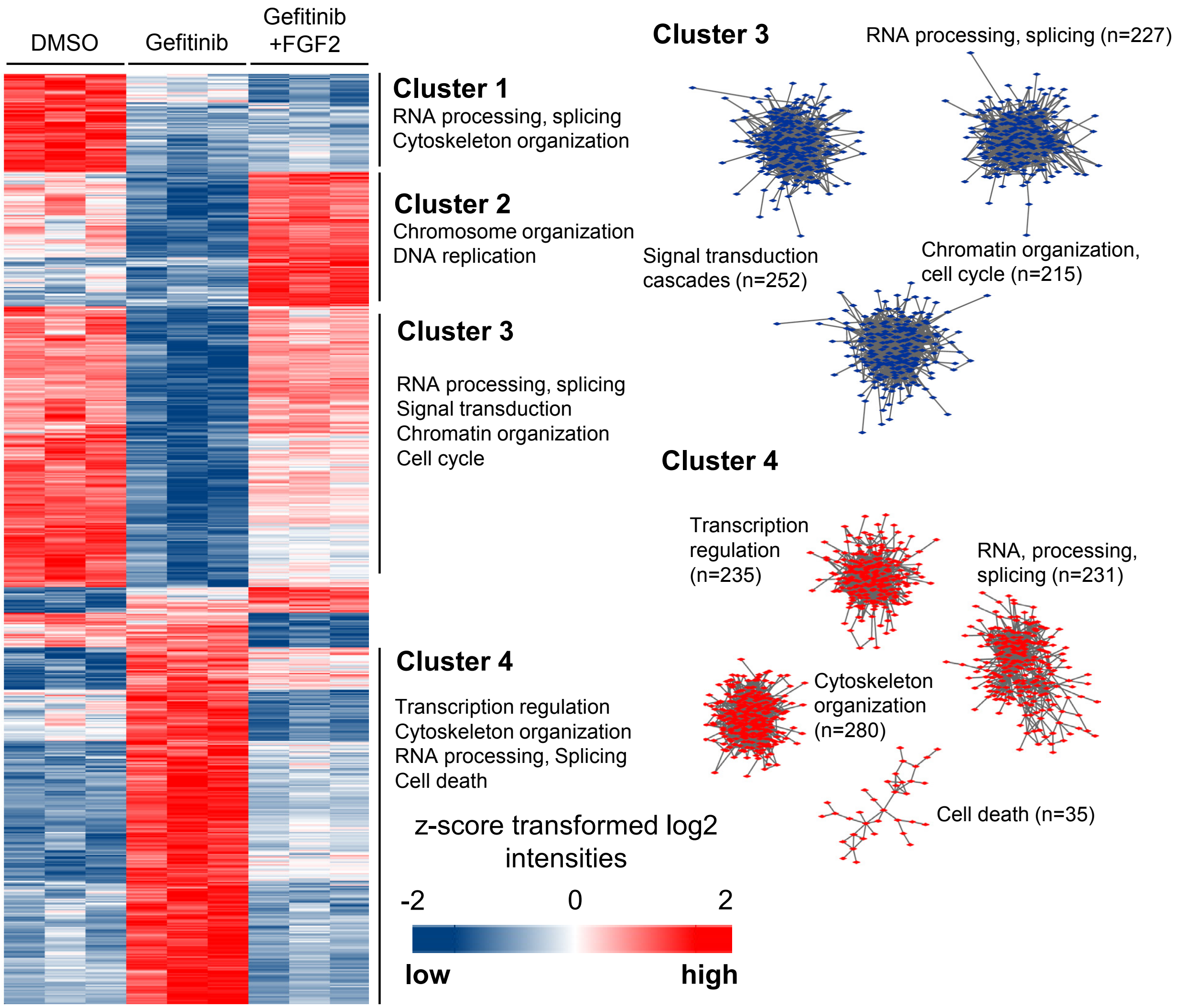

Figure 5: Widespread changes of the phosphoproteome in response to gefitinib and substantial reversal in the presence of FGF2. Unsupervised hierarchical clustering and GO term analysis of statistically significantly regulated phosphorylation site abundance (n=5,465; $p<0.01$, Benjamini-Hochberg corrected) induced by EGFR inhibition and FGF2 mediated resistance. The large clusters 3 and 4 were further characterized by community clustering (Glay algorithm) and functional related proteins are visualized as networks. For example, cluster 3 contains a large network of proteins that are involved in signal transduction. Phosphorylation sites on these proteins are partially or fully restored by FGF2.

Kinase activity, gefitinib mechanism of action and FGF2 mediated drug resistance

The very large number of statistically significant changes in protein phosphorylation observed above implies strong regulation of kinase expression and/or activity in response to drug and growth factor treatment. This data should, therefore, also contain information regarding the drugs' molecular mode of action as well as highlighting potential intrinsic or acquired resistance mechanisms. I quantified 286 kinases in the experiments, observed expression changes for 134 of these ($p<0.01$) and quantified 699 phosphorylation sites and phosphorylation level changes for 137 kinases (312 sites, $p<0.01$) which allowed investigating the above point in some detail. Most strongly downregulated by gefitinib were the autophosphorylation sites pY1197 and pY1172 of the EGF receptor confirming that EGFR activity is blocked by the drug (Fig. 6A). Sites on the receptor tyrosine kinase EPHA2 (pY772, pT771; pS897) were similarly affected by the drug. Co-immunoprecipitation experiments of EGFR and EPHA2 [56, 57] have shown that both proteins can interact physically. It is, therefore, possible that EGFR and EPHA2 activate each other via heterodimerization or signaling adaptors and that inhibition of EGFR results in the simultaneous inhibition of EPHA2 as EPHA2 itself is not a target of gefitinib. Sites on MAPK1 (ERK2, pY187) and MAPK3 (ERK1, pY204) were also negatively affected by gefitinib showing that the cellular mechanism of action of the drug proceeds via the inhibition of the RAS/MEK/ERK signaling axis.

Interestingly, gefitinib also induced phosphorylation on kinases, most prominently on MYLK (pS1653, pS1656, pS1659, pS1732), CDK14 (pT125), MAP2K2 (MAP2K2, pS312) and MAP3K1 (pS250). MYLK phosphorylates myosin II which is essential for stress fiber and focal adhesion formation and is intimately linked to EGFR and integrin mediated signaling. I found that MYLK expression and phosphorylation increases following gefitinib treatment (Fig. 4B, Fig. 6A). The functions of the respective phosphorylation sites are not known but prior work has shown that this kinase contributes to proliferation [58] and has anti-apoptotic potential [59]. Moreover, it can induce migration through cross-talk with MAPK1/3 [60]. Increased abundance and phosphorylation on MYLK may, therefore, constitute a pro-survival mechanism that prevents apoptosis in response to EGFR kinase inhibition. I also observed an increase in phosphorylation for CDK14 in response to gefitinib. This cell cycle regulating kinase has been shown to correlate with proliferation and migration in gastric cancer [61]. How CDK14 relates to EGFR signaling or inhibition thereof is unclear at present but the increased phosphorylation on pT125 of CDK14 observed here may have a similar effect and may thus serve as an intrinsic pro-survival adaptation mechanism to EGFR inhibition. MAP2K2 and MAP3K1 are also increasing in phosphorylation levels and both are involved in MAPK pathways. However, there are neither known kinases that phosphorylate MAP2K2 at pS312 and MAP3K1 at pS250 nor are the functions of these sites known.

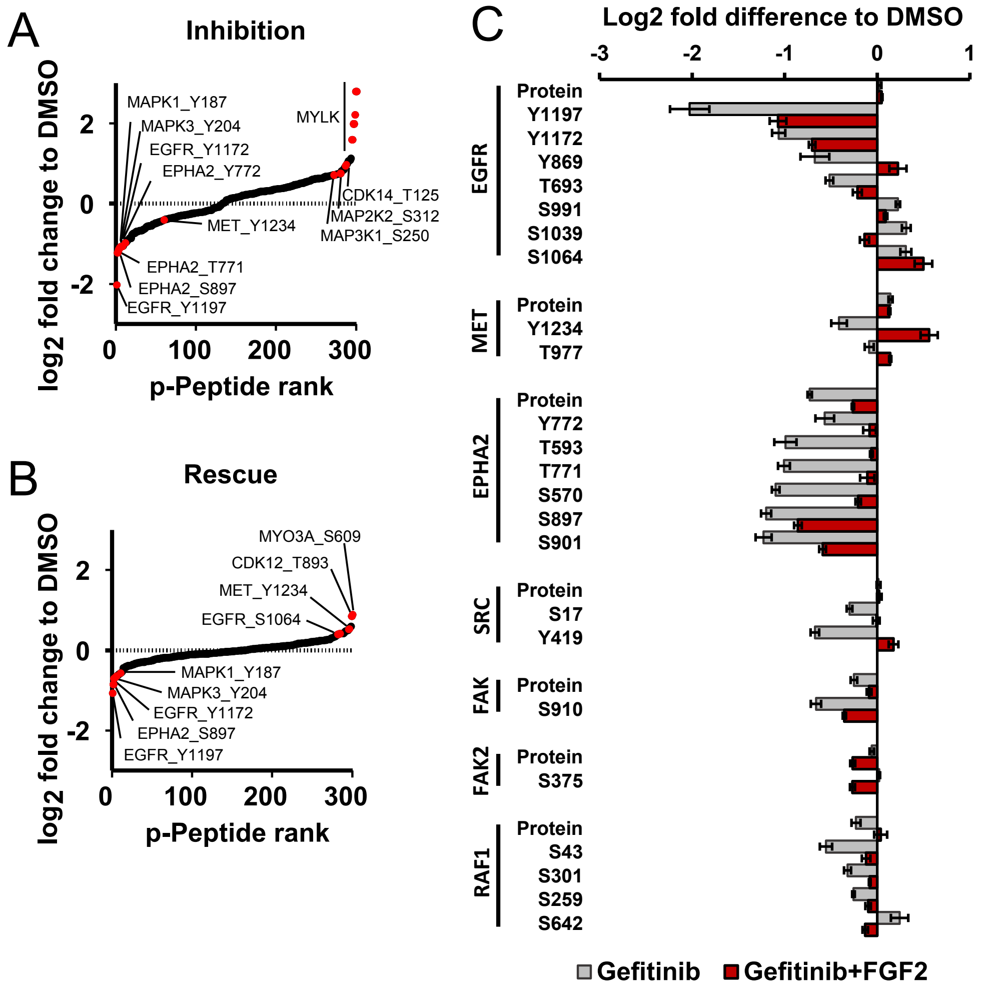

Figure 6: Regulation of phosphorylation sites on protein kinases. A) Ranked list of regulated phosphorylation sites upon gefitinib treatment. B) Same as panel A but for FGF2 treatment. C) Selected examples of protein kinases that are either regulated at the protein and phosphorylation level or only regulated at the protein phosphorylation level. For details, see main text. Error bars denote SD of biological triplicate experiments.

Many phosphorylation sites on protein kinases that were downregulated by gefitinib were also down in the presence of FGF2 albeit to a lesser extent, indicating a partial re-activation of the primary signaling elicited by the growth factor (Fig. 6). However, given that the cells are fully viable, this may also suggest that such re-activation processes may not always be essential or particularly important for cell survival. Instead, the full restoration of cellular viability (and thus gefitinib resistance) may be mediated by proteins such as c-MET the activity of which (pY1234) was much higher in the presence of FGF2 compared to gefitinib alone (Fig. 6A, 6B and 6C). The mechanism for this may be related to FGF2's ability to induce the production of HGF which in turn activates its receptor c-MET [62]. The data showed that the majority of regulated phosphorylation was restored to (close to) baseline levels by FGF2. Following three days of drug and growth factor treatment, this may be explained by changes in kinase abundance (kinome reprogramming), resulting in higher/lower phosphopeptide abundance, but also by changes in kinase activity without concomitant changes in kinase abundance (activity reprogramming). Both mechanisms are meaningful ways to regulate the activity of signaling pathways in cells. Regulating protein levels may provide for a more sustained adaptation whereas regulating activity provides for a means to respond rapidly to a cellular signal. The kinases EPHA2 and RAF1 are examples for which kinase abundance and activity are regulated together (Fig. 6C), whereas EGFR or SRC are examples for a lack of regulation at the protein level but instead show strong effects at the level of protein phosphorylation.

The broad coverage of the proteome and phosphoproteome obtained in this study enabled us to investigate this latter point in more detail. I quantified the (relative) abundance of ~8,500 proteins among which are 3,353 phosphoproteins with at least one quantified phosphorylation site (Fig. 7A). Of the 4,916 proteins that did not show expression changes ($p<0.01$, Benjamini-Hochberg corrected), there were 1,091 that did exhibit a statistically significant regulation at the phosphorylation site level (Fig. 7B). A more detailed analysis of the protein kinases in this set is shown in figure 7C providing further insights into kinase activity mediated responses to EGFR inhibition and FGF2 induced resistance. As mentioned before, EGFR activity was downregulated by gefitinib as expected and partially re-activated by FGF2. In addition, MAPK3 (ERK1, pY204) phosphorylation partially recovered, confirming the reactivation of ERBB and downstream MEK/ERK signaling induced by FGF2. Further examples include the splicing regulator CDK13 [63] and the histone regulators CDK17 and CDK18 [64] that show several phosphorylation sites that were regulated in response to EGFR inhibition and attenuated by addition of FGF2 (Fig. 7C). Most sites in CDKs were upregulated in response to EGFR inhibition and downregulated after addition of FGF2 (see also cluster 4 in Fig. 5). CDK 13 is a key regulator of transcription elongation and affects splicing [65] whereas CDK17 and CDK18 are related to cell cycle control [66]. These observations are in agreement with the interpretation that the cells are forced to reach a new steady state by altered gene transcription in response to gefitinib.

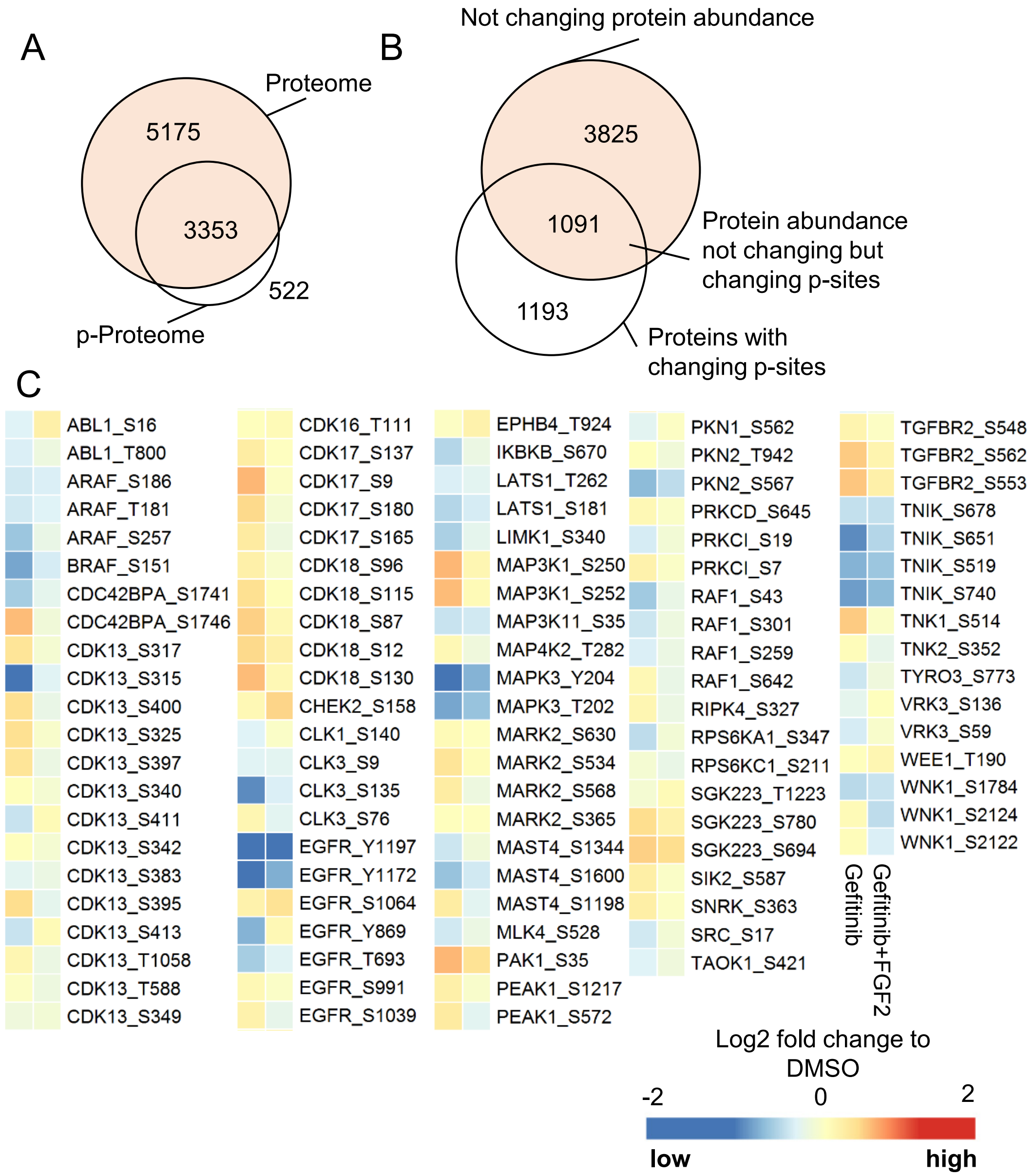

Figure 7: Protein activity adaptation to EGFR inhibition and FGF2 stimulation. A) Venn-diagram of quantified proteins and phosphoproteins showing substantial overlap. B) Venn-diagram of proteins that i) exhibit no protein abundance changes; ii) show no protein but phosphorylation level changes and iii) show changes at both levels ($p<0.01$, Benjamini-Hochberg corrected). Proteins in the intersection are particularly interesting as their phosphorylation stoichiometry changes indicating rapid and reversible regulatory mechanisms. C) Heatmaps for protein kinases (examples) for which no expression differences were detected but whose phosphorylation changes, indicating changes in kinase activity.

Protein phosphorylation profiling prioritizes candidate drug targets to growth factor mediated gefitinib resistance

This study has generated a rich set of phosphorylation regulation data in the context of gefitinib mode of action and growth factor mediated resistance. The kinases highlighted in this experimental setting may potentially be used as drug targets with the aim to overcome growth factor mediated resistance often occurring within the tumor microenvironment. Furthermore, the kinase substrates may be used as a molecular read-out for measuring engagement of the drug with its target in the cell. I, therefore, condensed the information obtained in this work into a model that focusses on the regulated phosphoproteome in the context of certain drugable cellular signaling pathways (Fig. 8). The activity of EGFR (pY1172, pY1197, pY869), MET (pY1234), EPHA2 (pY771) and SRC (pY419) was found to be positively regulated by FGF2. Each of these proteins is a drug target in its own right and the consequences of inhibiting these proteins can for example be captured by their downstream substrate CTNND1 (sites mapped to isoform 1A of p120-catenin) which was found to statistically significant changes on 17 phosphorylation sites. Motif based kinase-substrate relationship prediction using Networkin, suggests GSK3B (CTNND1_pT201), FYN, MET (CTNND1_pY228), SRC, IGF1R (CTNND1_pY296), SRC, FER (CTNND1_pY898) and AKT1 (CTNND1_pS914) as potential upstream kinases (Fig. 8). Except for the GSK3B target site (CTNND1_pT201), all other sites were downregulated after gefitinib treatment and increased again by FGF2 treatment, confirming activity of SRC and MET (Fig. 6C, Fig.8) and indicating IGFR and AKT1 activation in response to FGF2 treatment. Indeed, CTNND1 is known to be involved in growth factor dependent signaling [67] and phosphorylation regulates E-cadherin mediated cell adhesion [68]. Along the same lines, phosphorylation changes were observed for insulin receptor substrates 1 (IRS1) and 2 (IRS2). These are docking proteins that bind to SH2 domains, function downstream of activated cell surface receptors and thereby regulate signal transduction. The function of IRS1/2 has been extensively studied in insulin signaling and metabolism, but there is also growing evidence for their roles in altered signaling pathways in cancer [69]. Four and eight phosphorylation sites were found to be differentially regulated on IRS1 and IRS2, respectively (Fig. 8) and kinase-substrate relationships were predicted for AKT1 (IRS1_pS330, IRS1_pS527, IRS2_pS365, IRS2_pT1102, IRS2_pS1149), MAPK1/3 (IRS1_pS1078, IRS2_pT520, IRS2_pS915) and PDK1 (IRS1_pS1145). IRS1 and IRS2 interact with the catalytic subunit PIK3CA (p110α) of phosphoinositide 3-kinase (PI3K) [70] and the regulatory subunit PIK3R1 (p85α) [71, 72] of the PI3K complex and thereby initiate PI3K/AKT/mTOR signaling. From the data, it appears that MAPK1/3, AKT1 and PDK1 feedback regulate IRS1/2 and that this further affects downstream signaling as part of the response to

EGFR inhibition and FGF2 stimulation. As mentioned earlier, MAPK1/3 (pY185, pY204) activity was downregulated after EGFR inhibition and partially restored following FGF2 treatment.

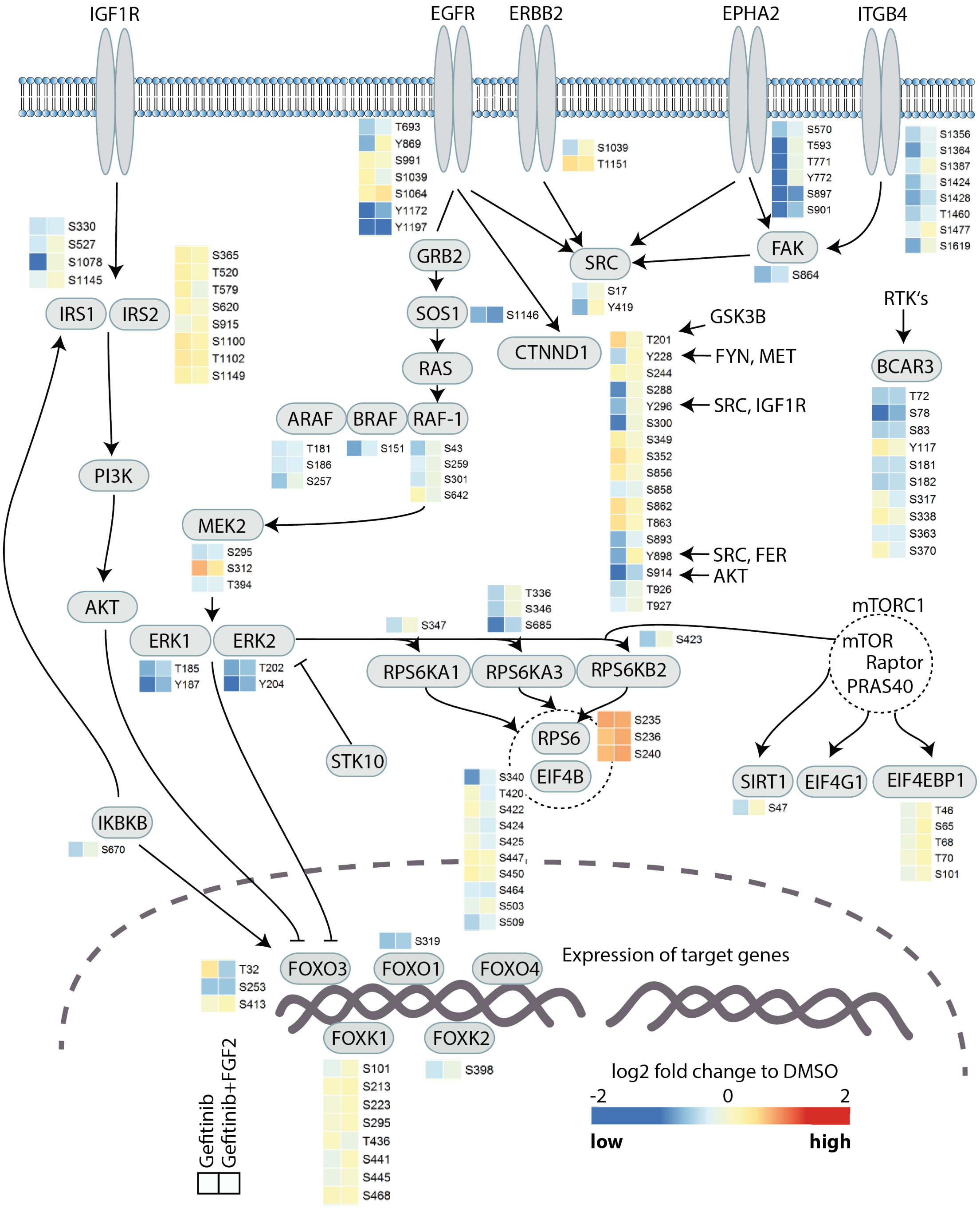
IGF1R
EGFR
ERBB2
EPHA2
ITGB4
T693
Y869
S991
S1039
S1064
Y1172
Y1197
S1039
T1151
S570
T593
T771
Y772
S897
S901
S1356
S1364
S1387
S1424
S1428
T1460
S1477
S1619
S330
S527
S1078
S1145
S365
T520
T579
S620
S915
S1100
T1102
S1149
GRB2
SRC
FAK
S864
S17
Y419
IRS1
IRS2
SOS1
S1146
CTNND1
GSK3B
T201
Y228
S244
S288
Y296
S300
S349
S352
S856
S858
S862
T863
S893
Y898
S914
T926
T927
FYN, MET
SRC, IGF1R
SRC, FER
AKT
RTK's
BCAR3
T72
S78
S83
Y117
S181
S182
S317
S338
S363
S370
RAS
ARAF
BRAF
RAF-1
T181
S186
S257
S151
S43
S259
S301
S642
PI3K
MEK2
S295
S312
T394
AKT
ERK1
ERK2
T185
Y187
T202
Y204
S347
T336
S346
S685
S423
mTORC1
mTOR
Raptor
PRAS40
RPS6KA1
RPS6KA3
RPS6KB2
RPS6
EIF4B
S235
S236
S240
STK10
S340
T420
S422
S424
S425
S447
S450
S464
S503
S509
SIRT1
EIF4G1
EIF4EBP1
S47
T46
S65
T68
T70
S101
IKBKB
S670
S319
T32
S253
S413
FOXO3
FOXO1
FOXO4
Expression of target genes
FOXK1
FOXK2
S101
S213
S223
S295
T436
S441
S445
S468
S398
Gefitinib
Gefitinib+FGF2
log2 fold change to DMSO
-2
0
2
low
high

Figure 8: Phosphoproteomic model of FGF2 mediated gefitinib resistance in A431 cells. Kinases and other proteins shown here all exhibited enhanced phosphorylation site abundance in response to gefitinib or FGF2 treatment implying differential activity of the kinases involved. This model formed the basis for the choice of drug combinations shown in figure 9.

Accordingly, other sites in the RAS/RAF/MEK/ERK pathway showed a similar behavior (RAF1 pS43, pS259, pS301; MEK2 pS295, pT394). As a consequence, it is worth considering MAPK1/3 as a regulator of IRS1/2 phosphorylation and modulator of PI3K/AKT/mTOR signaling. As a number of other MAPK1/3 and mTOR substrates (S6K, SIRT1, EIF4EBP1) were also significantly regulated, mTOR, PI3K, AKT, and MAPK1/3 appear to be important signaling nodes and may therefore serve as potential targets for combination treatments with gefitinib. The same applies for the SRC family kinases and IGF1R/INSR as potential upstream regulators of IRS1/2. Last but not least, the FGF receptor itself would seem an obvious target as its ligand FGF2 is driving the resistance of cells to gefitinib treatment. Unfortunately, I did not observe any phosphorylation sites on FGFR in the experiments, possibly as a result of low protein abundance of this receptor in the cells and insufficient sequence coverage obtained by a single protease digestion scheme.

To test the hypothesis that combinations of kinase inhibitors would overcome growth factor mediated gefitinib resistance, I measured cell viability using a number of inhibitors against the aforementioned priority targets. Figure 9A shows that the combination of the reasonably selective FGFR inhibitor AZD4547 with gefitinib was much more effective than either compound alone. The two drugs acted in a synergistic fashion as neither compound had an appreciable effect at 2.5 µM but the combination of 2.5 µM of each drug led to the complete killing of cells even in the presence of FGF2. In the context of gefitinib resistance, I have previously shown that growth factor receptors can activate each other and can thus render gefitinib monotherapy ineffective but that it can be completely overcome by co-treatment with a second kinase inhibitor [16]. Hence, it is not farfetched to speculate that the same or a similar mechanism may be at work here. This notion is strongly supported by the phosphoproteomic data from which it is evident that FGF2 leads to the re-activation of pY1172 and pY1197 of the EGFR as well as several downstream signaling members. Figure 9B shows drug combination experiments using further signaling nodes derived from the phosphoproteomic data. SRC family kinases were targeted by saracatinib, MEK by trametinib, AKT by AZD5364, IGF1R/INSR by OSI906 and PI3K/mTOR by NVP-BEZ235 or GSK2126458/omipalisib. In the absence of FGF2, saracatinib, trametinib and OSI-906 all showed additive efficacy in combination with gefitinib. However, only the combination of trametinib and gefitinib was effective in the presence of FGF2, making MEK inhibition a reasonable option for combination treatment (Fig. 9B). The reasons why the other combinations failed may be due to redundancy in bypass signaling mechanisms that are not targeted by these drugs. Very surprisingly, the dual PI3K/mTOR inhibitor GSK2126458 completely killed the cells whether or not it was used in combination with gefitinib or whether or not FGF2 was present.

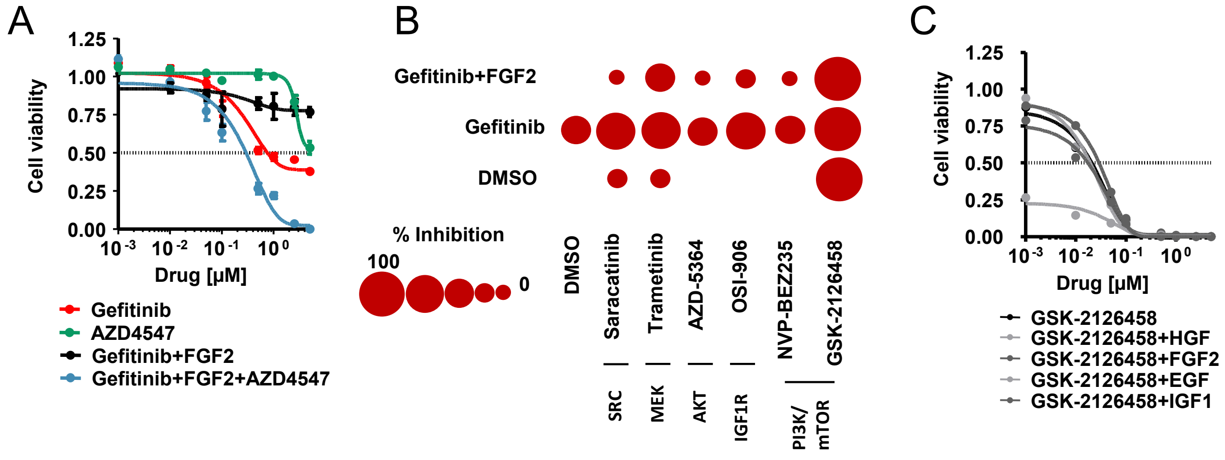

Figure 9: Drug combination treatment aiming to prevent growth factor mediated resistance to EGFR inhibition. A) Cell viability assays showing that the combination of gefitinib and the FGFR inhibitors prevents FGF2 mediated resistance. B) Extension of this analysis to six kinase inhibitors showing that only the MEK inhibitor trametinib synergizes with gefitinib in preventing FGF2 mediated resistance. Interestingly, the dual PI3K/mTOR inhibitor GSK2126458 killed cells in the presence or absence of gefitinib or FGF2 while the dual PI3K/mTOR inhibitor NVP-BEZ235 had practically no effect. For further details, see main text.

Conversely, the frequently used PI3K/mTOR inhibitor NVP-BEZ235 had no effect on its own, showed no added benefit in combination with gefitinib and was also largely ineffective in the presence of FGF2. The reasons for this discrepancy are unclear at present. Even though GSK2126458 is an immensely potent inhibitor of PI3K subunits (PI3Kα Ki = 0.04 nM, PI3Kβ Ki = 0.13 nM, PI3Kδ Ki = 0.024 nM, PI3Kγ Ki = 0.06 nM) and of mTORC1 (Ki = 0.18 nM) and much more potent than NVP-BEZ235 inhibitor (IC_{50} = 6 nM) [73, 74], the complete lack of efficacy of NVP-BEZ235 inhibitor in the cellular assay practically rules out PI3K/mTOR as the targets underlying the potent killing of cells by GSK2126458. It is possible, that GSK2126458 possesses as of yet unknown other targets which may explain its potency. Strikingly, GSK2126458 was effective even as a single agent at concentrations below 100 nM and prevented growth factor mediated resistance for HGF, FGF2, EGF and IGF1 (Fig. 9C) suggesting that the drug acts on an exceedingly important (yet currently unidentified) common pathway component.

In conclusion, this work provided a detailed molecular description and analysis of proteomic and phosphoproteomic changes of human epidermoid A431 cancer cells in response to EGFR inhibition by gefitinib and FGF2 mediated resistance as a simplified model for studying effects of the tumor microenvironment. The data revealed widespread changes at both molecular levels in response to gefitinib, most of which were reverted by the growth factor. The analysis highlighted kinases and signaling pathways underlying this form of kinase inhibitor resistance and thereby prioritized certain signaling nodes as targets for combination treatments that break growth factor mediated resistance. Combined MEK/EGFR was effective in this regard but this was overshadowed by an as of yet mechanistically unclear but phenotypically astounding efficacy of GSK2126458 that cannot be satisfactorily explained by inhibition of its presumed targets PI3K and mTOR. The underlying true mechanisms remain to be elucidated but in any case, it appears that GSK2126458 may be an attractive agent for targeting the tumor microenvironment.

Acknowledgments

I want to thank Jana Zecha for mass spectrometric measurements on the Q-Exactive plus mass spectrometer and Karl Kramer for discussions.

Abbreviations

AGC	Automatic gain control
DTT	Dithiothreitol
FC	Fold change
FDR	False discovery rate
FGF2	Fibroblast growth factor 2
FPLC	Fast preparative liquid chromatography
GO	Gene ontology
HPLC	High pressure liquid chromatography
hSAX	hydrophilic strong anion exchange chromatography
KEGG	Kyoto Encyclopedia of Genes and Genomes
NSCLC	Non-small cell lung cancer
PCA	Principle component analysis
pY/S/T	Phosphotyrosine, -serine, -threonine
RTK	Receptor tyrosine kinase
TMT	Tandem mass tags

References

1. Casalini P, Iorio MV, Galmozzi E, Menard S. Role of HER receptors family in development and differentiation. Journal of cellular physiology 2004, 200: 343-350

2. Yarden Y, Schlessinger J. The EGF receptor kinase: evidence for allosteric activation and intramolecular self-phosphorylation. Ciba Foundation symposium 1985, 116: 23-45

3. Goldman R, Levy RB, Peles E, Yarden Y. Heterodimerization of the erbB-1 and erbB-2 receptors in human breast carcinoma cells: a mechanism for receptor transregulation. Biochemistry 1990, 29: 11024-11028

4. Zhang H, Berezov A, Wang Q, Zhang G, Drebin J, Murali R, Greene MI. ErbB receptors: from oncogenes to targeted cancer therapies. The Journal of clinical investigation 2007, 117: 2051-2058

5. Tebbutt N, Pedersen MW, Johns TG. Targeting the ERBB family in cancer: couples therapy. Nature reviews Cancer 2013, 13: 663-673

6. Goss GD, Spaans JN. Epidermal Growth Factor Receptor Inhibition in the Management of Squamous Cell Carcinoma of the Lung. The oncologist 2016, 21: 205-213

7. Morita S, Okamoto I, Kobayashi K, Yamazaki K, Asahina H, Inoue A, Hagiwara K*, et al.* Combined survival analysis of prospective clinical trials of gefitinib for non-small cell lung cancer with EGFR mutations. Clinical cancer research 2009, 15: 4493-4498

8. Maemondo M, Inoue A, Kobayashi K, Sugawara S, Oizumi S, Isobe H, Gemma A*, et al.* Gefitinib or chemotherapy for non-small-cell lung cancer with mutated EGFR. The New England journal of medicine 2010, 362: 2380-2388

9. Roth P, Weller M. Challenges to targeting epidermal growth factor receptor in glioblastoma: escape mechanisms and combinatorial treatment strategies. Neuro-oncology 2014, 16 Suppl 8: viii14-19

10. Ioannou N, Seddon AM, Dalgleish A, Mackintosh D, Modjtahedi H. Expression pattern and targeting of HER family members and IGF-IR in pancreatic cancer. Frontiers in bioscience 2012, 17: 2698-2724

11. Quesnelle KM, Wheeler SE, Ratay MK, Grandis JR. Preclinical modeling of EGFR inhibitor resistance in head and neck cancer. Cancer biology & therapy 2012, 13: 935-945

12. Engelman JA, Cantley LC. The role of the ErbB family members in non-small cell lung cancers sensitive to epidermal growth factor receptor kinase inhibitors. Clinical cancer research 2006, 12: 4372-4376

13. Engelman JA, Zejnullahu K, Mitsudomi T, Song Y, Hyland C, Park JO, Lindeman N*, et al.* MET amplification leads to gefitinib resistance in lung cancer by activating ERBB3 signaling. Science 2007, 316: 1039-1043

14. Yang H, Wang R, Peng S, Chen L, Li Q, Wang W. Hepatocyte growth factor reduces sensitivity to the epidermal growth factor receptor-tyrosine kinase inhibitor, gefitinib, in lung adenocarcinoma cells harboring wild-type. Oncotarget 2016, 7: 16273-16281

15. Peled N, Wynes MW, Ikeda N, Ohira T, Yoshida K, Qian J, Ilouze M*, et al.* Insulin-like growth factor-1 receptor (IGF-1R) as a biomarker for resistance to the tyrosine kinase inhibitor gefitinib in non-small cell lung cancer. Cellular oncology 2013, 36: 277-288

16. Koch H, Busto ME, Kramer K, Medard G, Kuster B. Chemical Proteomics Uncovers EPHA2 as a Mechanism of Acquired Resistance to Small Molecule EGFR Kinase Inhibition. Journal of proteome research 2015, 14: 2617-2625

17. Ware KE, Hinz TK, Kleczko E, Singleton KR, Marek LA, Helfrich BA, Cummings CT*, et al.* A mechanism of resistance to gefitinib mediated by cellular reprogramming and the acquisition of an FGF2-FGFR1 autocrine growth loop. Oncogenesis 2013, 2: e39

18. Terai H, Soejima K, Yasuda H, Nakayama S, Hamamoto J, Arai D, Ishioka K*, et al.* Activation of the FGF2-FGFR1 autocrine pathway: a novel mechanism of acquired resistance to gefitinib in NSCLC. Molecular cancer research 2013, 11: 759-767

19. Duncan JS, Whittle MC, Nakamura K, Abell AN, Midland AA, Zawistowski JS, Johnson NL*, et al.* Dynamic reprogramming of the kinome in response to targeted MEK inhibition in triple-negative breast cancer. Cell 2012, 149: 307-321

20. Stuhlmiller TJ, Miller SM, Zawistowski JS, Nakamura K, Beltran AS, Duncan JS, Angus SP*, et al.* Inhibition of Lapatinib-Induced Kinome Reprogramming in ERBB2-Positive Breast Cancer by Targeting BET Family Bromodomains. Cell reports 2015, 11: 390-404

21. Zhang L, Yu H, Badzio A, Boyle TA, Schildhaus HU, Lu X, Dziadziuszko R*, et al.* Fibroblast Growth Factor Receptor 1 and Related Ligands in Small-Cell Lung Cancer. Journal of thoracic oncology : official publication of the International Association for the Study of Lung Cancer 2015, 10: 1083-1090

22. McMillin DW, Negri JM, Mitsiades CS. The role of tumour-stromal interactions in modifying drug response: challenges and opportunities. Nature reviews Drug discovery 2013, 12: 217-228

23. Wilson TR, Fridlyand J, Yan Y, Penuel E, Burton L, Chan E, Peng J*, et al.* Widespread potential for growth-factor-driven resistance to anticancer kinase inhibitors. Nature 2012, 487: 505-509

24. Paulo JA, McAllister FE, Everley RA, Beausoleil SA, Banks AS, Gygi SP. Effects of MEK inhibitors GSK1120212 and PD0325901 in vivo using 10-plex quantitative proteomics and phosphoproteomics. Proteomics 2015, 15: 462-473

25. Ruprecht B, Koch H, Medard G, Mundt M, Kuster B, Lemeer S. Comprehensive and reproducible phosphopeptide enrichment using iron immobilized metal ion affinity chromatography (Fe-IMAC) columns. Molecular & cellular proteomics : MCP 2015, 14: 205-215

26. Rappsilber J, Mann M, Ishihama Y. Protocol for micro-purification, enrichment, pre-fractionation and storage of peptides for proteomics using StageTips. Nature protocols 2007, 2: 1896-1906

27. Ritorto MS, Cook K, Tyagi K, Pedrioli PGA, Trost M. Hydrophilic Strong Anion Exchange (hSAX) Chromatography for Highly Orthogonal Peptide Separation of Complex Proteomes. Journal of proteome research 2013, 12: 2449-2457

28. Cox J, Mann M. MaxQuant enables high peptide identification rates, individualized p.p.b.-range mass accuracies and proteome-wide protein quantification. Nature biotechnology 2008, 26: 1367-1372

29. Cox J, Neuhauser N, Michalski A, Scheltema RA, Olsen JV, Mann M. Andromeda: a peptide search engine integrated into the MaxQuant environment. Journal of proteome research 2011, 10: 1794-1805

30. Huang da W, Sherman BT, Lempicki RA. Systematic and integrative analysis of large gene lists using DAVID bioinformatics resources. Nature protocols 2009, 4: 44-57

31. Franceschini A, Szklarczyk D, Frankild S, Kuhn M, Simonovic M, Roth A, Lin J*, et al.* STRING v9.1: protein-protein interaction networks, with increased coverage and integration. Nucleic acids research 2013, 41: D808-815

32. Morris JH, Apeltsin L, Newman AM, Baumbach J, Wittkop T, Su G, Bader GD*, et al.* clusterMaker: a multi-algorithm clustering plugin for Cytoscape. BMC bioinformatics 2011, 12: 436

33. Su G, Kuchinsky A, Morris JH, States DJ, Meng F. GLay: community structure analysis of biological networks. Bioinformatics 2010, 26: 3135-3137

34. Horn H, Schoof EM, Kim J, Robin X, Miller ML, Diella F, Palma A*, et al.* KinomeXplorer: an integrated platform for kinome biology studies. Nature methods 2014, 11: 603-604

35. Alanazi I, Ebrahimie E, Hoffmann P, Adelson DL. Combined gene expression and proteomic analysis of EGF induced apoptosis in A431 cells suggests multiple pathways trigger apoptosis. Apoptosis : an international journal on programmed cell death 2013, 18: 1291-1305

36. Kim K, Wu HG, Jeon SR. Epidermal growth factor-induced cell death and radiosensitization in epidermal growth factor receptor-overexpressing cancer cell lines. Anticancer research 2015, 35: 245-253

37. Olson OC, Joyce JA. Microenvironment-mediated resistance to anticancer therapies. Cell research 2013, 23: 179-181

38. Savitski MM, Mathieson T, Zinn N, Sweetman G, Doce C, Becher I, Pachl F*, et al.* Measuring and Managing Ratio Compression for Accurate iTRAQ/TMT Quantification. Journal of proteome research 2013, 12: 3586-3598

39. Suenaga M, Yamamoto M, Tabata S, Itakura S, Miyata M, Hamasaki S, Furukawa T. Influence of gefitinib and erlotinib on apoptosis and c-MYC expression in H23 lung cancer cells. Anticancer research 2013, 33: 1547-1554

40. Zhou X, Zheng M, Chen F, Zhu Y, Yong W, Lin H, Sun Y*, et al.* Gefitinib inhibits the proliferation of pancreatic cancer cells via cell cycle arrest. Anatomical record 2009, 292: 1122-1127

41. Shintani S, Li C, Mihara M, Yano J, Terakado N, Nakashiro K, Hamakawa H. Gefitinib ('Iressa', ZD1839), an epidermal growth factor receptor tyrosine kinase inhibitor, up-regulates p27KIP1 and induces G1 arrest in oral squamous cell carcinoma cell lines. Oral oncology 2004, 40: 43-51

42. Nakanishi Y, Walter K, Spoerke JM, O'Brien C, Huw LY, Hampton GM, Lackner MR. Activating Mutations in PIK3CB Confer Resistance to PI3K Inhibition and Define a Novel Oncogenic Role for p110β. Cancer research 2016, 76: 1193-1203

43. Bornet O, Nouailler M, Feracci M, Sebban-Kreuzer C, Byrne D, Halimi H, Morelli X*, et al.* Identification of a Src kinase SH3 binding site in the C-terminal domain of the human ErbB2 receptor tyrosine kinase. FEBS letters 2014, 588: 2031-2036

44. Thorpe LM, Yuzugullu H, Zhao JJ. PI3K in cancer: divergent roles of isoforms, modes of activation and therapeutic targeting. Nature reviews Cancer 2015, 15: 7-24

45. Mao P, Hever MP, Niemaszyk LM, Haghkerdar JM, Yanco EG, Desai D, Beyrouthy MJ*, et al.* Serine/threonine kinase 17A is a novel p53 target gene and modulator of cisplatin toxicity and reactive oxygen species in testicular cancer cells. The Journal of biological chemistry 2011, 286: 19381-19391

46. Mao P, Hever-Jardine MP, Rahme GJ, Yang E, Tam J, Kodali A, Biswal B*, et al.* Serine/threonine kinase 17A is a novel candidate for therapeutic targeting in glioblastoma. PloS one 2013, 8: e81803

47. Bush EW, Helmke SM, Birnbaum RA, Perryman MB. Myotonic Dystrophy Protein Kinase Domains Mediate Localization, Oligomerization, Novel Catalytic Activity, and Autoinhibition. Biochemistry 2000, 39: 8480-8490

48. Mulders SAM, van Horssen R, Gerrits L, Bennink MB, Pluk H, de Boer-van Huizen RT, Croes HJE*, et al.* Abnormal actomyosin assembly in proliferating and differentiating myoblasts upon expression of a cytosolic DMPK isoform. Biochimica et Biophysica Acta (BBA) - Molecular Cell Research 2011, 1813: 867-877

49. Wei W, Liu W, Serra S, Asa SL, Ezzat S. The breast cancer susceptibility FGFR2 provides an alternate mode of HER2 activation. Oncogene 2015: 1-9

50. Yamagishi Y, Honda T, Tanno Y, Watanabe Y. Two histone marks establish the inner centromere and chromosome bi-orientation. Science 2010, 330: 239-243

51. Roberts PJ, Der CJ. Targeting the Raf-MEK-ERK mitogen-activated protein kinase cascade for the treatment of cancer. Oncogene 2007, 26: 3291-3310

52. Meng Z, Moroishi T, Mottier-Pavie V, Plouffe SW, Hansen CG, Hong AW, Park HW*, et al.* MAP4K family kinases act in parallel to MST1/2 to activate LATS1/2 in the Hippo pathway. Nature communications 2015, 6: 8357

53. Dai J, Sultan S, Taylor SS, Higgins JM. The kinase haspin is required for mitotic histone H3 Thr 3 phosphorylation and normal metaphase chromosome alignment. Genes & development 2005, 19: 472-488

54. Bernard S, Eilers M. Control of cell proliferation and growth by Myc proteins. Results and problems in cell differentiation 2006, 42: 329-342

55. Lepique AP, Moraes MS, Rocha KM, Eichler CB, Hajj GN, Schwindt TT, Armelin HA. c-Myc protein is stabilized by fibroblast growth factor 2 and destabilized by ACTH to control cell cycle in mouse Y1 adrenocortical cells. Journal of molecular endocrinology 2004, 33: 623-638

56. Larsen AB, Pedersen MW, Stockhausen MT, Grandal MV, van Deurs B, Poulsen HS. Activation of the EGFR gene target EphA2 inhibits epidermal growth factor-induced cancer cell motility. Molecular cancer research 2007, 5: 283-293

57. Gusenbauer S, Vlaicu P, Ullrich A. HGF induces novel EGFR functions involved in resistance formation to tyrosine kinase inhibitors. Oncogene 2013, 32: 3846-3856

58. Connell LE, Helfman DM. Myosin light chain kinase plays a role in the regulation of epithelial cell survival. Journal of cell science 2006, 119: 2269-2281

59. Cui W-j, Liu Y, Zhou X-l, Wang F-z, Zhang X-d, Ye L-h. Myosin light chain kinase is responsible for high proliferative ability of breast cancer cells via anti-apoptosis involving p38 pathway. Acta Pharmacol Sin 2010, 31: 725-732

60. Zhou X, Liu Y, You J, Zhang H, Zhang X, Ye L. Myosin light-chain kinase contributes to the proliferation and migration of breast cancer cells through cross-talk with activated ERK1/2. Cancer letters 2008, 270: 312-327

61. Yang L, Zhu J, Huang H, Yang Q, Cai J, Wang Q, Zhu J*, et al.* PFTK1 Promotes Gastric Cancer Progression by Regulating Proliferation, Migration and Invasion. PloS one 2015, 10: e0140451

62. Blanquaert F, Delany AM, Canalis E. Fibroblast growth factor-2 induces hepatocyte growth factor/scatter factor expression in osteoblasts. Endocrinology 1999, 140: 1069-1074

63. Even Y, Durieux S, Escande ML, Lozano JC, Peaucellier G, Weil D, Geneviere AM. CDC2L5, a Cdk-like kinase with RS domain, interacts with the ASF/SF2-associated protein p32 and affects splicing in vivo. Journal of cellular biochemistry 2006, 99: 890-904

64. Chaput D, Kirouac L, Stevens SM, Jr., Padmanabhan J. Potential role of PCTAIRE-2, PCTAIRE-3 and P-Histone H4 in amyloid precursor protein-dependent Alzheimer pathology. Oncotarget 2016, 7: 8481-8497

65. Even Y, Durieux S, Escande M-L, Lozano JC, Peaucellier G, Weil D, Genevière A-M. CDC2L5, a Cdk-like kinase with RS domain, interacts with the ASF/SF2-associated protein p32 and affects splicing in vivo. Journal of cellular biochemistry 2006, 99: 890-904

66. Malumbres M. Cyclin-dependent kinases. Genome biology 2014, 15: 1-10

67. Cozzolino M, Stagni V, Spinardi L, Campioni N, Fiorentini C, Salvati E, Alemà S*, et al.* p120 Catenin Is Required for Growth Factor–dependent Cell Motility and Scattering in Epithelial Cells. Molecular Biology of the Cell 2003, 14: 1964-1977

68. Petrova YI, Spano MM, Gumbiner BM. Conformational epitopes at cadherin calcium-binding sites and p120-catenin phosphorylation regulate cell adhesion. Molecular Biology of the Cell 2012, 23: 2092-2108

69. Shaw LM. The insulin receptor substrate (IRS) proteins: at the intersection of metabolism and cancer. Cell Cycle 2011, 10: 1750-1756

70. Hao Y, Wang C, Cao B, Hirsch BM, Song J, Markowitz SD, Ewing RM*, et al.* Gain of interaction with IRS1 by p110alpha-helical domain mutants is crucial for their oncogenic functions. Cancer cell 2013, 23: 583-593

71. Hadari YR, Tzahar E, Nadiv O, Rothenberg P, Roberts CT, Jr., LeRoith D, Yarden Y*, et al.* Insulin and insulinomimetic agents induce activation of phosphatidylinositol 3'-kinase upon its association with pp185 (IRS-1) in intact rat livers. The Journal of biological chemistry 1992, 267: 17483-17486

72. Argetsinger LS, Norstedt G, Billestrup N, White MF, Carter-Su C. Growth hormone, interferon-gamma, and leukemia inhibitory factor utilize insulin receptor substrate-2 in intracellular signaling. The Journal of biological chemistry 1996, 271: 29415-29421

73. Knight SD, Adams ND, Burgess JL, Chaudhari AM, Darcy MG, Donatelli CA, Luengo JI*, et al.* Discovery of GSK2126458, a Highly Potent Inhibitor of PI3K and the Mammalian Target of Rapamycin. ACS medicinal chemistry letters 2010, 1: 39-43

74. Maira SM, Stauffer F, Brueggen J, Furet P, Schnell C, Fritsch C, Brachmann S*, et al.* Identification and characterization of NVP-BEZ235, a new orally available dual phosphatidylinositol 3-kinase/mammalian target of rapamycin inhibitor with potent in vivo antitumor activity. Molecular cancer therapeutics 2008, 7: 1851-1863

Chapter IV

Time resolved proteomic and phosphoproteomic analysis of adaptation to kinase inhibition

Summary

Although substantial progress has been achieved with the use of targeted cancer therapies, resistance to small molecule kinase inhibition invariably develops and often occurs in very short time scales. From recent studies and the data presented in the previous chapter it becomes more evident that drug adaptation mechanisms appear in very short time and that adaptation in these short time scales already reflects clinically observed resistance mechanisms. To improve the understanding of fast adaptation mechanisms I profiled the time resolved adaptation to EGFR inhibition by gefitinib and FGFR inhibition by AZD4547 on the proteome and phosphoproteome level over 72 h. Application of TMT 10plex labeling enabled the quantification of 10 time points in a single experiment. Moreover, MS3-based quantification on an Orbitrap Fusion mass spectrometer reduced the ratio compression known from MS2-based workflows. Multiplexing facilitated the analysis of time resolved responses in four cell lines and for two inhibitors on the proteome and phosphoproteome level in only eight days of measurement time. Analysis was performed to a depth of up to 4,000 proteins and for up to 7,000 p-sites for each cell line and inhibitor with quantitative data for all time points without missing values. I found that time dependent data can provide information of potential kinase substrate relationships. For instance activity sites in MAPK1/3 were found to correlate very well in all cell lines with the pS2155 in the potential downstream substrate TPR. Moreover, gefitinib treatment induced time dependent overexpression of E-cadherin and ICAM1, leading to cellular aggregation in PC9 lung cancer cells and potential adhesion mediated resistance. Time resolved profiles also revealed that adaptation mechanisms are highly diverse between cell lines and general adaptation mechanisms are less common. Hence, the acquired data provide a proof-of-principle for the conduction of time resolved experiments and a resource for further investigations.

Introduction

Targeted cancer therapies often fail even if there are high initial response rates [1, 2]. Genetic alterations were found to mediate resistance in different targets and tumor entities [3-7]. Moreover, bypass activation to the target is another often observed resistance mechanism [8-13]. Tumor cells evade the action of the drugs by using the whole repertoire of cellular plasticity. In a healthy individual this allows the cells to adapt to different situations and tasks. However, this flexibility also allows fast evasion from targeted cancer therapies by modulation of pathway signaling dependencies and activation of bypass signaling tracks. Recently, it became more evidence that adaptive reprogramming, without affection of genetic mechanisms, appears in very short timescales in response to targeted kinase inhibition [14, 15]. The authors showed that targeted inhibition can result in altered gene transcription and overexpression of receptor tyrosine kinases. This so called adaptive kinome response resulted in elevated expression of DDR1, DDR2, PDGFR, MET, FGFR2, MERTK, EPHA4, EGFR, IGF1R in response to MEK [14] and ERBB2 [15] inhibition.

Proteomic investigation of drug adaptation mechanisms are most often based on binary comparisons or few time points [15]. However, the application of 10plex tandem mass tagging allows time resolved experiments with narrow time points in a reasonable amount of measurement time. The availability of MS3-based quantification [16] in the Fusion Lumos moreover reduces ratio distortion effects usually observed for MS2-based quantifications and allows the coverage of the whole range of fold changes. A narrow time point coverage has the potential to improve the understanding of early, intermediate and late adaptation mechanisms.

In the previous chapter it was shown that the combination of the EGFR inhibitor gefitinib and the FGFR inhibitor AZD4547 is more effective than the single agent treatment. Because the lack of effectiveness of single agent treatments may be a result of fast adaptation and bypass activation, I decided to investigate adaptation mechanisms to the two inhibitors in more detail. The aforementioned TMT labeling was used for time resolved analysis of the drug adaptation mechanisms on the proteome and phosphoproteome level over three days.

Experimental procedures

Cell viability assays

An Alamar Blue (Thermo Fischer Scientific) cell viability assay was performed in 96-well plates with each well containing 2,000 cells. A431 (epidermoid cancer) and PC9 (lung cancer) cells were cultivated in RPMI-1640, ACHN (renal cancer) and IGROV1 (ovarian cancer)) were cultivated in IMDM, supplemented with 10% heat-inactivated FBS (all from Biochrom) in a humidified atmosphere at 5% CO_2 and 37 °C. At the following day, the cells were exposed to different concentrations of gefitinib (LC laboratories) and AZD4547 (Selleckchem) ranging from 10 nM to 10 µM. The cells were then incubated for 72 h at 37 °C and 5% CO_2. Subsequently, Alamar Blue cell viability assays were performed by adding 10 µl Alamar Blue reagent to each well. The reduction from resazurin to the resorufin was measured after 2 h and 4 h using a fluorescence spectrophotometer (BMG Labtech) at 544 nm (excitation) and 590 nm (emission). This assay does not distinguish between viability and proliferation. For simplicity, I refer to viability throughout this thesis, acknowledging that this may also mean proliferation.

Cell culture and cell lysis

A431, ACHN, PC9, and IGROV1 cancer cells were cultivated in RPMI-1640 and IMDM, supplemented with 10% heat-inactivated FBS in a humidified atmosphere at 5% CO_2 and 37 °C. The cells were plated onto 100 mm cell culture dishes on day 0. The next day, A431 cells were treated with 1 µM gefitinib or 5 µM AZD4547, ACHN cells with 1 µM gefitinib or 1 µM AZD4547, PC9 cells with 100 nM gefitinib or 5 µM AZD4547 and IGROV1 with 100 nM gefitinib or 1 µM AZD4547. The cells were then lysed after 2 h, 4 h, 8 h, 12 h, 24 h, 36 h, 48 h, 60 h and 72 h in 200 µl lysis buffer (40 mM Tris/HCl pH 7.6, 8 M urea, EDTA-free protease inhibitor complete mini from Roche, phosphatase inhibitor cocktail 1, 2 and 3 from Sigma Aldrich at 1x final concentration according to the manufacturer instructions). Afterwards, the lysate was transferred into reaction vessels and centrifuged at 22,000 x g to precipitate insoluble material. The protein concentration in the supernatant was determined with a Bradford assay (Pierce).

Immunofluorescence staining

Cells were seeded on µ-slides (Ibidi) in a volume of 50 µl to allow adhesion in a duration of 3 h. Afterwards 100 µl of complete medium was added and the slides were incubated at 5% CO_2 and 37 °C. At the next day the cells were treated with 100 nM gefitinib. The Medium was replaced every 24 h. After 72 h the cells were fixed with 4% formaldehyde for 15 min at room temperature and the channels were washed three times with PBS containing Ca^{2+} and Mg^{2+}. Cells were blocked with washing buffer (5% BSA, 0.3% TritonX-100 in PBS containing Ca^{2+} and Mg^{2+}) for 60 minutes. The blocking solution was aspirated and cells were washed with 200 µl PBS containing Ca^{2+} and Mg^{2+}. The cells were stained with an E-cadherin specific antibody AlexaFluor 488 fluorescent dye conjugate (Cell Signaling Technology) in a 1:800 dilution (1 % BSA, 0.3 % TritonX-100 in PBS containing Ca^{2+} and Mg^{2+}) and the DNA was counterstained with DAPI (0.1 µg/ml). Incubation was performed at 4 °C overnight. Next day, cells were washed with PBS and mounting medium (Ibidi) was applied to visualize specific staining at 460-490 nm in a fluorescence microscope.

Protein digestion and peptide purification

For each time point in the experiment 200 µg were digested. Disulfide bonds were reduced with DTT at a final concentration of 10 mM for 45 min at 37 °C. Cysteine residues were alkylated using 55 mM chloroacetamide for 30 min at room temperature in the dark. The sample was diluted with three volumes of 40 mM Tris/HCl pH 7.6 to decrease the urea concentration to 1.5 M. Trypsin was added to a protease-to-protein ratio of 1:50 (w/w) and digestion was performed for 4 h at 37 °C and 700 rpm using a thermoshaker. A second aliquot of trypsin was added, again at a ratio of 1:50 (w/w) and the samples were incubated at 37 °C overnight. The following day, the samples were cooled to room temperature and acidified using 0.5% FA. Following the precipitation of insoluble debris at 5,000 x g, the supernatant was desalted using 50 mg Sep-Pak columns (Waters) and a vacuum manifold. Columns were primed with 1 ml of solvent B (0.1% FA, 50% ACN) and equilibrated with 3 ml solvent A (0.1% FA in deionized water). The sample was then slowly passed through the column to allow proper peptide binding. Peptides were washed three times with 1 ml solvent A and then eluted into a reaction vessel using 2 times 250 µl solvent B. Finally, the samples were frozen at -80 °C and dried to completeness in a speed vac.

Peptide labeling using tandem mass tags (TMT10)

Lyophilized peptides (300 µg) were dissolved for 10 min at 700 rpm in 62.5 µl of 50 mM TEAB buffer (Sigma Aldrich). TMT reagents (Thermo Scientific) were dissolved in water-free ACN at a concentration of 60 mM. Afterwards, 7.5 µl TMT solution was added to each of the 10 samples, resulting in a final concentration of 6.5 mM TMT. The samples were incubated at 700 rpm for 1 h at room temperature before the labeling reaction was stopped by adding hydroxylamine to a concentration of 0.4%. Following 15 min incubation at room temperature, the samples were acidified and diluted with 750 µl 0.1% FA in deionized water to dilute the ACN concentration to below 1%. In order to correct for potential sample loss and varying labeling efficiency, a labeling test was performed by measuring defined sample mixtures by LC-MS/MS. Peptides were then mixed in equimolar ratios, desalted according to the procedure described above and prepared for proteomic and phosphoproteomic analysis.

Phosphopeptide enrichment using Fe-IMAC columns

Phosphopeptide enrichment was essentially performed as previously described [17]. Briefly, a Fe-IMAC column (ProPac IMAC-10 column, 4 x 50 mm, Thermo Scientific) was charged with Fe^{3+} ions using 3 ml $FeCl_3$ (Sigma Aldrich). Next, the column was equilibrated with solvent A (30% ACN, 0.07% TFA) and connected to an Aekta FPLC system (GE Healthcare). Subsequently, 1.5 mg TMT-labeled peptides were reconstituted in 500 µl solvent A and loaded onto the column (5 min, 0.2 ml/min). Peptides were eluted with solvent B (0.3% NH4OH) in a stepwise gradient of 0-16% (5-6.72 min, 3 ml/min), 16-26.25% (6.7-11.7 min, 0.55 ml/min), 26.25-50% (11.7-12.35 min, 3 ml/min), and 12.35-15 min 0% (3 ml/min). The phosphopeptide-containing fraction (UV) was collected in a reaction vessel (1 ml) and was evaporated to dryness in a speed vac.

High pH reversed-phase micro-column fractionation

High pH reversed-phase micro-columns were prepared in 200 µl pipette tips. Five discs (Ø 1.5 mm) of C18 material (3M Empore) per micro-column were squeezed into a 200 µl pipette tip that was fixed in a 1.5 ml reaction vessel. All solvents were passed through the columns by centrifugation. Columns were primed with 40 µl 50% ACN, 25 mM NH_4COOH (pH 10) and equilibrated with two times 40 µl 25 mM NH_4COOH (pH 10). The sample was then slowly passed through the column and the flow-through was collected and applied to a low pH micro-column for desalting as described previously [18]. Peptides were fractionated using solvents with increasing ACN concentrations. A gradient comprising of 5%, 10%, 15%, 20%, 25%, 30% and 50% ACN in 25 mM NH_4COOH was used for peptides and 5%, 7.5%, 10%, 12.5%, 15%, 17.5% and 50% ACN in 25 mM NH_4COOH for phosphopeptides The desalted flow-through was combined with the second last fraction and the 50% fraction was combined with the 5% fraction, leading to a total of six fractions. The fractionated samples were dried down prior to mass spectrometric analysis.

LC-MS/MS

Peptides were reconstituted in 0.1% FA and phosphopeptides were reconstituted in 0.1% FA and 50 mM citric acid, in order to chelate residual Fe^{3+}-ions. LC-MS/MS measurements were performed by coupling an Ultimate 3000 (Thermo Scientific) to an Orbitrap Fusion Lumos mass spectrometer. Peptides were delivered to a trap column (ID 75 µm, ReproSil-Gold 120 C18 3 µm, Dr. Maisch) for 10 min at a flow rate of 5 µl/min in loading solvent (0.1% FA in water). Peptides were then separated on the analytical column using a 110 min gradient (solvent A: 0.1% FA, 5% DMSO; solvent B: 0.1% FA, 5% DMSO in ACN) at a flow rate of 300 nl/min (0 - 1 min: 2 - 4% B; 101 min: 32% B; 103-105 min: 80% B, 107-110 min: 2%). The Orbitrap Fusion operated in data-dependent mode, automatically switching between MS1, MS2 and MS3 at a cycle time of 2 s. Full-scan MS1 spectra were acquired at 360 to 1300 m/z, 60,000 resolution, automatic gain control (AGC) target value of 4 x 10^5 charges and a maximum injection time of 50 ms. MS2 spectra were acquired at 400 to 2000 m/z at an AGC target value of 1.8 x10^4 charges, 35% collision energy and maximum injection time of 55 ms in the ion trap. Precursor ion isolation width was fixed at 0.7 Th. 10 MS2 notches were selected for MS3 spectra. Acquisition was performed at 100 to 1000 m/z at 30,000 resolution, an AGC target value of 1.2 x10^5 charges and maximum injection time of 55 ms in the orbitrap. Precursor ion isolation width was fixed at 1.3 Th and dynamic exclusion was set to 60 s.

Data analysis

MaxQuant [19] version 1.5.2.8 was used together with its integrated search engine Andromeda [20] for the analysis of LC-MS/MS data. Raw files were searched against the UniProtKB database (v.22.07.13, containing 88,381 entries). Carbamidomethylated cysteine was set as a fixed modification. For raw files of phosphopeptide fractions, phosphorylation of serine, threonine and tyrosine, as well as oxidation of methionine and N-terminal protein acetylation were allowed as variable modifications. For raw files of full proteome fractions, only oxidation of methionine and N-terminal protein acetylation were allowed as variable modifications. Enzyme specificity was set to trypsin/P, allowing for cleavage after proline to account for in-source fragmentation. The minimum peptide length was set to seven amino acids and a maximum of two missed-cleavages were allowed. Quantification was performed on TMT reporter ions in MS3 for protein and phosphopeptide analysis. All tandem mass tags were corrected for their isotopic impurities. The mass tolerance was set to 4.5 ppm for precursor ions and to 20 ppm for fragment ions. The dataset was adjusted to 1% FDR on the level of proteins and peptide spectrum matches (PSMs). Data were further processed using Perseus (v. 1.5.1.6, Max Plank Institute of Biochemistry, Munich), Microsoft Excel and GraphPad Prism. Known potential contaminants and modified peptides with an Andromeda score below 40 were excluded from analysis. Data of cell viability assays were analyzed using GraphPad Prism v.5.01. Four parameter logistic models and nonlinear regression analysis were applied to fit dose-response curves and calculate EC_{50} values. The quantitative values of TMT reporter ions were normalized to the same sum and log2 transformed to get a normal distribution. Log2 transformed data were z-scored to transform variations on the fold change axis to a similar range.

Results and discussion

Time resolved analysis of adaptation mechanisms to EGFR and FGFR inhibition

Cancer cells from different human origins (PC9, lung; A431, skin; IGROV1, ovarian; ACHN, renal) were treated with the inhibitors gefitinib and AZD4547 in a dose dependent manner. A sigmoidal dose response curve was fitted to the data to determine the EC_{50} of both drugs in the four cell lines. The treatment dose that is close to the EC_{50} was selected for a time dependent treatment for 10 time points at 0 h, 2 h, 4 h, 8 h, 12 h, 24 h, 36 h, 48 h, 60 h, 72 h. By selection of a treatment dose that is close to the EC_{50}, the induction of apoptotic signaling should be avoided while the cells are under uncomfortable conditions and experience selection pressure to activate alternative bypass signaling mechanisms. Cell lysates from different time points were chemically labeled with TMT 10plex and the phosphoproteome and full proteome was measured on an Orbitrap Fusion mass spectrometer. An MS3 workflow enabled the reduction of ratio compression for the 10 time points of one TMT experiment (Fig. 1).

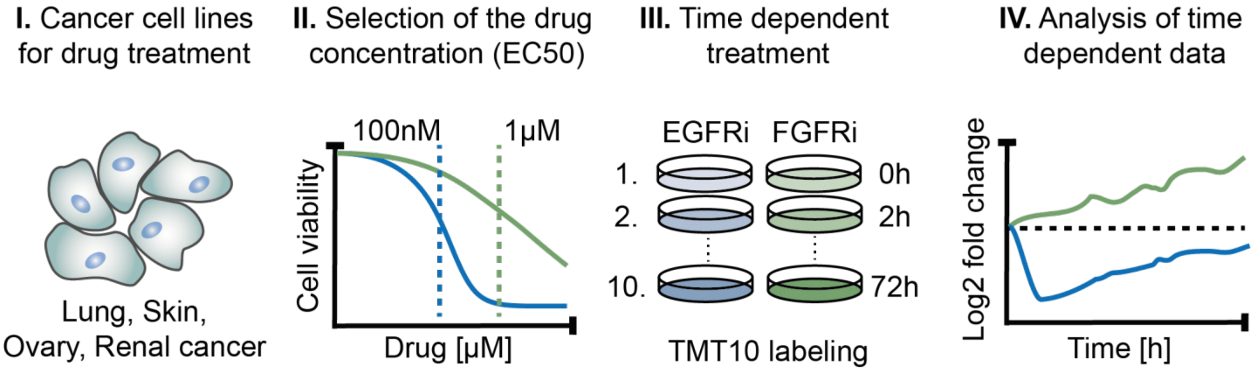
I. Cancer cell lines for drug treatment
Lung, Skin, Ovary, Renal cancer
II. Selection of the drug concentration (EC50)
100nM
1μM
Cell viability
Drug [μM]
III. Time dependent treatment
EGFRi
FGFRi
1.
2.
10.
0h
2h
72h
TMT10 labeling
IV. Analysis of time dependent data
Log2 fold change
Time [h]

Figure 1: Illustration of the proteomic analysis of drug adaptation mechanisms. Cancer cells of the lung, skin, ovar and renal adenocarcinoma were treated dose dependently with the EGFR inhibitor gefitinib and the FGFR inhibitor AZD4547. A treatment dose close to the EC_{50} was selected for time dependent investigation of adaptation mechanisms. TMT 10plex labeling enabled multiplexing of 10 time points in one experiment and comprises high precision for time dependent analysis.

Selection of a treatment dose that inhibits cell proliferation without killing the cells

In the first step the cells were treated with gefitinib, AZD4547 and the combination of both drugs in concentrations ranging from 10 nM to 10 μM. EGFR inhibition is effective in all of the cells and EC_{50} values are between 255 nM (A431) and 14 nM (PC9) (Fig. 2). The PC9 cells are a well investigated model system for non-small cell lung cancer with EGFR activating mutations and are known to be sensitive to gefitinib. However, also all other cell types and wild type EGFR show sensitivity to gefitinib in a nanomolar range. The cells are less sensitive to AZD4547 and EC_{50} values could not be determined due to missing dose dependent response in the selected inhibitor interval (10 nM – 10 µM, Fig. 2). Unfortunately, the AZD4547 inhibitor concentration could not be increased above 10 µM due to lacking solubility in aqueous solutions. However, it is apparent that the combination of both inhibitors is more effective in all cell lines. This confirms the observation of the previous chapter that FGFR mediated signaling can bypass EGFR inhibition (Fig. 2).

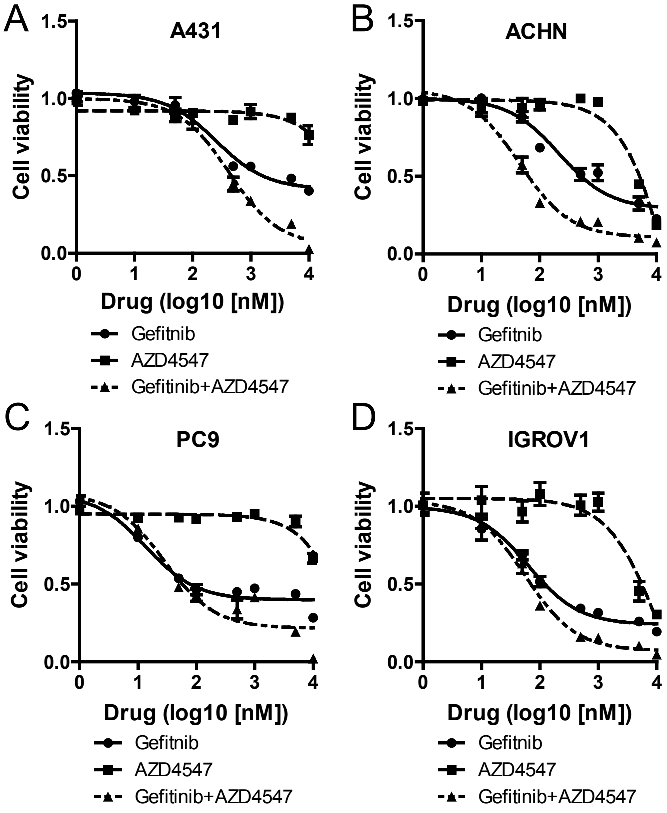

Figure 2: Cell viability after dose dependent EGFR and FGFR inhibition. A) EGFR inhibition is more effective in A431 cells than FGFR inhibition but combined inhibition outperforms single inhibitor treatment and kills the cells. B-D) Same as A but for ACHN, PC9 and IGROV1 cells.

Next, the inhibitor concentrations for time dependent treatments were selected based on the dose response curves. A431 cells and ACHN cells were treated with 1 µM and PC9 cells and IGROV1 cells were treated with 100 nM gefitinib. In contrast, the selected dose of AZD4547 was 5 µM for A431, PC9, IGROV1 and 1 µM for ACHN. As apparent from the viability data (Fig. 2 A-D) this dose was not always sufficient to influence cell viability. By knowing this fact, there may be not enough selection pressure for the cells to adapt to bypass signaling. However, the inhibitor was not soluble at concentrations above 10 µM and treatment at these concentrations was not possible. Phenotypically there is a clear effect visible after gefitinib treatment on all of the cells. Cellular proliferation is inhibited after gefitinib treatment in A431, ACHN, PC9 and IGROV1 cells (Fig. 3). Importantly, the cells do not show an apoptotic phenotype (cell blebbing, apoptotic bodies).

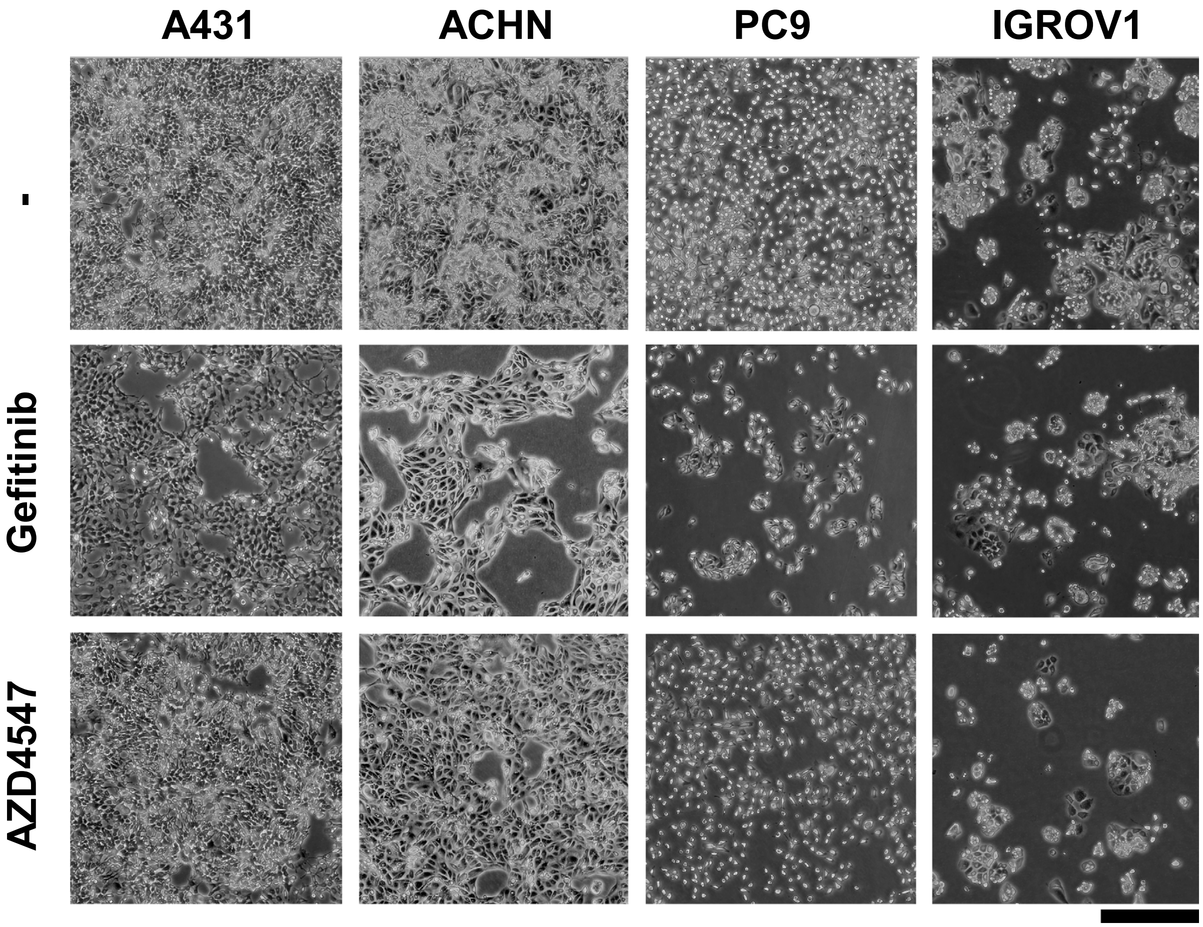

Figure 3: Phenotype of cells after treatment with gefitinib and AZD4547 for 72 h. The selected gefitinib concentration inhibits cell proliferation in all cell lines. The antiproliferative effect of AZD4547 treatment on cells is less pronounced than the effect of gefitinib. Differences in cellular confluence are visible for PC9 cells and IGROV1 cells. Importantly, the selected inhibitor concentrations do not induce apoptotic phenotypes. The phenotype of A431, ACHN and IGROV1 is affected by gefitinib which is not evident for AZD4547. Scale bar represents 500 µm.

However, A431 cells seem to loose cell to cell contacts, ACHN cells become more spindle shaped and most interesting PC9 cells clearly aggregate into distinct colonies from scattered single cells, whereas IGROV1 cell shape seems to be largely unaffected (Fig. 3). The differences in the phenotypic adaptation already indicate that the molecular adaptation mechanisms to EGFR inhibition are largely diverse (shown later on the molecular the profiles on proteome and p-proteome). Inhibition of the FGFR receptor by AZD4547 does not result in a clear antiproliferative effect in A431 and AZD4547 cells (Fig. 3) which is in agreement to the viability assays (Fig. 2A and B, 5 μM and 1 μM used). Cell proliferation in PC9 and IGROV1 cells is reduced without a visible effect on the cell shape (Fig. 3).

Time resolved profiles reveal diverse adaptation mechanisms to EGFR and FGFR inhibition

The proteomic dataset reveals insights into the time dependent profile of 3,000-4,000 proteins in each cell line. This coverage is achieved for the treatment with gefitinib and AZD4547, respectively (Fig. 4A). The coverage on the phosphoproteome level includes the time dependent profiles of up to almost 7,000 p-sites in ACHN cells and 4,500 p-sites in PC9 cells (Fig. 4B). Differences in the number of phosphorylation sites may be explained by general differences of protein phosphorylation between the cell lines. This would also explain the similar numbers of proteins and p-sites that were identified in independent TMT experiments in the same cell line (Fig. 4).

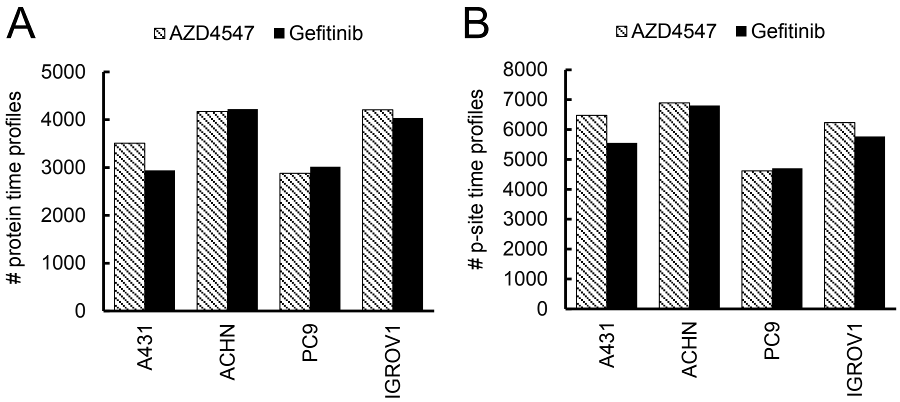

Figure 4: Number of quantitative time profiles for proteins and p-sites after treatment with gefitinib and AZD4547. A) Number of protein profiles for A431, ACHN, PC9 and IGROV1 for the time dependent treatment with gefitinib and AZD4547. B) Same as in A but for the p-site profiles. Time profiles are complete and contain no missing values for any time point.

Importantly, the time profiles for the proteome and phosphoproteome contain no missing values which illustrates the advantage of TMT labeling over label free approaches in time dependent studies. I noticed that the selected treatment concentrations with the AZD4547 inhibitor were inappropriate to expect adaptation mechanisms. The selected concentrations often showed no effect on viability (Fig. 2) and proliferation (Fig. 3), also the time profiles did not show proper curves. In the following I will therefore mostly focus on the results of the gefitinib treatment. The time profiles of the proteome and phosphoproteome changes after gefitinib treatment reflect that the adaptation mechanisms are often diverse. There were large profiles found in each cell line but a considerable number of smaller profiles that are not clearly defined. These smaller profiles that are not clearly defined may contain interesting biological observations but are highly diverse between the cell lines. The larger profiles show some similarity between the cell lines but still differ in the time domain, if the shape of the profile is similar. Figure 5 serves as an example for clearly defined p-site profiles after gefitinib treatment in the four cell lines. Similarities can be found between A431 cells and PC9 cells.

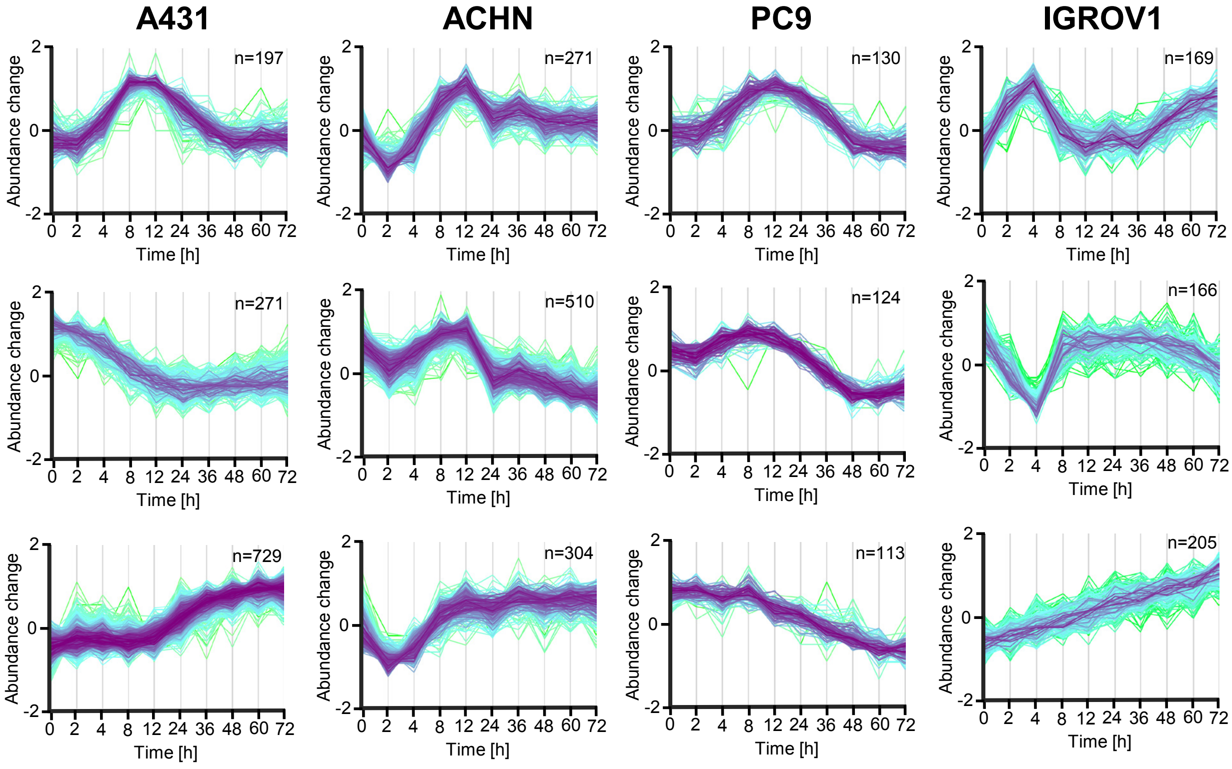

Figure 5: Time resolved profiles of phosphorylation site changes after EGFR inhibition. Phosphorylation site profiles between inhibitors are partially diverse but include similar patterns as transient up- and downregulation or sustained up- and downregulation to a new steady state.

In A431 cells 197 p-sites are temporarily upregulated after 4 h and return to basal level after 36 h. A similar profile can be found in PC9 cells (130 and 124 p-sites found in two similar profiles). Phosphorylation sites in these profiles potentially induce altered expression of genes for adaptation. After reprogramming of the cell, a new steady state is reached and the signaling returns to basal level (Fig. 5). Also in A431 cells and PC9 cells there is a profile of p-sites (n=271 and n=113, respectively) that represents a slow decrease of phosphorylation. However, there is a difference in the time span until a steady state is reached. After just 24 hours p-sites reach a stable level in A431 cells whereas this is not apparent in PC9 cells. Notably, the two clusters do not represent the same p-sites, it is therefore questionable whether this kind of comparison can explain similarities in adaptation processes. Further examples include upregulation of p-sites to a new steady state which is apparent in A431 (n=729) or ACHN (n=304) cells. Even if the time domain is different, the profiles could explain adaptation to a new steady state of signal transduction that possibly reflects a drug resistant phenotype (Fig. 5). The illustrated p-site profiles for IGROV1 cells reflect a fast response to gefitinib. Fast downregulation potentially reflects p-sites that are directly downstream of the EGFR receptor (n=166). The reverse effect is also evident (n=169) and could be linked to feedback activation mechanisms and fast bypass signaling that compensates downregulation of p-sites related to EGFR signaling. Continuous upregulation as shown for the IGROV1 cells (n=205) could be related to inhibitor independent cellular processes like cell proliferation or cell to cell adhesion (Fig. 5). As evident by the different cellular phenotypes that appear in response to gefitinib treatment (Fig. 4) and different p-site profiles, adaptation to EGFR inhibition is largely diverse. A more detailed view on kinases involved in the MAPK pathway confirms these heterogeneous adaptation mechanisms on the protein level (Fig. 6A). After 72 h proteins involved in the MAPK pathway (AKT2, AURKB, MAP2K3, PKN1, RPS6KA3) are differentially regulated between the cell lines in response to gefitinib treatment. The time resolved profile of the AKT2 abundance reveals that changes are only small for all cell lines and the fluctuations (log2 fold change ~0.5) could also be a result of technical noise. Only in the last three time points AKT2 is upregulated in ACHN cells (Fig. 6B). This could serve as a late adaptation mechanism that upregulates AKT2 as a bypass signaling mechanism. The aurora kinase B (AURKB) is an important component of the chromosomal passenger complex, which is a key regulator of mitosis [21, 22]. It is interesting that the abundance of AURKB is not affected for 8 h but is afterwards at least slightly decreasing in all cell lines. The decrease in kinase abundance is most evident in PC9 cells where this kinase is 8 times less abundant than at time point 0 (Fig. 6B). From this data it seems likely that the cells enter the cell cycle less frequently which is reflected by the lower number of cells in phase contrast pictures (Fig. 3). Also A431 cells show a strong decrease of the AURKB abundance but this is only transiently apparent, suggesting that the cells could overcome mitotic arrest. MAP2K3 is involved in the p38 pathway and has been shown to contribute to resistance in chemotherapy [23, 24]. The abundance of this kinase is not affected in IGROV1 and ACHN cells but is continuously decreasing in A431 and PC9 cells. It may be possible that the loss of abundance is associated with a more resistant phenotype but also that this is only a bystander effect of adaptation and only reflects the change to another steady state (Fig. 6B).

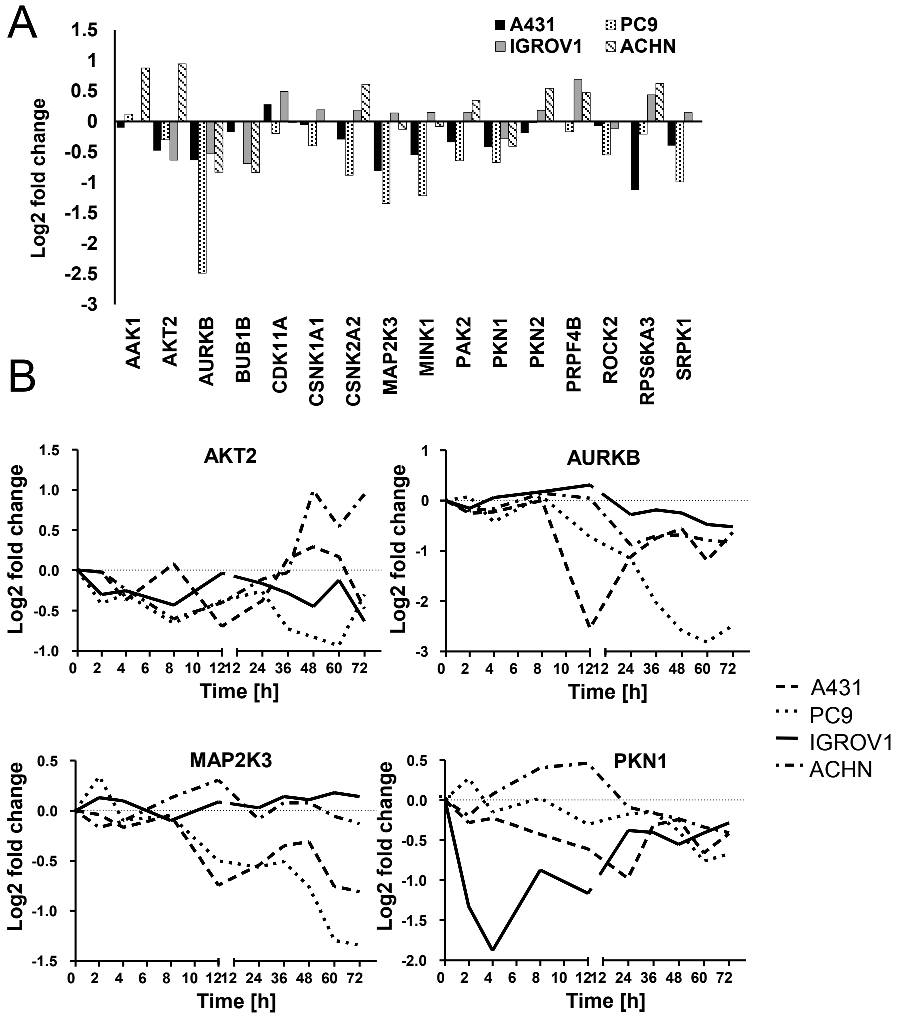

Figure 6: Kinases in the MAPK pathway after treatment with gefitinib. A) Diverse kinase regulation after 72 h in the four investigated cell lines. B) Time resolved response for AKT2, AURKB, MAP2K3 and PKN1.

The serine threonine kinase PKN1 regulates cell migration [25] and targets HDAC proteins [26] which influences transcription of various genes. An interesting observation is the fast but transient decrease of the PKN1 kinase abundance in IGROV1 cells (Fig. 6B) whereas all other cells do not show this initial drop. Decreased abundance could affect the expression of hundreds of other genes via HDAC modification and may therefore be part of a fast adaptation process. However, that this effect is only evident in one cell line illustrates again that adaptation is a diverse process and general effects are at least rarely found on the single protein level.

Time resolved profiles suggest that phosphorylation on S2155 of the nuclear core complex protein (TPR) is a substrate of MAPK1 and MAPK3

The RAS/RAF/MAPK signaling cascade is a known downstream pathway of activated EGFR signaling and activated signaling results in enhanced cell proliferation [27]. In this regard inhibition of the EGFR was expected to result in decreased activity of members in this pathway. Activity sites of ERK1 (MAPK3 pY204) and ERK2 (MAPK1 pY187) phosphorylated peptides were identified and show time dependent inhibition curves in response to gefitinib treatment (Fig. 7A). Interestingly, MAPK1_pY187 and MAPK3_pY204 A431 in A431 and ACHN cells are mostly inhibited after 2 h and start to be increasingly reactivated from 4 h to 72 h. Late reactivation (24 h - 72 h) could be a result of metabolic degradation of gefitinib and reactivation of EGFR but the early reactivation starting after 4 h is too fast to be a result of inhibitor degradation. More likely, the reactivation results from bypass activation mechanisms that activate MAPK1 and MAPK3 independent of EGFR. It is important to note that IGROV1 cells do not show markedly reduced phosphorylation on MAPK1_pY187 and no inhibition on MAPK3_pY204 after gefitinib treatment (Fig. 7A). Because cell viability and proliferation are affected by gefitinib in all cell lines (Fig. 2D and Fig. 3) it is apparent that IGROV1 cells have a different downstream signaling from the EGFR receptor than the other three cell types, but the phenotypical outcome is the same. The nuclear core complex protein (TPR) shows inhibition on pS2155 that follows the same time dependent profile as the inhibition of the activity site pY187 in MAPK1 in all cell lines. Interestingly, it was demonstrated by Vormastek et al. that phosphorylation sites in the C-terminal region of TPR (not including pS2155) are phosphorylated by MAPK1 and that phosphorylation stabilizes the interaction between MAPK1 and TPR [28]. The high correlation of time dependent data in this study add further evidence that TPR_pS2155 is phosphorylated by MAPK1 and possibly also by MAPK3 (Fig. 7A). The profiles of FGFR inhibition by AZD4547 indicate that MAPK activation and also TPR phosphorylation is not affected by the drug (Fig. 7B), which would be in agreement to the phenotypic data. However, also for AZD4547 there is a correlation between all three phosphorylation site profiles. Especially the similarity between the phosphosite profile of MAPK1/MAPK3 and TPR_S2155 in the IGROV1 cells is clearly visible (Fig. 7B).

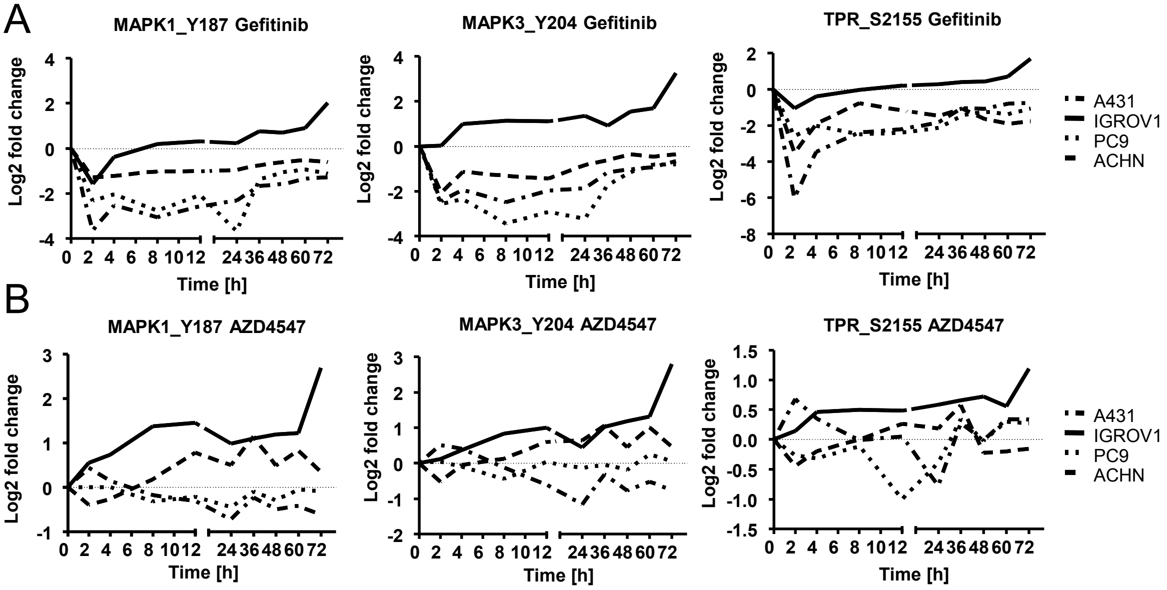

Figure 7: Time resolved phosphorylation suggests TPR_S2155 as a substrate of MAPK1/3. A) Activation of MAPK1/3 and TPR phosphorylation after gefitinib treatment. B) Same as A but for AZD4547.

Elevated expression of E-cadherin and ICAM1 is a marker for gefitinib induced cell-cell aggregation in PC9 cells

As already mentioned above, gefitinib induces phenotypic changes in A431, ACHN and PC9 cells. Whereas the changes in A431 and ACHN are rather small and affect mostly proliferation (Fig. 3), in PC9 the changes are clearly visible. Untreated cells show a strong scattering and almost no contact to other cells (Fig. 8A) In contrast, cells treated with 100 nM gefitinib cluster closely together which results in the formation of cellular aggregates (Fig. 8A upper panel). Higher magnification illustrates that the cells are in very close contact and wind around each other (Fig. 8A lower panel). Also treatment with AZD4547 showed a slightly different phenotype (stretched shape) compared to the control (Fig. 8A lower panel). The visible adaptation on the phenotypic level also confirms the observed extensive molecular adaptation on the proteome and phosphoproteome level (Fig. 5). To get a deeper insight into the adaptation mechanisms that could explain the aggregative phenotype of gefitinib treated PC9 cells, proteins with functions in cell to cell adhesion (GO-term annotations) were considered for further interpretation.

Interestingly, the abundance of cell adhesion proteins E-cadherin (CDH1 gene) and ICAM1 is 8-fold upregulated after 72 h treatment with gefitinib (Fig. 8B).

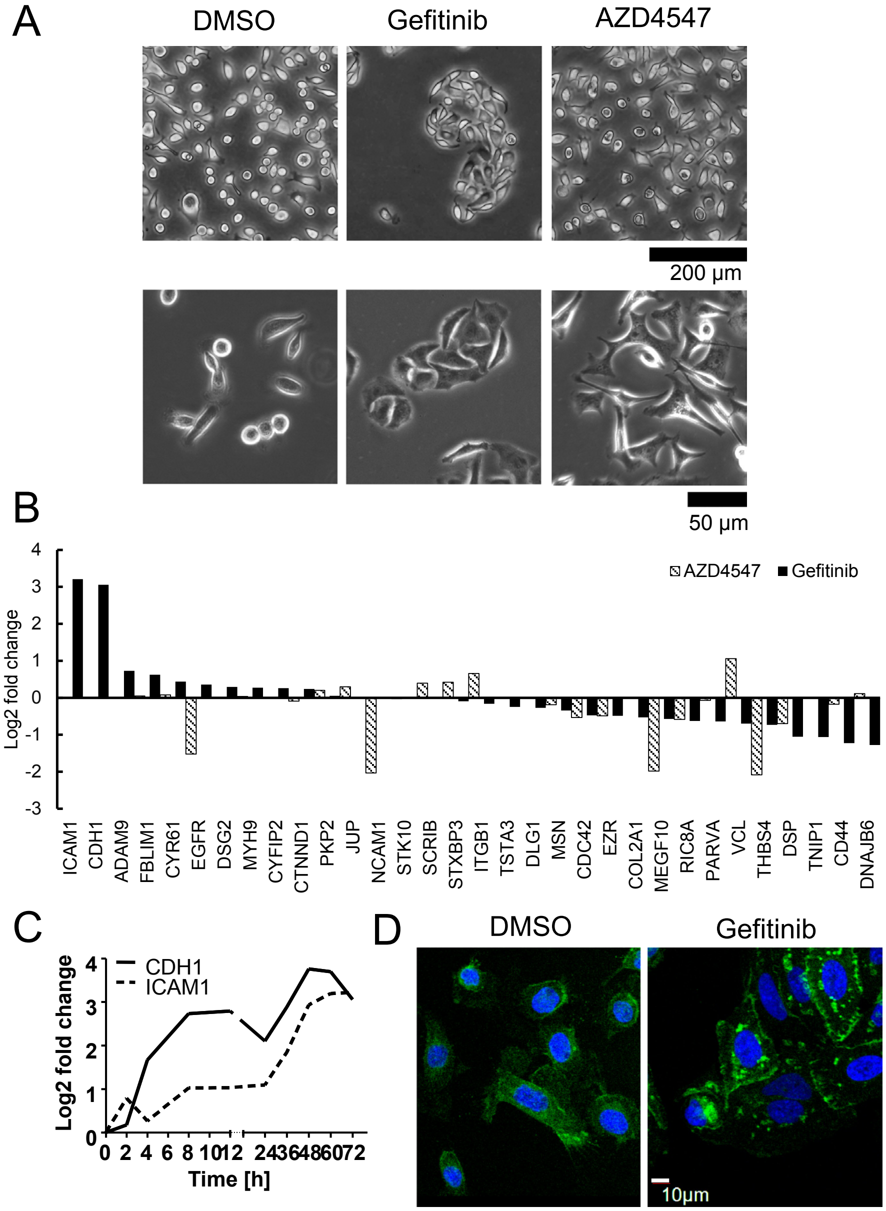

Figure 8: Gefitinib treatment induces cell-cell interaction via overexpression of CDH1 and ICAM1. A) Gefitinib treatment induces cell-cell interaction and colony formation after 72 h while the effect of AZD4547 on the phenotype is less pronounced and a stretched shape is visible. B) Fold changes of proteins involved in cell adhesion (GO term) after 72 h treatment with gefitinib and AZD4547. Gefitinib treated cells show strong induction of CDH1 and ICAM1 that are involved in cell-cell interactions. C) Time dependent profile of CDH1 and ICAM1 expression after gefitinib treatment. D) Immunofluorescence staining of CDH1 (green; DAPI counterstaining, blue) indicates overexpression and spot-like localization in gefitinib treated cells (72 h treatment).

The time resolved data illustrate that ICAM1 is 2 fold upregulated after 24 h and reaches a maximum of 8 fold upregulation after 48 h (Fig. 8C). E-cadherin is upregulated very fast in response to gefitinib treatment and is upregulated 4 fold after 2 h, 8 fold after 8 h and reaches a maximum of 16 fold upregulation after 48 h (Fig. 8C). Interestingly, E-cadherin is localized in spot like structures at the cell to cell interaction surface after gefitinib treatment as revealed by immunofluorescence staining (Fig. 8D). This spot like structure could enhance the cell to cell interactions and force the aggregative behavior of the cells. Altered E-cadherin expression has been found in various cancers, but most often decreased levels were reported to be associated with epithelial-mesenchymal transition (EMT) and a poor prognosis [29-31]. Conversely, the switch from a sensitive mesenchymal phenotype to a resistant epithelial phenotype with elevated E-cadherin expression was found for cells that became resistant to the drug salinomycin [32]. Accordingly, it seems possible that PC9 cells become resistant to gefitinib by induction of a more epithelial phenotype with more E-cadherin and ICAM mediated cell to cell contacts. Enhanced cell to cell contacts could initiate cell interaction based pro survival signaling that let the cells become independent on EGFR signaling. Importantly, cell adhesion-mediated drug resistance (CAM-DR) has been found in different cancer cell types [33-36] and can be a result of cell matrix or cell-cell interactions. It is possible that enhanced interactions of the PC9 cells provide a better microenvironment to circumvent killing by EGFR inhibition.

Time dependent proteomic and phosphoproteomic data can improve our understanding of adaptation mechanisms to small molecule kinase inhibitors as illustrated by the time resolved adaptation to EGFR inhibitor gefitinib and FGFR inhibitor AZD4547. Chemical labeling with tandem mass tags minimizes the analysis time due to sample multiplexing and reduces the number of missing values between time points tremendously. Time dependent analysis can help to understand kinase substrate relationships or the reactivation and bypass activation of kinases. It can also contribute to the understanding of molecular mechanisms that induce visible phenotypic changes, as exemplified by the CHD1 and ICAM1 induction after treatment with gefitinib. However, a major drawback is the difficulty to understand proteomic and phosphoproteomic time profiles, the connection between proteins and phosphorylation sites in cellular networks and the diversity of adaptation mechanisms between cell lines. Hence, the acquired data provide a proof of principle for the conduction of time resolved experiments and a resource for further investigations.

Acknowledgments

The author wants to thank Melanie Schoof for the conduction of experiments during her M. Sc. thesis under my supervision, Daniel Zolg for mass spectrometric measurements on the Orbitrap Fusion Lumos and Karl Kramer for discussions.

Abbreviations

MS2	Fragment mass spectrum from MS1 precursor
MS3	Isolated fragment ion spectrum from MS2 precursors
IMAC	Immobilized metal affinity chromatography
FC	Fold change
TMT	Tandem mass tags
pY/T/S	Phosphotyrosine, -treonine, -serine
GO	Gene ontology
TMT	Tandem mass tags
FPLC	Fast preparative liquid chromatography

References

1. Amado RG, Wolf M, Peeters M, Van Cutsem E, Siena S, Freeman DJ, Juan T*, et al.* Wild-type KRAS is required for panitumumab efficacy in patients with metastatic colorectal cancer. Journal of clinical oncology : official journal of the American Society of Clinical Oncology 2008, 26: 1626-1634

2. Riely GJ, Pao W, Pham D, Li AR, Rizvi N, Venkatraman ES, Zakowski MF*, et al.* Clinical course of patients with non-small cell lung cancer and epidermal growth factor receptor exon 19 and exon 21 mutations treated with gefitinib or erlotinib. Clinical cancer research : an official journal of the American Association for Cancer Research 2006, 12: 839-844

3. Karvela M, Helgason GV, Holyoake TL. Mechanisms and novel approaches in overriding tyrosine kinase inhibitor resistance in chronic myeloid leukemia. Expert Review of Anticancer Therapy 2012, 12: 381-392

4. Jabbour E, Kantarjian H, Jones D, Talpaz M, Bekele N, O'Brien S, Zhou X*, et al.* Frequency and clinical significance of BCR-ABL mutations in patients with chronic myeloid leukemia treated with imatinib mesylate. Leukemia 2006, 20: 1767-1773

5. Emery CM, Vijayendran KG, Zipser MC, Sawyer AM, Niu L, Kim JJ, Hatton C*, et al.* MEK1 mutations confer resistance to MEK and B-RAF inhibition. Proceedings of the National Academy of Sciences 2009, 106: 20411-20416

6. Cools J, Mentens N, Furet P, Fabbro D, Clark JJ, Griffin JD, Marynen P*, et al.* Prediction of Resistance to Small Molecule FLT3 Inhibitors: Implications for Molecularly Targeted Therapy of Acute Leukemia. Cancer research 2004, 64: 6385-6389

7. Suda K, Onozato R, Yatabe Y, Mitsudomi T. EGFR T790M Mutation: A Double Role in Lung Cancer Cell Survival? Journal of Thoracic Oncology 2009, 4: 1-4

8. Engelman JA, Zejnullahu K, Mitsudomi T, Song Y, Hyland C, Park JO, Lindeman N*, et al.* MET amplification leads to gefitinib resistance in lung cancer by activating ERBB3 signaling. Science 2007, 316: 1039-1043

9. Tang MKS, Zhou HY, Yam JWP, Wong AST. c-Met Overexpression Contributes to the Acquired Apoptotic Resistance of Nonadherent Ovarian Cancer Cells through a Cross Talk Mediated by Phosphatidylinositol 3-Kinase and Extracellular Signal-Regulated Kinase 1/2. Neoplasia 2010, 12: 128-IN125

10. Zhou J, Wang J, Zeng Y, Zhang X, Hu Q, Zheng J, Chen B*, et al.* Implication of epithelial-mesenchymal transition in IGF1R-induced resistance to EGFR-TKIs in advanced non-small cell lung cancer. 2015

11. Zhou L, Liu XD, Sun M, Zhang X, German P, Bai S, Ding Z*, et al.* Targeting MET and AXL overcomes resistance to sunitinib therapy in renal cell carcinoma. Oncogene 2015: 1-11

12. Suda K, Mizuuchi H, Sato K, Takemoto T, Iwasaki T, Mitsudomi T. The insulin-like growth factor 1 receptor causes acquired resistance to erlotinib in lung cancer cells with the wild-type epidermal growth factor receptor. International journal of cancer Journal international du cancer 2014, 135: 1002-1006

13. Ware KE, Hinz TK, Kleczko E, Singleton KR, Marek LA, Helfrich BA, Cummings CT*, et al.* A mechanism of resistance to gefitinib mediated by cellular reprogramming and the acquisition of an FGF2-FGFR1 autocrine growth loop. Oncogenesis 2013, 2: e39

14. Duncan JS, Whittle MC, Nakamura K, Abell AN, Midland AA, Zawistowski JS, Johnson NL*, et al.* Dynamic reprogramming of the kinome in response to targeted MEK inhibition in triple-negative breast cancer. Cell 2012, 149: 307-321

15. Stuhlmiller TJ, Miller SM, Zawistowski JS, Nakamura K, Beltran AS, Duncan JS, Angus SP*, et al.* Inhibition of Lapatinib-Induced Kinome Reprogramming in ERBB2-Positive Breast Cancer by Targeting BET Family Bromodomains. Cell reports 2015, 11: 390-404

16. McAlister GC, Nusinow DP, Jedrychowski MP, Wühr M, Huttlin EL, Erickson BK, Rad R*, et al.* MultiNotch MS3 Enables Accurate, Sensitive, and Multiplexed Detection of Differential Expression across Cancer Cell Line Proteomes. Analytical chemistry 2014, 86: 7150-7158

17. Ruprecht B, Koch H, Medard G, Mundt M, Kuster B, Lemeer S. Comprehensive and reproducible phosphopeptide enrichment using iron immobilized metal ion affinity chromatography (Fe-IMAC) columns. Molecular & cellular proteomics : MCP 2015, 14: 205-215

18. Rappsilber J, Mann M, Ishihama Y. Protocol for micro-purification, enrichment, pre-fractionation and storage of peptides for proteomics using StageTips. Nature protocols 2007, 2: 1896-1906

19. Cox J, Mann M. MaxQuant enables high peptide identification rates, individualized p.p.b.-range mass accuracies and proteome-wide protein quantification. Nature biotechnology 2008, 26: 1367-1372

20. Cox J, Neuhauser N, Michalski A, Scheltema RA, Olsen JV, Mann M. Andromeda: a peptide search engine integrated into the MaxQuant environment. Journal of proteome research 2011, 10: 1794-1805

21. Wang F, Ulyanova Natalia P, van der Waal Maike S, Patnaik D, Lens Susanne MA, Higgins Jonathan MG. A Positive Feedback Loop Involving Haspin and Aurora B Promotes CPC Accumulation at Centromeres in Mitosis. Current Biology, 21: 1061-1069

22. Goto H, Yasui Y, Nigg EA, Inagaki M. Aurora-B phosphorylates Histone H3 at serine28 with regard to the mitotic chromosome condensation. Genes to Cells 2002, 7: 11-17

23. Galan-Moya EM, de la Cruz-Morcillo MA, Valero ML, Callejas-Valera JL, Melgar-Rojas P, Losa JH, Salcedo M*, et al.* Balance between MKK6 and MKK3 Mediates p38 MAPK Associated Resistance to Cisplatin in NSCLC. PloS one 2011, 6: e28406

24. Dumka D, Puri P, Carayol N, Lumby C, Balachandran H, Schuster K, Verma AK*, et al.* Activation of the p38 Map Kinase Pathway is Essential for the Antileukemic Effects of Dasatinib. Leukemia & lymphoma 2009, 50: 2017-2029

25. Lachmann S, Jevons A, De Rycker M, Casamassima A, Radtke S, Collazos A, Parker PJ. Regulatory Domain Selectivity in the Cell-Type Specific PKN-Dependence of Cell Migration. PloS one 2011, 6: e21732

26. Harrison BC, Huynh K, Lundgaard GL, Helmke SM, Perryman MB, McKinsey TA. Protein kinase C-related kinase targets nuclear localization signals in a subset of class IIa histone deacetylases. FEBS letters 2010, 584: 1103-1110

27. Roberts PJ, Der CJ. Targeting the Raf-MEK-ERK mitogen-activated protein kinase cascade for the treatment of cancer. Oncogene 2007, 26: 3291-3310

28. Vomastek T, Iwanicki MP, Burack WR, Tiwari D, Kumar D, Parsons JT, Weber MJ*, et al.* Extracellular signal-regulated kinase 2 (ERK2) phosphorylation sites and docking domain on the nuclear pore complex protein Tpr cooperatively regulate ERK2-Tpr interaction. Mol Cell Biol 2008, 28: 6954-6966

29. Qian X, Ma X, Zhou H, Yu C, Zhang Y, Yang X, Shen X*, et al.* Expression and prognostic value of E-cadherin in laryngeal cancer. Acta Oto-Laryngologica 2016, 13: 1-7

30. Liu J, Sun XIN, Qin S, Wang H, Du N, Li Y, Pang Y*, et al.* CDH1 promoter methylation correlates with decreased gene expression and poor prognosis in patients with breast cancer. Oncology Letters 2016, 11: 2635-2643

31. Farmakovskaya M, Khromova N, Rybko V, Dugina V, Kopnin B, Kopnin P. E-Cadherin repression increases amount of cancer stem cells in human A549 lung adenocarcinoma and stimulates tumor growth. Cell Cycle 2016, 15: 1084-1092

32. Kopp F, Hermawan A, Oak PS, Ulaganathan VK, Herrmann A, Elnikhely N, Thakur C*, et al.* Sequential Salinomycin Treatment Results in Resistance Formation through Clonal Selection of Epithelial-Like Tumor Cells()(). Translational Oncology 2014, 7: 702-711

33. Tsubaki M, Takeda T, Yoshizumi M, Ueda E, Itoh T, Imano M, Satou T*, et al.* RANK-RANKL interactions are involved in cell adhesion-mediated drug resistance in multiple myeloma cell lines. Tumour Biol 2016,

34. Wu Y, Xu X, Miao X, Zhu X, Yin H, He Y, Li C*, et al.* Sam68 regulates cell proliferation and cell adhesion-mediated drug resistance (CAM-DR) via the AKT pathway in non-Hodgkin's lymphoma. Cell Prolif 2015, 48: 682-690

35. Sun L, Liu L, Liu X, Wang Y, Li M, Yao L, Yang J*, et al.* MGr1-Ag/37LRP induces cell adhesion-mediated drug resistance through FAK/PI3K and MAPK pathway in gastric cancer. Cancer science 2014, 105: 651-659

36. Meads MB, Gatenby RA, Dalton WS. Environment-mediated drug resistance: a major contributor to minimal residual disease. Nature reviews Cancer 2009, 9: 665-674

Chapter V

General Discussion

General Discussion

Mass spectrometry-based proteomics represents a high performance technology for quantification of proteins and protein phosphorylations. Recently, the use of MS-based proteomics lead to the identification of 17,294 proteins from different organs of the human body [1], indicating that proteomics reached a level to cover proteomes to a very high depth. The use of proteomics also provides a certain and unique possibility for the characterization of resistance mechanisms which is not covered by other “omics” techniques. Essentially, this is the measurement of alterations directly at the protein or protein activity level which serves as a pivotal information layer to derive targetable molecules and better combination of targeted treatments. Hence, proteomic technologies were applied to investigate the molecular basis for resistance in detail.

Targeted cancer therapies are designed to target kinases due to their pivotal role as executors of signal transduction in the cell. Because treatment resistance often occurs by kinase reactivation or bypass signaling, kinases are directly connected to emerging resistance. Hence, a chemical proteomics approach was chosen to evaluate resistance mechanisms directly on the kinase level. In the beginning of this thesis it was assumed that the chemical proteomics approach is generally able to derive information about the activation status of kinases [2]. This would have been a great advantage, because the large scale assessment of kinase activation can reflect activity dependent resistance mechanisms that are inaccessible by many other techniques. However, it became increasingly evident that activity dependent enrichment is largely dependent on the type of inhibitor that is immobilized to the sepharose matrix of the beads [3]. This denotes that chemical proteomics is not generally suited to derive activity dependent resistance mechanisms but covers resistance mechanisms that are based on changes in kinase abundance. This was proven to be useful to get insights into differential kinome adaptations after long term treatment with EGFR inhibitor gefitinib. Chemical proteomics revealed different expressions of kinases in response to EGFR inhibition and suggested EPHA2 as a new resistance mechanism. This could be confirmed by further cell based assays and thereby proves that chemical proteomics is a suitable sub-proteome enrichment tool to facilitate mass spectrometry-based analysis of resistance mechanisms.

The lacking ability of chemical proteomics for kinase activity profiling required an alternative for the assessment of kinase activity. The global quantification of protein phosphorylation provides the possibility to derive a kinase activity centric picture which is however, much more complicated than the direct information from kinases. In chapter three and chapter four I have applied phosphoproteomics to evaluate signatures that lead to growth factor mediated resistance and time dependent adaptation to kinase inhibition. The investigations resulted in the quantification of up to 22,000 phosphorylation sites, a number that could be further improved by more fractionation. In another study, up to 50,000 phosphorylated peptides were derived by extensive fractionation from a single human cancer cell line [4]. These numbers are impressive when compared to traditional immunoblot or antibody arrays. However, even if the numbers are high, they do not reflect our understanding of the biology in these studies. The information that is achieved from phosphoproteomics is often extremely difficult to understand. Apart from some known phosphorylation sites in kinase activation loops (activity sites) that directly represent the kinase activation status, phosphoproteomics provides mostly an indirect information on kinases activity. Kinases phosphorylate their substrates which in turn reflects the kinase activity. However, a single substrate can be phosphorylated by several kinases under different physiological conditions, the inference from a substrate to the activated kinase is therefore often difficult. Moreover, most kinase substrate relationships are still not known or only based on predicted phosphorylation motifs [5, 6] which renders the majority of information from phosphoproteomics inaccurate or inaccessible. In this thesis signaling nodes could be identified from the conducted phosphoproteomics experiments, but it was also obvious from the data that biological interpretations often suffer from a gap of knowledge in the functional role of protein phosphorylations. The long term success of phosphoproteomics will therefore largely rely on the functional understanding of phosphorylation events. So far, deep phosphoproteomics improves the chance to cover phosphorylation events that can be interpreted with our current knowledge but also unfolds the large parts of a problem; the higher the number of identified phosphorylation sites, the higher the proportion of phosphorylation sites with unknown functions. Large scale functional studies that can further define kinase substrate relationships will be needed and are vital for future phosphoproteomics investigations.

Isobaric tagging with tandem mass tags was applied to reduce measurement time by sample multiplexing and the number of missing values between proteomics experiments. Both of these issues were successfully addressed and allowed the quantification of 22,000 p-peptides and 8,500 proteins without missing values in the data matrix in a 9 times reduced measurement time, when compared to a label free approach. The changes of the growth factor mediated rescue from EGFR inhibition could be hereby analyzed to a tremendous depth without losing the possibility to include biological replicates. Importantly, the data set contained a lot of markers including ERBB3, AKT, FGFR overexpression or cMET activation that were found as markers of resistance in previous studies [7-9]. This adds increasing confidence into the methods applied and the results obtained. Nevertheless, there are known issues with a compressed dynamic range arising from precursor co-isolation and MS2 based quantification [10-13]. The compressed dynamic range results in small fold changes that do not represent the real fold changes. The precision in TMT labeled samples is usually much higher, but the interpretation of small changes, even if statistically significant, can be difficult as small changes may not have a biological meaning. The use of MS3 based workflows where multiple ions are selected in MS2 for recording of TMT reporter ions in MS3 largely overcomes the problem of ratio compression due to a two steps ion selection process [14]. In this thesis, MS3 based quantification of TMT reporter ions was applied to monitor adaptation mechanisms to kinase inhibition. In contrast to the MS2 approach, MS3 based quantification resulted in clearly visible time profiles that also showed reasonable fold changes. However, the MS3 approach suffers from a large machine duty cycle that increases issues with data dependent acquisition (DDA). The number of identifications in the same measurement time is reduced when compared to MS2 because of additional recording of MS3 spectra. The increased duty cycle and stochastic nature of precursor selection in DDA experiments lowered the number of overlapping identification between experiments. This was especially apparent in phosphoproteomics experiments. Within one TMT time point experiment, quantification of all time points was most often possible. However, between TMT experiments the number of missing values is even more severe than in label free quantification due to the long duty cycle of MS3. This demonstrates that tandem mass tagging is very helpful to reduce measurement time, missing values and to increase measurement precision within one batch. Across batches there are unsolved issues, especially the low overlap of phosphopeptide identifications will decrease the identified core phosphoproteome to a low number, if the number of samples increases. The development of new mass spectrometers with more speed will reduce the duty cycle and successful implementation of ion mobility [15, 16] could help to separate co-eluting and co-selected peptides to prevent ratio compression. It is thus promising that multiplexing techniques will be applicable to large scale applications without the aforementioned shortcomings.

Abbreviations

DDA	Data dependent acquisition
MS	Mass spectrometry
MS2	Fragment mass spectrum from MS1 precursor
MS3	Isolated fragment ion spectrum from MS2 precursors
TMT	Tandem mass tags

References

1. Wilhelm M, Schlegl J, Hahne H, Moghaddas Gholami A, Lieberenz M, Savitski MM, Ziegler E*, et al.* Mass-spectrometry-based draft of the human proteome. Nature 2014, 509: 582-587

2. Duncan JS, Whittle MC, Nakamura K, Abell AN, Midland AA, Zawistowski JS, Johnson NL*, et al.* Dynamic reprogramming of the kinome in response to targeted MEK inhibition in triple-negative breast cancer. Cell 2012, 149: 307-321

3. Ruprecht B, Zecha J, Heinzlmeir S, Médard G, Lemeer S, Kuster B. Evaluation of Kinase Activity Profiling Using Chemical Proteomics. ACS chemical biology 2015, 10: 2743-2752

4. Sharma K, D'Souza RC, Tyanova S, Schaab C, Wisniewski JR, Cox J, Mann M. Ultradeep human phosphoproteome reveals a distinct regulatory nature of Tyr and Ser/Thr-based signaling. Cell reports 2014, 8: 1583-1594

5. Horn H, Schoof EM, Kim J, Robin X, Miller ML, Diella F, Palma A*, et al.* KinomeXplorer: an integrated platform for kinome biology studies. Nature methods 2014, 11: 603-604

6. Schwartz D, Gygi SP. An iterative statistical approach to the identification of protein phosphorylation motifs from large-scale data sets. Nature biotechnology 2005, 23: 1391-1398

7. Chakrabarty A, Sanchez V, Kuba MG, Rinehart C, Arteaga CL. Feedback upregulation of HER3 (ErbB3) expression and activity attenuates antitumor effect of PI3K inhibitors. Proceedings of the National Academy of Sciences of the United States of America 2012, 109: 2718-2723

8. Engelman JA, Zejnullahu K, Mitsudomi T, Song Y, Hyland C, Park JO, Lindeman N*, et al.* MET amplification leads to gefitinib resistance in lung cancer by activating ERBB3 signaling. Science 2007, 316: 1039-1043

9. Ware KE, Hinz TK, Kleczko E, Singleton KR, Marek LA, Helfrich BA, Cummings CT*, et al.* A mechanism of resistance to gefitinib mediated by cellular reprogramming and the acquisition of an FGF2-FGFR1 autocrine growth loop. Oncogenesis 2013, 2: e39

10. Ow SY, Salim M, Noirel J, Evans C, Rehman I, Wright PC. iTRAQ Underestimation in Simple and Complex Mixtures: “The Good, the Bad and the Ugly”. Journal of proteome research 2009, 8: 5347-5355

11. Karp NA, Huber W, Sadowski PG, Charles PD, Hester SV, Lilley KS. Addressing Accuracy and Precision Issues in iTRAQ Quantitation. Molecular & Cellular Proteomics 2010, 9: 1885-1897

12. Savitski MM, Mathieson T, Zinn N, Sweetman G, Doce C, Becher I, Pachl F*, et al.* Measuring and Managing Ratio Compression for Accurate iTRAQ/TMT Quantification. Journal of proteome research 2013, 12: 3586-3598

13. Sandberg A, Branca RMM, Lehtiö J, Forshed J. Quantitative accuracy in mass spectrometry based proteomics of complex samples: The impact of labeling and precursor interference. Journal of proteomics 2014, 96: 133-144

14. McAlister GC, Nusinow DP, Jedrychowski MP, Wühr M, Huttlin EL, Erickson BK, Rad R*, et al.* MultiNotch MS3 Enables Accurate, Sensitive, and Multiplexed Detection of Differential Expression across Cancer Cell Line Proteomes. Analytical chemistry 2014, 86: 7150-7158

15. Meier F, Beck S, Grassl N, Lubeck M, Park MA, Raether O, Mann M. Parallel Accumulation–Serial Fragmentation (PASEF): Multiplying Sequencing Speed and Sensitivity by Synchronized Scans in a Trapped Ion Mobility Device. Journal of proteome research 2015, 14: 5378-5387

16. Helm D, Vissers JPC, Hughes CJ, Hahne H, Ruprecht B, Pachl F, Grzyb A*, et al.* Ion Mobility Tandem Mass Spectrometry Enhances Performance of Bottom-up Proteomics. Molecular & cellular proteomics : MCP 2014, 13: 3709-3715

Danksagung | Acknowledgment

Nach guten drei Jahren ist es nun geschafft. Diese Arbeit wäre jedoch ohne die Hilfe von Kollegen, Freunden und Familie nicht möglich gewesen und ich schulde vielen Menschen meinen herzlichen Dank.

An erster Stelle geht mein Dank an Bernhard, der mit seinen Vorlesungen überhaupt erst mein Interesse an der Proteomik geweckt hat und später als Doktorvater meine Dissertation betreut hat. Ihm verdanke ich eine große Freiheit in der Umsetzung meines Dissertationsvorhabens und die wissenschaftliche Diskussion vieler guter Ideen die Einzug in diese Arbeit gefunden haben.

Des Weiteren gilt mein Dank Prof. Dr. Florian Bassermann der sich dazu bereit erklärt hat diese Arbeit als Zweitprüfer zu begutachten und Prof. Dr. Dieter Langosch, der sich bereit erklärt hat den Prüfungsvorsitz zu übernehmen.

Natürlich gilt mein Dank auch meinen ehemaligen Studenten Matthias, Andreas und Melanie, die während ihrer Masterarbeiten und als Forschungspraktikanten einen wichtigen Beitrag zu dieser Arbeit geleistet haben. Besonders die Ergebnisse von Melanie haben ihren Weg in Kapitel vier dieser Dissertation gefunden.

Ein weiterer Dank geht an die Kollegen am Lehrstuhl für Proteomik die immer für gute Stimmung gesorgt haben und mit denen man jedes Thema in aller Tiefe bei kollegialer Atmosphäre besprechen konnte. Ein gesonderter Dank geht an unsere Bioinformatiker und Betreuer von Massenspektrometern, die den Routinebetrieb am Laufen halten und an Susan und Scarlet für das aufmerksame Korrekturlesen der Arbeit.

Mein Dank gilt auch dem Deutschen Konsortium für Translationale Krebsforschung für die finanzielle Förderung meines Promotionsprojektes.

Nun möchte ich meinen Dank an meine Familie richten, die immer für mich da ist, ohne euch wäre ich nicht da wo ich jetzt bin. Scarlet, du hast mich immer unterstützt und jetzt wo unsere kleinen Tochter Emilie bei uns ist, ist alles noch viel schöner als zuvor.

List of publications

Koch H., Busto, M. E. D. C., Kramer, K., Médard, G., and Kuster, B. (2015) Chemical Proteomics Uncovers EPHA2 as a Mechanism of Acquired Resistance to Small Molecule EGFR Kinase Inhibition. ***J. Proteome Res.***; 14, 2617–2625

Ruprecht B., **Koch H.**, Medard G., Mundt M., Kuster B., and Lemeer S. (2015) Comprehensive and reproducible phosphopeptide enrichment using iron immobilized metal ion affinity chromatography (Fe-IMAC) columns. ***Mol. Cell. Proteomics***; 14(1):205-15.

Koch H., Wilhelm M., Ruprecht B., Frejno M., Beck S., Klaeger S., and Kuster B. (2016) Phosphoproteome profiling reveals molecular mechanisms of growth factor mediated kinase inhibitor resistance in EGFR overexpressing cancer cells; ***J. Proteome Res.*** *(*accepted)

Ruprecht B., **Koch H.**, Domasinska P., Frejno M., Kuster B., and Lemeer S. Optimized enrichment of phosphoproteomes by Fe-IMAC column chromatography. ***Methods in Molecular Biology***; (in press)

Curriculum vitae

Personal information

Name	Heiner Matthias Koch
Date and place of birth	1985/11/14, Peine, Germany
Address	Zschokkestraße 67, 80686 Munich, Germany
E-mail	heiner.koch@tum.de
Nationality	German

Professional Experience

Since 05/2013	Doctoral candidate at the Technical University of Munich (Chair of Proteomics and Bioanalytics) and German Cancer Research Center (DKFZ) *”Application of mass spectrometry-based proteomics to study cancer drug resistance mechanisms”*
04/2008 – 09/2010	Intern in research departments at Roche Diagnostics GmbH, Penzberg

Education

10/2010 – 02/2013	Master of Science in Molecular Biotechnology, Technical University of Munich
01/2012 – 06/2012	Semester abroad, Master of Science in Medical Bioscience, Linköping University, Sweden
10/2007 – 09/2010	Bachelor of Science in Molecular Biotechnology, Technical University of Munich

Conference attendance (Poster presentations)

ASMS 2016, San Antonio, USA

HUPO 2015, Vancouver, Canada

Annual meeting of the German Consortium for Translational Cancer Research (DKTK) 2015, Heidelberg, Germany

HUPO 2014, Madrid, Spain

Annual meeting of the German Consortium for Translational Cancer Research (DKTK) 2014, Heidelberg, Germany